Parenteral controlled drug delivery by novel direct injectable polymer (DIPO) - *in situ* forming implant

Dissertation

zur Erlangung des akademischen Grades
Doctor rerum naturalium (Dr. rer. nat.)
vorgelegt der
Naturwissenschaftlichen Fakultät I
Biowissenschaften
der Martin-Luther-Universität Halle-Wittenberg
von
M.Sc. Alexandre Gomes Rodrigues
geb. am: 12.11.1983 in: Ribeirão Pires (São Paulo)

Gutachter /in

1. Prof. Dr. Karsten Mäder
2. Prof. Dr. Jörg Kreßler
3. Prof. Dr. Dagmar Fischer

Datum der öffentlichen Verteidigung: 18.04.2018

Science is organized knowledge.

Wisdom is organized life.

Immanuel Kant (1724-1804)

Table of contents

List of symbols and abbreviations

^{13}C NMR	^{13}C nuclear magnetic resonance
^{1}H NMR	^{1}H nuclear magnetic resonance
δ	Chemical shift
θ	Contact angle
API	Active pharmaceutical ingredient
Asp	Aspartic acid
ATR-IR	Attenuated total reflectance infrared
BA	Benzoyl alcohol
BB	Benzyl benzoate
BT-MRI	Bench-top magnetic resonance imaging
BT-NMR	Bench-top nuclear magnetic resonance
CAL-B	*Candida antartica* lipase - B
CCD	Charge-coupled device
COSY	Correlation spectroscopy
CT	Computer tomography
CuCl$_2$	Copper (II) chloride
DDS	Drug delivery system
DG	Degree of grafting
DIPO	Direct injectable polymers
DiR	1,1'-Dioctadecyl-3,3,3',3'-tetramethylindotricarbocyanine iodide
DLS	Dynamic light scattering
DMSO	Dimethyl sulfoxide
DSC	Differential scanning calorimetry
DTG	Differential thermogravimetry
DVA	Divinyl adipate
EC 3.1.1.3	Enzyme Commission number of triacylglycerol lipase (3 = represents the hydrolysis group)
e.g.	Exempli gratia
EMEA	European Medicines Evaluation Agency
FA	Fatty acid
FCS	Fetal calf serum
G	Gauge
GIT	Gastrointestinal tract
GMO	Glyceryl monooleate
GnRH	Gonadotropin-releasing hormone
GPC	Gel permeation chromatography
HCl	Hydrochloric acid
hexPLA	Hexylsubstituted poly(lactide)
His	Histidine
HPG	Hypothalamic-pituitary-gonadal
HPLC	High-pressure liquid chromatography
HSQC	Heteronuclear single quantum coherence
ISFI	*In situ* forming implant
ISO	International system organization
IVIS$^{®}$	*In vivo* imaging system

kGy	Kilogray
LDH	Lactate dehydrogenase
LH-RH	Luteinizing-hormone releasing-hormone
MEM	Modified Eagle Medium
MHz	Megahertz
M_n	Number-average molar mass
MRI	Magnetic resonance imaging
MTS	3-(4,5-Dimethylthiazol-2-yl)-5-(3-carboxymethoxyphenyl)-2-(4-sulfophenyl)-2H-tetrazolium
M_w	Weight-average molar mass
NMP	*N*-methyl-2-pyrrolidone
NIH/3T3	National Institute of Health/fibroblasts cell line
NIR	Near-infrared
P_2O_5	Phosphorus pentoxide
PCL	Poly(ε-caprolactone)
PCS	Photon correlation spectroscopy
PDI	Polydispersity index
PEG	Poly(ethylene glycol)
PEO	Poly(ethylene oxide)
PEO-PPO-PEO	Poly(ethylene oxide)-poly(propylene oxide)- poly(ethylene oxide)
PET	Poly(ethylene terephthalate)
PET	Positron emission tomography
PGA	Poly(glycerol adipate)
PGA-*g*-Ox	Poly(glycerol adipate)-*graft*-oleate; x = degree of grafting
PGA-L25	Poly(glycerol adipate), L25 represents laureate 25 mol% grafting
PGA-L95	Poly(glycerol adipate), L95 represents laureate 95 mol% grafting
PLA	Poly(lactic acid)
PLGA	Poly(lactic-*co*-glycolic acid)
ppm	Parts per million
PPO	Poly(propylene oxide)
PSA	Prostate-specific antigen
rpm	Revolution per minute
RT	Room temperature
s.c.	Subcutaneous
SEC	Size exclusion chromatography
Ser	Serine
SKH-1	Hairless albino mouse strain
TE	Exposition time
T_g	Glass transition temperature
TGA	Thermo-gravimetric analysis
THF	Tetrahydrofuran
TMS	Tetramethylsilane
TR	Repetition time
vol%	Volume percent
ZnSe	Zinc selenide

1 Introduction

1.1 Drug delivery systems

The progress in biotechnology and analytical methods has contributed to many advances in drug development [1]. As a result, proteins and peptides play a key role as a novel class of therapeutic biomolecules [1,2]. Nowadays a great part of new molecules with therapeutic potential investigated consists of peptides and proteins. These compounds have increasingly occupied a strategic place within the (bio)pharmaceutical sector by repositioning major companies and research centers and generating billions of dollars in revenues [2-6]. In this scenario, improvements in drug delivery technologies to provide an adequate therapy are on demand [4,7].

Most patients and health professionals prefer the oral route for drug administration due to its readiness, painless use, and easy adjustment, resulting in a higher patient compliance when compared to other routes [8,9]. However, many new peptides and proteins suffer from a rapid enzymatic degradation in the gastrointestinal tract (GIT) and are poorly absorbed when administered orally, which makes them unsuited for oral dosage form [10]. Moreover, the administration of drugs using conventional dosage forms results in unspecific targeting and possibly undesired side effects, due to a fast and systemic bioavailability of the active ingredient [10].

Parenteral drug administration is a delivery route that overcomes the absorption barrier and avoids the first pass metabolism. Despite the attractiveness of this route from a formulation point of view, researchers must address the drawbacks it presents in order to reach effective and improved therapy with biomolecules. The short half-life of many drugs remains a problem because the maintenance of the necessary therapeutic drug concentration on the site of action requires either infusions or frequent injections [11]. Furthermore, poor drug concentration in the target tissue is one of the main problems in pharmacotherapy, which leads to poor efficacy and unwanted side effects due to drug presence in non-target healthy tissue [12].

Parenteral controlled release systems may be the key to solving these dilemmas. These systems are important for local and systemic drug delivery applications. They can provide increased local drug concentrations (e.g., for brain tumors or local inflammation) and decrease the

frequency of administrations. Scientists have been exploring several strategies as drug delivery systems (DDS) during the last few decades. Among these strategies nanoparticles [13], liposomes [14], microparticles [15], hydrogels [16], implants [17] and other systems [18,19] have been investigated to formulate and release active pharmaceutical ingredients (API). The objective is to offer a final product that suits the needs of patients by increasing patient compliance and reducing undesired side effects on healthy locations (cells, tissues, organs) while maintaining the drug concentration within the therapeutic window [18]. DDS enable a controlled and sustained drug release during the period of the therapy that can be days [20], weeks [21], months [22] or even years [23].

1.1.1 Pre-formed implants

Over the past three decades, the design of parenteral formulations has resulted in the achievement of elegant and sophisticated DDS. Among them, implants have received great attention [24,25]. The first implants, pre-formed implants, were a solid polymer formulation that had to be inserted into the body through a microsurgery or a large internal diameter needle [11]. Commercial implants from this category include Vantas®, a hydrogel containing histrelin acetate, and Viadur®, a titanium alloy reservoir with a controlling membrane, a piston and a diffusion moderator, containing leuprolide acetate [11,26], the later discontinued. These devices offer advantages, such as control of the implant shape. Based on that, properties such as surface area and diffusion of the drug are reproducible.

1.1.2 Non-biodegradable polymers

Even though pre-formed implants have important characteristics concerning drug therapy, their use is suboptimal because the implantation is invasive, not offering comfort to the patient. Besides that, the implant has to be removed when the treatment has finished, in the case of non-biodegradable polymers [12]. The removal of the material is painful due to the fibrous encapsulation formed in the site, as a host response to the foreign body [12]. These non-biodegradable implants were made using materials like silicone elastomers and polyacrylates. The first pre-formed implant to reach the market was Norplant®, a system based on silicone elastomer rods, used as a contraceptive [23]. Various other polymers have been employed to obtain pre-formed implants, among them triblock copolymers of

poly(ethylene oxide) and poly(propylene oxide) (traded as Poloxamers, Pluronics, and Synperonics) (Figure 1). However, the limitations imposed by this type of implant encouraged researchers to work on more suitable systems.
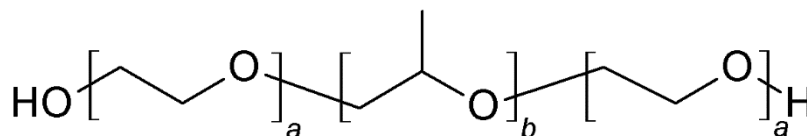

Figure 1. Chemical structure of the triblock copolymer of poly(ethylene oxide)-poly(propylene oxide)-poly(ethylene oxide) (PEO-PPO-PEO) used in hydrogel-based systems.

1.1.3 Biodegradable polymers

To overcome the limitations of implantable devices, as the removal procedure required by the non-biodegradable polymers, researchers came up with materials that degrade in the body, including polyesters, poly(orthoesters), poly(anhydrides), advancing the therapy. Biodegradable polymeric implants have turned into products, such as Gliadel®. It is a wafer used to treat malignant recurrent glioblastoma multiforme (GBM), a brain tumor [12]. Although extending the life of patients, this system presents inconveniences such as postoperative wound infections and cerebral edema [27].

1.1.3.1 *In situ* forming implants (ISFI)

Dunn et al. [28] designed and first reported the concept of an injectable formulation that turns into a semi-solid or solid drug depot and degrades in the body. After being injected into the body, the fluid implant (as a solution or suspension) forms a gel or solid depot, delivering the drug continuously. Compared to pre-formed implants, these characteristics cause less pain and improve patient acceptance [29]. *In situ* forming implants are already important as parenteral controlled release dosage forms and have been gaining research interest in recent years. The depot can be formed by *in situ* cross-linking, *in situ* solidifying organogels or *in-situ* phase separation [11], as elaborated in the following sections.

1.1.3.2 *In situ* cross-linking

In the case of *in situ* forming cross-linked systems, researchers have made polymer networks by photo-initiated polymerization such as Irgacure® 2959 [30], cross-linking with chemical or plant extract agents [31,32] and physical cross-linking of specific monomers [11,33]. Several factors that must be considered when developing depot systems, such as the demands for *in vivo* reaction conditions, which are quite restricted imposing developmental challenges, the need for non-toxic monomers, cross-linking agents and solvents used, oxygen-rich environments, narrow range of physiologically acceptable temperatures and suitable rates of polymerization. Hydrogels are part of this category and have been extensively studied [34,35].

1.1.3.3 *In situ* solidifying organogels

Organogels are semi-solid materials, consisting of a gelator and a solvent, with the appearance and rheological behavior of solids [36]. The self-assembled gelator is a 3-D network (a polymer or a low molar mass gelator), and an organic solvent as a continuous liquid phase. The balance between the gelator and the organic phase, as well as the physicochemical properties of the gel components and their interactions, control the properties of the gel [36]. Gels are prepared by dissolving the gelator in a heated solvent, in concentrations typically lower than 15% (wt). Upon cooling the solubility of the gelator decreases. Consequently, the gelator self-assembles into aggregates, which form the network by intermolecular physical interactions, immobilizing the organic solvent [36]. Various systems have been reported using different gelators. Among them, L-alanine, lecithin, and vegetable oils have been employed for the release of peptides (leuprolide and somatostatin) and hormones (levonorgestrel), in the pharmaceutical field [21].

1.1.3.4 *In situ* phase separation

In situ phase separation systems are the only ones that have resulted in products to the patients to date. They can be divided into fast and slow forming phase inversion implants [37]. This variant of ISFI consists of a solution or suspension of a biodegradable polymer with the drug and organic solvents injected intramuscularly or subcutaneously. Subsequently, the solvent diffuses out, and the polymer transforms into a semi-solid or solid

depot upon contact with aqueous body fluids. The system enables sustained drug release over a designed period. The advantages of this drug delivery system include prolonged delivery period, simple application and no need for large needles or microsurgery. Moreover, the implants are manufactured without complex processes and equipment [11]. In this category, polymers may compose the system without the use of solvents. However, the implant is not injectable at room or body temperature due to the physical characteristics of the polymer. As a result, it must be heated before injection, what limits its use since temperatures up to 60 °C are needed to inject the formulation, leading to a painful procedure [38]. The most common biodegradable polymers investigated for *in situ* implants are chitosan [39], alginate [40], poly(ε-caprolactone-*co*-lactide) [41], poly(lactic acid) (PLA) and poly(D,L-lactic-*co*-glycolic acid) (PLGA) [42].

One biodegradable material, which has been the most successful used for *in situ* forming implant so far, is the copolymer of poly(lactic acid) and poly(glycolic acid). PLA and PLGA, both synthetic biodegradable and biocompatible poly(esters), prevailed over other polymers and are widely employed in commercial products. An example of such case is Eligard® (Sanofi-Aventis), an implant consisting of PLGA dissolved in *N*-methyl-2-pyrrolidone (NMP) containing the gonadotropin-releasing hormone (GnRH) analog leuprolide for the treatment of prostate cancer [22]. Despite the products on the market to treat prostate cancer [22] and periodontitis [43] (Eligard® and Atridox®) [44] and clinical trials currently underway, there are drawbacks related to these materials that need to be addressed. PLA and PLGA degrade into lactic and glycolic acids monomers in an autocatalytic process (Figure 2) and are eliminated through metabolic pathways in the body. The degradation path often leads to an acidic microclimate, drug degradation prior release, heterogeneous degradation, and release profiles. These processes have been characterized by a series of studies using electron paramagnetic spectroscopy [45], potentiometry [46], radiometry based on laser confocal scanning microscopy imaging [47] and multispectral fluorescence imaging [48].
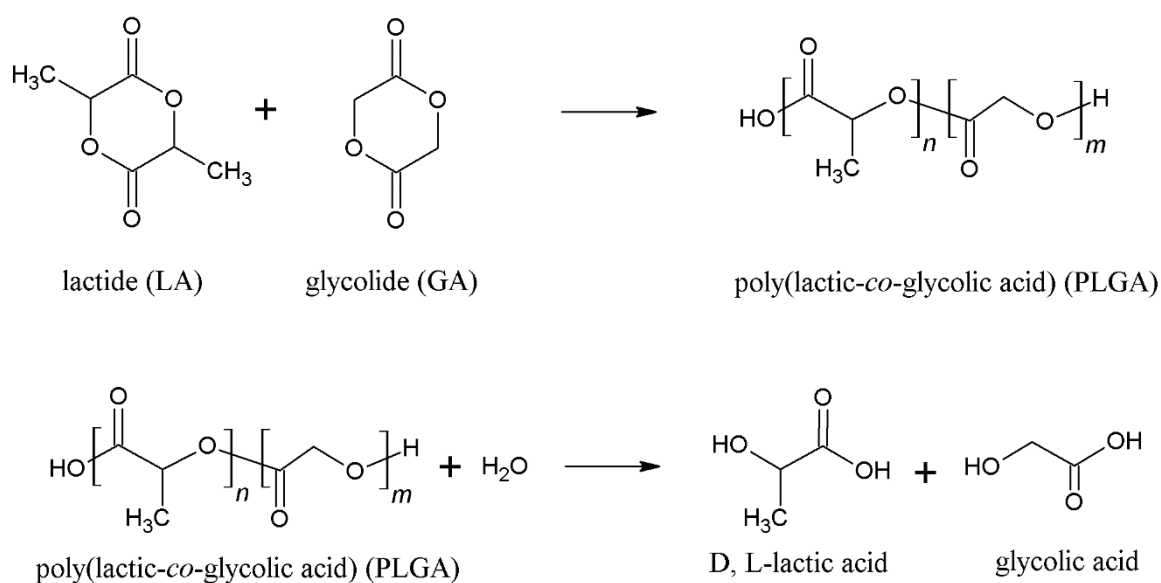
Figure 2. Route of poly(lactic-co-glycolic acid) (PLGA) synthesis from lactide (LA) and glycolide (GA) (top) and its degradation products (bottom).

The need for a high amount of organic solvent in these systems plays an important role in the formulation development [49]. Usually, solvents such as NMP and dimethyl sulfoxide (DMSO) are the choice to compose *in situ* forming implants [50]. It has been shown that the properties of the solvent also influence the release system performance [51]. Other organic solvents including benzyl alcohol (BA) and benzyl benzoate (BB) have been employed as well [37]. Researchers have been studying low molar mass PEG as a solvent to the PLGA system and its effects on the formulation stability [52]. As described in the literature, they have a controversial effect concerning toxicity, despite regulatory approval. Other features also influence the effectiveness of the implant, such as the concentration and type of PLGA, type of solvent, co-solvent, and additives [49]. Furthermore, to achieve better results from *in situ* forming implants researchers must solve other aspects, such as the variability of the implant shape and structure, avoidance of burst release during implant formation and toxicity issues [11]. It is therefore of great interest to develop new materials to overcome the problems of the products currently on the market. Several studies have reported results to circumvent these bottlenecks and improve fundamental aspects of implants preparation and use, as in the case of periodontitis treatments [53]. Gurny at al., have developed a system based on alkyl substituted poly(lactides), coined "hexPla" [54,55].

It is a lipophilic polymeric system that can be injected with (or without) a minimal amount of solvent and releases a drug within a certain period of time, consisting of a promising material. Ki et al. [56], reported a system based on sorbitan monooleate (SMO) mixed with phosphatidylcholine and tocopherol acetate to deliver leuprolide. They presented interesting results concerning drug release profile and *in vivo* compatibility. Other systems based on polyols have emerged as potential platforms to deliver drugs such as poly(glycerol sebacate), which has been investigated during the last two decades due to its tunable properties [57-60]. Other components as sorbitol [61], xylitol [62], sunflower oil [63], and diacids have also shown potential as drug carriers, as well as other biomedical applications, as bone regeneration [64-67]. However, the range of parameters that influence the performance of implants as drug delivery systems is wide and complicates the development of an ideal system. Among these factors are the shape and size of the implant [11], the site of implantation [68] and the physical and chemical nature of the implant [37].

1.2 *In vivo* investigation of drug delivery systems

Non-invasive *in vivo* monitoring of DDS degradation and drug release processes is a difficult task. Despite the advances in the imaging systems applied to humans, such as Computer Tomography and Positron Emission Tomography (CT and PET) [69,70], these techniques require a high investment and were unsuited for experimentation in small animals [71]. Technical developments enabled researchers to obtain 3-D images of animals. However, the costs remain a challenge compared to other methods [72].

Ultrasound imaging has been employed to monitor the behavior of implants *in vivo* with valuable results [73-75]. The technique has been employed to disclose important characteristics of materials implanted subcutaneously. Other techniques, such as magnetic resonance imaging (MRI) and electron paramagnetic resonance (EPR) spectroscopy, are suited for *in vivo* measurements and fit the need for experiments in small animals [76-78]. MRI has been applied to investigate pharmaceutical formulations *in vitro*/*in vivo* [79] and tumor-targeted delivery systems [80]. Nonetheless, high costs limit the application range of MRI [77]. Benchtop-NMR (BT-NMR) systems are an attractive alternative since they are commercially available and have been used in the food and chemical industry for years at a lower cost than high field superconducting NMR machines [77,81].

BT-NMR and BT-MRI have been applied to characterize tissue engineering scaffold [82], monitor contrast agent [83], *in vitro* and *in vivo* drug delivery systems [84], in tumor studies [85], ISFI [86], and inflammatory processes [87]. Besides that, it has been used to monitor chemical reactions *in situ* [88] and in academic teaching [89] that otherwise would require a larger number of animals (when performing *in vivo* experiments) and larger facilities.

1.3 *In vivo* fluorescence imaging

Since its discovery [90] fluorescence has been present in our daily lives and its evolution, combined with technological advances, has resulted in many important applications. Multispectral optical imaging is a valuable tool for non-invasive preclinical imaging [71, 91,92]. Fluorescence *in vivo* imaging plays a key role in preclinical studies due to the widespread facilities and availability of the technique, probes, and equipment [93,94]. It enables not only the monitoring of *in vivo* fate of fluorescent probes and its distribution into the body/organs, but it has also been used to characterize processes such as the pH environment in the body after implantation [48], and dynamic cellular processes [95]. NIR dyes have been used to monitor *in vivo* process of biomaterials, with minimized absorption and autofluorescence from organisms and tissues in the NIR spectral range [96]. Among them, DiR is an interesting and valuable cyanine dye that has been used in many recent studies in drug delivery [94,97,98].

1.4 Functional Polyesters

1.4.1 Enzymatic polycondensation

Esterifications in organic chemistry are usually performed using catalysts such as sulfuric and hydrochloride acids [99] or metal-based catalysts at high temperatures (180-280 ℃) [100]. A wide range of products we use is based on such process, from packages to food, healthcare products, and medicines. The combination of a need for sustainable processes and the fact that the synthesis becomes a challenging task when it comes to stereo- and regioselectivity have driven the attention of researchers. Consequently, the need for an eco-friendly synthesis has become evident [101,102]. Because of the specific functions performed on living organisms, enzymes are highly specialized biocatalysts [103]. Lipases (EC 3.1.1.3) are present in many types of living organisms. In the body, it hydrolyzes dietary

triglycerides, fats, and oil [104]. In the presence of organic media, however, it catalyzes esterification reactions, through a mechanism called interfacial activation [105]. The role of lipases is not restricted to physiological functions though. It has been used to produce detergents, food ingredients and biopolymers [106].

Candida antartica lipase B is an enzyme isolated from the yeast *Candida antartica* and traded under the commercial names CAL-B and Novozym 435 immobilized on a macroporous resin (Lewatit VP OC 1600) poly(methyl methacrylate-*co*-divinylbenzene). It is selective to primary alcohols and has been explored in a variety of reactions and for the esterification of alcohols with diacids [107]. The enzyme possesses a catalytic triad comprised of Ser105, His187 and Asp224 and its active site consists of an acyl binding pocket [104]. Enzymatic esterification using CAL-B is a green process that can be conducted under mild conditions at low temperature, reducing energy costs. All these factors promote enzymatic polycondensation as an attractive and intelligent way to carry out polymer synthesis, and they have been comprehensively studied [101,108,109].

1.4.2 Poly(glycerol adipate) (PGA)

Uppenberg et al. [104], elucidated the selectivity of CAL-B towards primary alcohol. Next, Kline et al. [110] described the synthesis of poly(glycerol adipate), a linear polyester with a pendant hydroxyl group that can be further grafted (Figure 3). It is synthesized from glycerol and adipic acids or its derivatives. Glycerol is a trialcohol derived from animals and plants triacylglycerides breakdown. It is a cheap and abundant by-product of biofuel and has over 2000 uses [111]. Divinyl adipate is a derivative of dicarboxylic acid that has been under research for biomedical applications [112-114]. It is an aliphatic compound used to obtain polyesters and polyamides by polycondensation [115].
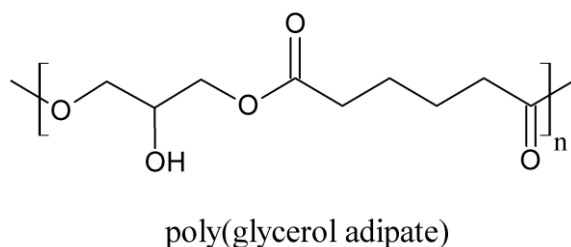

poly(glycerol adipate)

Figure 3. The structure of poly(glycerol adipate) with a pendant hydroxyl group.

Kallinteri at al. [116] were the first to report the synthesis of PGA nanoparticles applied in drug delivery as well as toxicity data about the polymer. Since then several studies have explored the possibilities that PGA offers.

PGA has been investigated in many publications [107,112,117-120). The use of PGA as a platform for drug delivery as opposite to PLGA-based polymers has the advantage of the hydroxyl pendant group (absent in PLGA) that is an opportunity for further grafting, thereby tuning the properties according to the desired situations. To be used in the biomedical field, a polymer must be well characterized concerning its physico-chemical characteristics as well as to properties relevant as a biomaterial. PGA has been tested concerning being scaled-up [121], its abilities to form different structures such as nanoparticles [116,122], its biocompatibility [116], drug incorporation and release [117,116], as well as its behavior in the physiological environment [123].

1.4.3 Fatty acid grafted PGA

In line with an environment-friendly approach, the components of the PGA are products already extensively used [124-126). The characteristics of nanoparticles made of PGA esterified with stearic acid were reported earlier [122]. In this work, Weiss et al. showed that the particles had a different shape as the degree of grafting changed, what may influence important factors in pharmaceutical use, as drug loading capacity. Further studies including lauric and behenic acids were performed and characterized the amphiphilic nature of PGA-based nanoparticles [112]. Studies conducted by the groups of Kressler and Mäder (Halle) and Garnett (Nottingham) also contributed to elucidate the characteristics of PGA grafted with fatty acids of different length and degree of substitution [118,127]. Wersig et al. [128] described a drug conjugate system in which PGA was esterified with indomethacin and presented interesting behavior regarding drug release. The change in hydrophilicity, pH, and the presence of lipase in the medium affected the drug release profile, while no burst release occurred in a one-month period.

Also, Weiss [129] performed preliminary studies using PGA as a depot system grafted with lauric acid. The results revealed interesting properties when applied *in vivo*. Carrying a lipophilic dye, a variation of PGA grafted with laureate (PGA-L95) (95% grafted with

respect to PGA molar mass) exhibited a faster release when compared to PGA-L25. Following *ex vivo* examinations, residual parts of the polymer remained in the subcutaneous tissue after six months [129]. Based on such explorations, a patent was issued covering the mentioned polymer and its fatty acids derivatives [130].

Recently, the synthesis of PGA grafted with different amounts of oleic acid was published and presented the results regarding the phase behavior of the polymer mixed with glycerol monooleate (GMO) [131]. The study found that adding PGA grafted with 22 mol% oleic acid (PGA-*g*-O22) to GMO/water system induced swelling and enlargement of water channels of double diamond cubic phase. PGA-*g*-O22 was proposed as a stabilizer for dispersed structured nanoparticles. These findings advanced our knowledge about fatty acid acylation of PGA towards precise properties tailoring.

Oleic acid is an attractive fatty acid source for grafting polymers as it is the most common fatty acid in plants and animals [132] and part of our diet [133]. It is a renewable source that is already well implemented into drug delivery systems [108,134]. Moreover, lipid carriers offer advantages to the formulator [135,136] and when used in implants have the advantages of resulting in a less acidic environment, in contrast to the case of PLGA-based polymers [137].

Objectives

Based on the current panorama of drug delivery systems, particularly *in situ* forming implants, a deeper understanding of the properties and characteristics that govern the performance of these materials is required. Novel materials must overcome the challenges faced by the currently commercialized products and be clinically superior, contributing to improve its usage from a patient's perspective.

The general aim of the present study was to synthesize poly(glycerol adipate) grafted with oleic acid to be used as an *in situ* forming implant for parenteral controlled drug release. As stated above, PGA-*g*-Ox has been described in the literature. However, it has not been explored as an ISFI for drug delivery. The initial steps involved the synthesis of PGA-*g*-Ox, here coined as Direct Injectable Polymer (DIPO), and its characterization, to understand practical aspects of PGA-*g*-Ox use. After synthesis via enzymatic polycondensation using *Candida antartica* lipase B as a catalyst, PGA-*g*-Ox was characterized regarding its fundamental aspects using classical methods such as size exclusion chromatography (SEC), nuclear magnetic resonance (NMR) and infrared spectroscopy (IR). Further characterization was performed concerning the use of the material in the pharmaceutical field. Its syringeability, without organic solvents, and amphiphilicity were determined because these aspects influence the clinical performance of biomaterials. Subsequently, the incorporation of an active substance and its release from the *in situ* implants were performed. A suspension of leuprolide acetate, used in the treatment of prostate cancer, endometriosis, and precocious puberty [138], was prepared with PGA-*g*-Ox as ISFI. The aim was to prevent the burst release of the drug. Leuprolide was ion-paired with sodium oleate and presented a controlled *in vitro* release profile. Next, studies were carried out to assess the *in vitro* biocompatibility profile of PGA-*g*-Ox.

Further steps included the impact of the implants *in vivo* along with non-invasive monitoring. A preclinical experiment was carried out to gain insight into PGA-*g*-Ox *in vivo* performance. To this end, SKH1-Elite mice using formulations of the polymer containing a fluorescent probe were injected subcutaneously. In the final step, *ex vivo* investigations were performed to understand the effect the material has on the target tissue, completing a cycle of studies to screen the designed system and its function as a biomaterial for *in situ* forming implant.

2 Materials and Methods

2.1 Materials

Glycerol was purchased from Grüssing GmbH (Filsum, Germany), divinyl adipate was acquired from TCI GmbH (Eschborn, Germany). Lipase from *Candida antarctica B,* tetrahydrofuran (anhydrous, 99.9%), oleoyl chloride (90%), trimethylamine (99.5%) and sodium oleate were purchased from Sigma-Aldrich Chemicals (Steinheim, Germany). DiR (1,1'-Dioctadecyl-3,3,3',3'-tetramethylindotricarbocyanine iodide) was purchased from Thermo Fisher Scientific (USA). Modified Eagle Medium (MEM) was obtained from Roche Applied Science GmbH (Manheim, Germany). DAKO® hematoxylin and eosin (H&E) were obtained from Agilent (Ratingen, Germany). Round glass slides were acquired from H. Saur, (Reutlingen, Germany). Leuprolide acetate was purchased from Chemos GmbH (Regenstauf, Germany), HPLC grade acetonitrile (99.9%) was purchased from VWR International GmbH (Dresden, Germany), fetal calf serum (FCS) was obtained from Biochrom (Berlin, Germany). Roti®-Histol (Xylol), sodium sulfate and other organic solvents (e.g., methanol, toluene, dichloromethane) were obtained from Carl Roth GmbH (Karlsruhe, Germany).

2.2 Methods and procedures applied

2.2.1 Preparation of linear poly(glycerol adipate)

In a typical synthesis procedure, glycerol (3 g, 32.6 mmol) and divinyl adipate (DVA) (6.46 g, 32.6 mmol) were placed into a 100 mL three-necked round bottom flask. The flask was sealed with a rubber septum and equipped with a Teflon half-moon mechanical stirrer produced in-house and a condenser containing $CaCl_2$ drying tube at its outlet under a nitrogen atmosphere, following a protocol published by Kallinteri et al. [116]. Anhydrous THF (15 mL) was added, and the reaction was stirred for 30 min at 250 rpm at 50 ºC. Afterward, CAL-B beads (2 wt% of monomers), dried under vacuum and over P_2O_5 for 48 h were added, and the oil bath temperature was kept at 50 ºC. The reaction was left under stirring for 11 h in a fume hood.

The catalyst beads were removed by filtration, after diluting the reaction mixture with a small amount of THF. The filtrate was concentrated by using a rotary evaporator and heated

for 1 h at 90 ℃ to deactivate the enzyme residue. The polymer was then dissolved in 10 mL THF and precipitated thrice in 200 mL diethyl ether to remove oligomers. The solvent was evaporated under reduced pressure. A slightly yellowish viscous liquid was obtained. The purity of the product was confirmed by ^{1}H NMR spectroscopy and further analyzed with ^{13}C NMR spectroscopy using deuterated chloroform as a solvent. The product was named as poly(glycerol adipate) (PGA).

2.2.2 Poly(glycerol adipate) grafting

The grafting of poly(glycerol adipate) with oleate, was carried out by reacting PGA with oleoyl chloride using triethylamine as an HCl acceptor in THF. Dried PGA (3 g) was placed in a 100 mL three neck round flask with a magnet stirrer, equipped with a condenser and a calcium chloride drying tube. Anhydrous THF was added (30 mL) and stirred for 10 min at 250 rpm at room temperature. Triethylamine (13.17 g, 130.3 mmol) was poured into the reaction under a nitrogen atmosphere. The reaction flask was cooled down with ice for 20 min. Oleoyl chloride was dissolved in THF at RT and added dropwise to the reaction via a syringe in the desired molar mass concentration (with an excess of about 6 mol% per hydroxyl group), according to the targeted degree of grafting. The reaction was left to warm up slowly, and the temperature was raised to 80 ℃ and kept for 3 h under continuous stirring.

Following that, the reaction was stopped, and the solvent was evaporated at 60 ℃ under reduced pressure. The resulting polymer was dissolved in 100 mL toluene and filtered. Extraction of the product was performed 5 times (with 100 mL of brine each time) in a 250 mL separation funnel to remove trimethylamine and its salt traces. The organic phase was dried over sodium sulfate until a transparent yellow color appeared. The solvent was removed in a rotary evaporator at 60 ℃, and the polymer was precipitated thrice in methanol (200 mL each time) at RT. The solvent was removed under reduced pressure. Samples were analyzed using SEC, ^{1}H /^{13}C NMR, COSY, HSQC and ATR IR spectroscopy and their thermal properties were determined by DSC and TGA. The product, named as PGA-*g*-Ox, where x represents the degree of grafting. Figure 4 shows the synthesis pathway of PGA-*g*-Ox.

2.2.3 Size exclusion chromatography (SEC)

Size exclusion chromatography (microGPC) measurements molar mass of PGA and its grafted versions were performed in a Viscotek GPCmax VE 2001. THF was used as eluent with a flow rate of 0.3 mL/min through CLM3008 and CLM3087SMT3000 columns (Viscotek, mixed bed) at 30 ℃, equipped with a refractive index detector (VE 3580 RI detector, Viscotek, Malvern) (Worcestershire, UK). The injection volume was 20 μL. All samples were analyzed at a concentration of 3 mg/mL. Polystyrene standards were used for calibration.
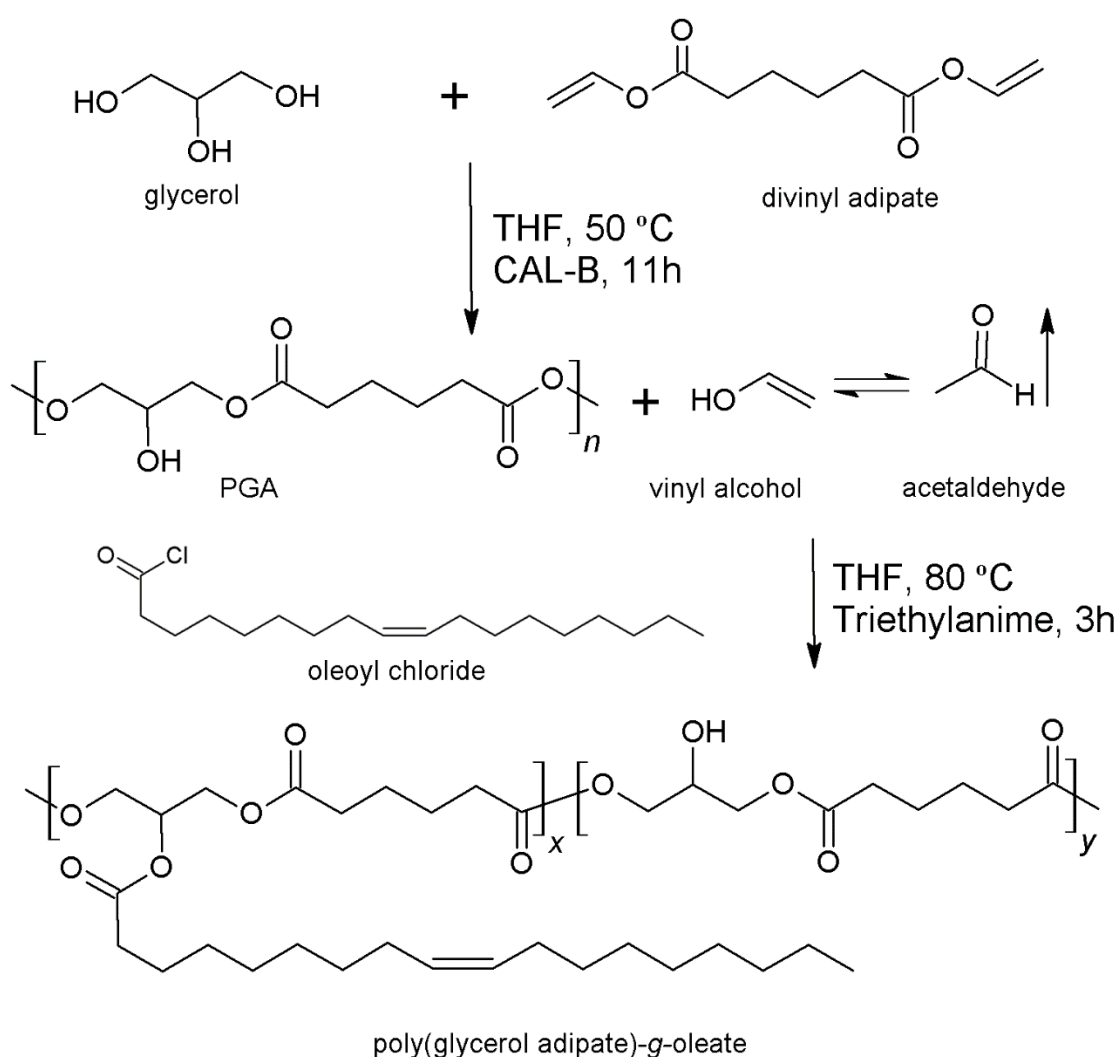

Figure 4. Scheme of poly(glycerol adipate)-graft-oleate synthesis using CAL-B in the esterification of glycerol with divinyl adipate at 50 °C followed by grafting, using triethylamine as HCl acceptor at 80 °C.

2.2.4 ^{1}H NMR and ^{13}C NMR spectroscopy

^{1}H NMR and ^{13}C NMR spectra were recorded using Agilent Technologies 400 MHz VNMRS spectrometer (Santa Clara, CA, USA) at 400 MHz for ^{1}H and ^{13}C NMR spectroscopy at 27 °C. Samples were prepared at a concentration of 12 mg/mL for ^{1}H NMR and 30 mg/mL for ^{13}C NMR spectroscopy, using deuterated chloroform. Chemical shifts were referred to tetramethylsilane (TMS) at 0 ppm. NMR spectra are interpreted using the software MestRec v.4.9.9.6. (Mestrelab Research, Santiago de Compostela, Spain). Chemical shifts are displayed in ppm.

PGA: ^{1}H NMR (400 MHz, CDCl$_3$) δ 7.19 (m, 1H), 5.04 (m, 1H), 4.82 (dd, J = 14.0, 1.6 Hz, 1H), 4.51 (dd, J = 6.3, 1.6 Hz, 1H), 4.20 – 3.98 (dd, J = 14.0, 1.6 Hz, 5H), 3.73 – 3.54 (m, 2H), 2.41 – 2.20 (m, 4H), 1.86 – 1.55 (m, 4H).

PGA-g-Ox: ^{1}H NMR (400 MHz, CDCl$_3$) δ 7.28 (m, 1H), 5.36 – 5.24 (m, 2H), 5.24 – 5.11 (m, 1H), 4.22 (m, J = 11.9, 4.0 Hz, 4H), 4.07 (s, J = 11.9, 6.0 Hz, 1H), 2.36 – 2.17 (m, 6H), 1.96 (m, J = 11.0 Hz, 4H), 1.66 – 1.43 (m, 6H), 1.18 (d, J = 27.3, 10.5 Hz, 20H), 0.81 (t, J = 6.8 Hz, 3H).

2.2.5 Attenuated total reflection infrared spectroscopy (ATR-IR)

Infrared (IR) spectra were recorded on a Bruker IFS 28 (Bruker Optik GmbH, Ettlingen, Germany), ZnSe crystal (20 mm) equipped with attenuated total reflectance (ATR) top plate MkII. Opus 4.2 software was used to analyze the data. The semi-solid samples were measured by spreading them on the crystal with the help of the tip of the spatula. Spectra were recorded in the range of 4000 to 500 cm^{-1}.

2.2.6 Differential scanning calorimetry (DSC)

Differential scanning calorimetry measurements were carried out using Mettler Toledo DSC823e module. In a typical procedure of sample preparation, 8 to 12 mg of sample material was enclosed in an aluminum pan and placed in the DSC module at room temperature. All measurements were performed under the constant flow of nitrogen (40 mL/min) for the sake of maintaining an inert environment. Samples were firstly heated up

to 100 °C with the heating rate of 5 °C/min to remove the moisture and residual solvent traces along with any previous thermal history of the material. The sample was kept at the same temperature for another 10 min while the temperature becomes homogenous throughout the material and then cooled to -80 °C with the rate of 5 °C/min. Again, the sample was kept at -80 °C for 10 min and is then heated up to 80 °C with the rate of 5 °C/min. Later, the data were analyzed using Origin® 8.5.1 (OriginLab, Northampton, MA, USA).

2.2.7 Thermogravimetric analysis (TGA)

TGA measurements were performed using a NETZSCH TG 209® equipment (NETSCH-Gerätebau GmbH, Selb, Germany) in the temperature range 20-600 ºC. Samples (40 mg) were placed in an alumina crucible and heated from ambient temperature to 600 ºC with a heating rate of 10 ºC/min in a 10 mL/min flow of N_2 and continuous record of sample temperature, its first derivative, and heat flow was taken. An empty alumina crucible was used as a reference.

2.2.8 Contact angle measurements

Contact angle measurements were made using a thin film of each polymer on a glass slide. For the measurements, round glass slides of (32 mm diameter, 0.17 mm thick) (H. Saur, Reutlingen, Germany) were extensively washed with Milli-Q® (Milli-Pore) ion-exchanged purified water, ethanol, acetone, and dried under a nitrogen stream. Subsequently, the slides were covered with 400 µL of a polymer solution (3 mg/mL) prepared in toluene. The glass slides were spin coated at 2000 rpm for 60 s (Meadway Research Incop., Garland, USA, model PWM 32) at RT. Afterward, the coated slides dried in a desiccator for at least 48 h. The samples, dried on round glass, were analyzed using a Goniometer (DataPhysics, Filderstadt, Germany) (Figure 5) and at least 5 measurements were performed for each sample. For the measurements, 10 µL of deionized water was used at a rate of 2 µL/s. The results were recorded using the software OCA 20 (DataPhysics, Filderstadt, Germany).
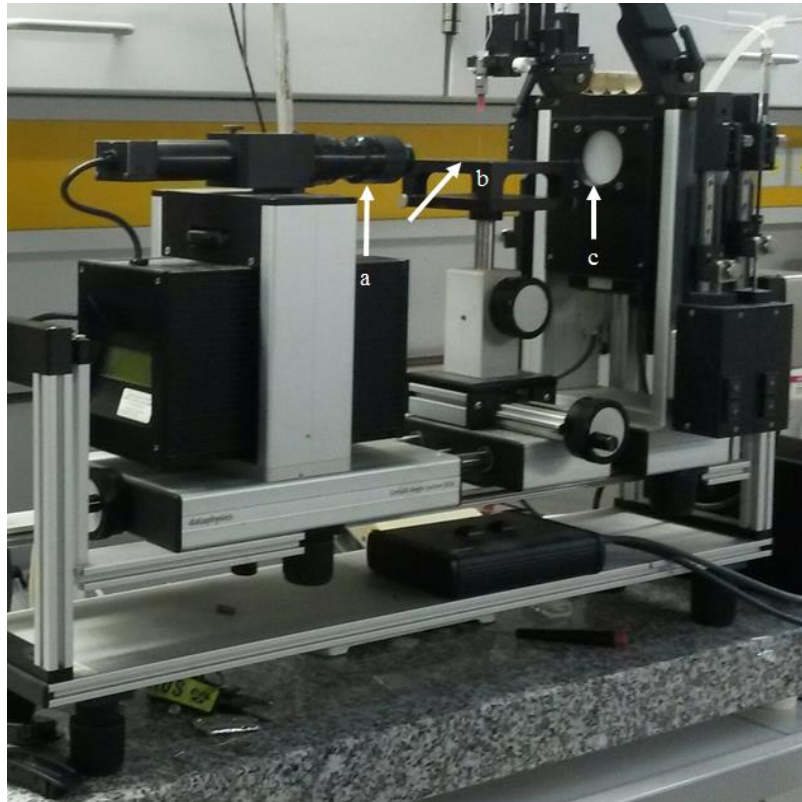
Figure 5. Set-up from Dataphysics used for contact angle measurements. a) camera; b) sample platform and needle; c) light source.

2.2.9 Magnetic resonance imaging (MRI)

For the MRI measurements, a 20 MHz NMR benchtop system (prototype based on Maran DRX2, Oxford Instruments Molecular Biotools, UK) was used. The system is capable of T_1 and T_2 relaxation time measurements and keeps a constant temperature of 37 ℃ inside the coil. The samples were placed in test tubes. A standard spin-echo sequence with a spin-echo time (TE) of 9.8 ms was applied and a repetition time (TR) of 200 ms. Third two averages were used resulting in an acquisition time of about 410 s for each image, and the field of view was 64 mm x 64 mm.

2.2.10 Syringeability

Syringeability experiments were carried out using a Texture Analyzer (Brookfield CT3™-4500) (Brookfield Engineering Laboratories, Middleboro, USA) (Figure 6). The set of parameters used to perform the experiments were as follows: metal cylindrical probe TA44 of 4 mm diameter, speed of 0.2 mm/s in compression mode, data recording 20 points/s and trigger point 0.004 N. Recording and data processing were carried out with the software TexturePro CT V1.4. The syringe used was a 1 mL (Luer-Lok™) (Becton Dickinson, New Jersey, USA). Needles (Terumo Europe, Leuven, Belgium or B. Braun, Melsungen, Germany) of 21, 23 and 25 G were used, with internal diameters of 0.8, 0.6 and 0.5 mm with a length of 40, 25 and 16 mm, respectively. Each measurement was repeated three times at RT using a fresh sample in each case. The syringe was placed on a metallic support and immobilized, ensuring no extra movement or deformation that could affect the measurement during the experiment.

Figure 6. Texture analyzer set-up for injection force measurements. Figure 6A depicts the set-up mounted and Figure 6B shows the tools available for such system, while an arrow indicates the tool used.

2.2.11 Electron-beam sterilization

The irradiation experiment was conducted by Dr. Wolfgang Knolle, at the Leibniz Institute for Surface Modification, Leipzig, Germany. The samples were irradiated by electron irradiation produced using a 10 MeV high energy linear accelerator (LINAC, Torjy Company, Russia). Samples were exposed to an irradiation dose of 25 kGy in 2 steps of 12.5 kGy each. They were packed at RT in sealed Eppendorf type vials and glass vials. The material was irradiated at RT and under liquid nitrogen.

Peptide formulation

2.3 Leuprolide ion-pairing

The ion-pairing of leuprolide acetate (Figure 7) with sodium oleate was performed based on previous results [139]. Leuprolide was dissolved in 5 mL deionized water and sodium oleate dissolved in 2 mL deionized water. The reaction was carried out using 1:1 molar concentration of sodium oleate to the peptide. The solution of sodium oleate was added dropwise into the leuprolide solution, forming a turbid solution immediately. It was stirred for 3 h at 200 rpm and RT.
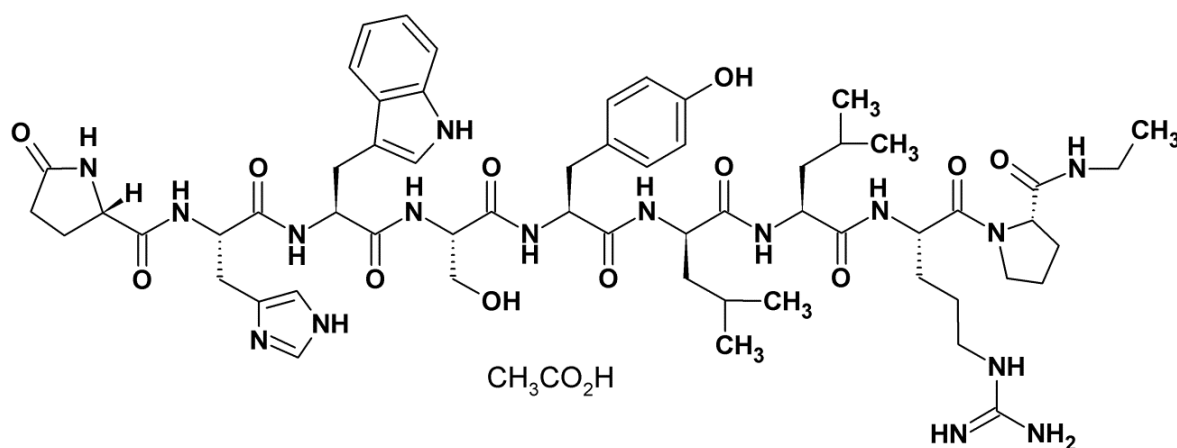

Figure 7. Chemical structure of leuprolide acetate [192]. The peptide is composed of nine amino acids and is commercialized in its acetate form.

2.4 Photon correlation spectroscopy (PCS) and zeta potential measurements

The size and zeta potential of the formed particles were measured by photon correlation spectroscopy performed in the backscattering mode (173 °), using a Zetasizer (Malvern Instruments, Malvern, UK), at 25 ℃. Each sample was measured three times with 12–16 runs each. Zeta-average diameters and polydispersity index (PDI) were determined by the cumulant analysis software of the instrument (Dispersion Technology Software 4.20, Malvern or Zetasizer Software 6.30, Malvern, UK). Afterward, the particles were lyophilized.

2.5 *In vitro* drug release

Leuprolide particles were mixed with pre-warmed polymers (under 50 ℃) on a heat plate using a spatula. The polymer containing the drug was placed into the sample holder and covered with a poly(ethylene terephthalate) net (Figure 8). The release was carried out over 28 days with triethylamine buffer adjusted with phosphoric acid to pH 7.4 and 0.02 wt% sodium azide, at 37 ℃ (calibration in Figure 9). To analyze the release, HPLC Waters E600 was used, with a Terra X 120 C18Q 3 µm column (150 x 3 mm), with an isocratic flow of 0.5 mL/min, of acetonitrile/water 78/22 vol% with 0.05 vol% trifluoroacetic acid at 40 ℃ and an injection volume of 10 µL. 1 mL was taken from the medium at predetermined time intervals and replaced with fresh medium.
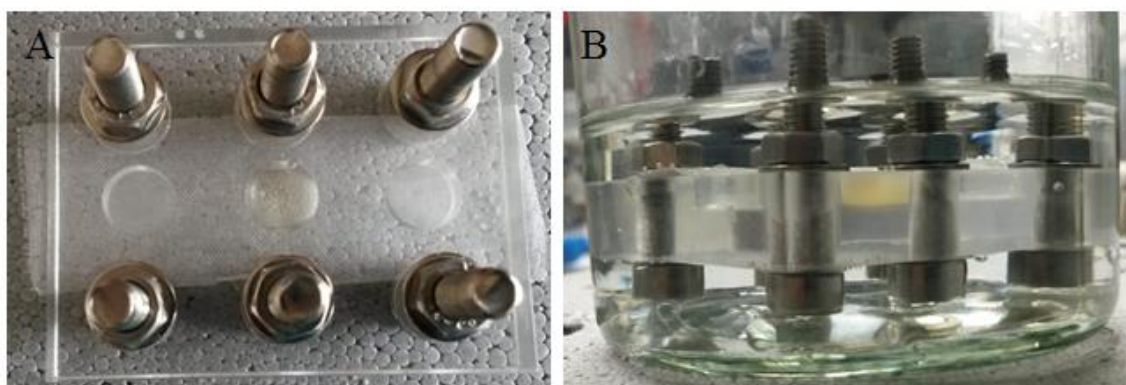

Figure 8. A) Drug release device made in-house used to perform in vitro release studies. B) Assembled apparatus as used in the studies.
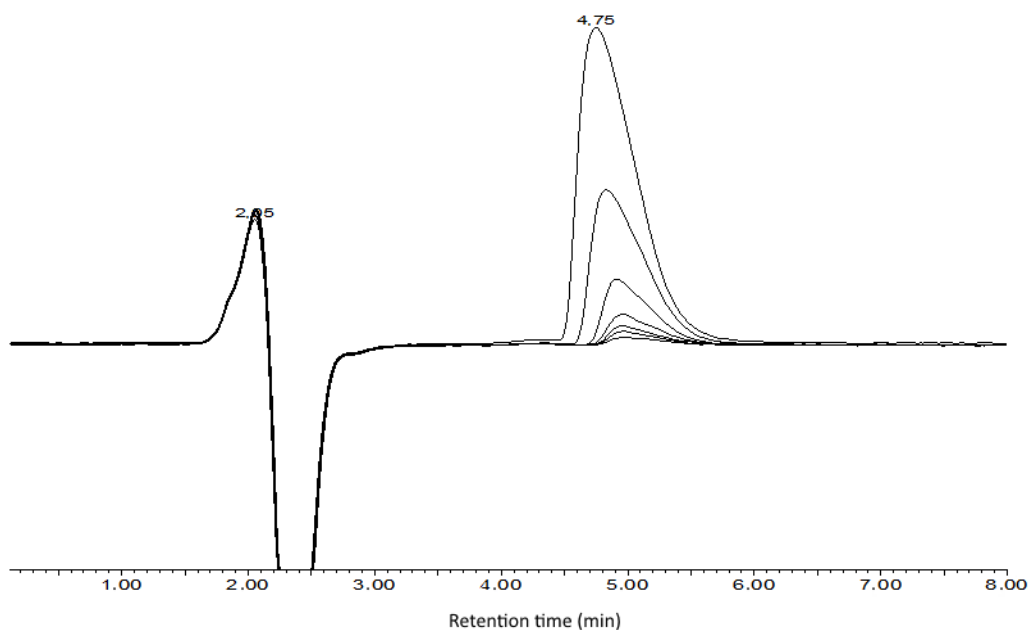
Figure 9. HPLC calibration chromatogram of leuprolide acetate in triethylamine buffer, pH 7.4 at 40 °C.

2.6 *In vitro* cytotoxicity

2.6.1 Extract production

Polymer extracts were prepared to evaluate its potential cytotoxicity, according to the EN ISO 10993-12 guidelines for biocompatibility test. The experiment was conducted in the laboratory of Prof. Dr. Hiebl (Faculty of Medicine – Martin Luther Halle-Wittenberg University). The material was prepared by making a film and drying it for 24 h. Twelve milliliters of MEM supplemented with 10 vol% fetal calf serum (FCS), and the bottle was incubated at 37 °C for 24 h under a continuous horizontal shaking (20 rpm, Julabo SW23, Germany).

2.6.2 Cell culture

The assays were performed with 3T3 cells. The cells were used for testing from a cell confluence of 80%. The cultivation took place at 37 °C, 5 vol% CO_2 in a water-vapor-saturated atmosphere supplemented MEM (10 vol% FCS, Biochrom AG, Berlin, Germany). 3T3 cell culture medium was used as negative control and $CuCl_2$ (1 mM) was used as a

positive control by incubation of the test specimens in serum-supplemented cell culture medium (MEM + 10 vol% FCS) at 37 °C.

2.6.3 MTS assay

The MTS test (CellTiter 96® Aqueous Non-Radioactive Cell Proliferation Assay, Promega) measures the activity of the mitochondrial and cytosolic dehydrogenases and allows corresponding conclusions to be made regarding the cell activity. The test was carried out according to the manufacturer's instructions [140].

2.6.4 LDH assay

The cell membrane integrity was assessed by the extracellular activity of lactate dehydrogenase determination (Cytotoxicity Detection Kit (LDH)), Roche Applied Science, Sigma-Aldrich Chemicals (Steinheim, Germany). This enzyme is predominantly intracellular. An increased extracellular appearance is an indication of damage to the cell membrane. The test was carried out according to the manufacturer's instructions [141].

2.6.5 Statistics

Data on the LDH and MTS test are given as mean values ± standard deviation (based on eight measurements) and were analyzed with Student's t-test or the Chi-Square test. Deviations with a $p < 0.05$ were considered significant.

2.7 SKH1-Elite mice

All *in vivo* experiments were carried out in compliance with the regional guidelines for animal and approved by the animal care and use committee of Saxony-Anhalt. SKH1 – Elite hairless, immunocompetent, adult male mice (Charles River, Sulzfeld, Germany) of 35-42 g of weight, were used for the implantation. All mice were housed in cages under controlled conditions (12 h light/dark schedule/cycle, 24 °C, feed and water *ad libitum*) and relative humidity of 50%. The weight and health aspects, such as pain, were monitored constantly. All animals were observed visually for the signal of inflammatory symptoms. The inflammatory response to the implants was scored as 0 (normal), 1 (mild), 2 (moderate),

3 (severe). The presence of redness, exudates, scratching or touch response was recorded.

2.8 Subcutaneous administration of implants and *in vivo* imaging

DiR, a near-infrared fluorescent lipophilic dye, was used as a reporter (Figure 10). The dye was dissolved in 50 µL of dichloromethane. Afterward, the solution was mixed with the polymers and peanut oil, and the mixture was let to dry overnight in a desiccator. SKH1 – Elite adult mice were used for the implantation. For each mouse, 200 µL of the polymer were injected subcutaneously (s.c.). Fifteen mice were randomized into 3 groups with 5 subjects each.
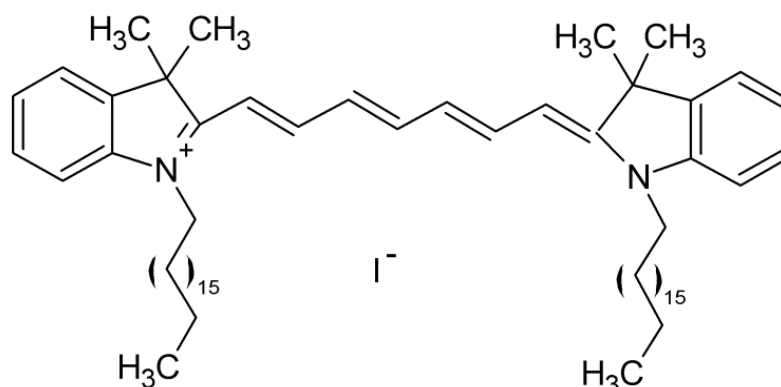

Figure 10. Chemical structure of the lipophilic dye DiR (1,1'-Dioctadecyl - 3,3,3',3' tetramethylindotricarbocyanine iodide).

Before injection, the mice were sedated with isoflurane in an induction chamber. Group 1 received the formulation with PGA-*g*-O100 and dye while group 2 received formulation containing PGA-*g*-O75 and the group 3 received peanut oil and dye. Before injection, the site of implantation was disinfected with ethanol 70%. Each mouse received 200 µL of polymer or peanut oil containing DiR. The formulations were injected subcutaneously in the right flank of the mice using a 25 G needle and 1 mL syringe.

Fluorescence experiments were performed at predetermined time intervals using the IVIS® Spectrum *in vivo* imaging system (PerkinElmer, Hopkinton, MA, USA) (Figure 11). The mice were placed in a prone position in a dark box, and light emission was recorded with a

CCD camera cooled at -90 ºC. The fluorescence signal was detected using epi-fluorescence mode with excitation at 750 nm and emission at 780 nm.

During the imaging procedure, a mixture of isoflurane/oxygen was used as anesthesia gas with an initial dose of 2.5 vol% isoflurane (Forene®, Abbot, Germany) (3.0 L/min oxygen) and a steady-state dose of 1.8 vol% isoflurane (1.5 L/min oxygen). For the imaging experiments, the mice were placed at a warming plate (35 ºC) to prevent a decrease of body temperature and imaged with an IVIS® Spectrum *in vivo* imaging system (Caliper Life Science, MA, USA). The exposure time was automatically set to optimum values to ensure highest information content by the software (autoexpose function). The software used to quantify light emission was Living image® 4.5.2.

Figure 11. IVIS® in vivo imaging system (A), inside vision of the plate (B), animals sedated placed on the imaging platform (C) and gas system (D). The white arrow in (D) points to isoflurane container and black arrow points to the induction chamber used to sedate the animals.

2.9 *Ex vivo* study of the surrounding tissue and implanted polymers

For *ex vivo* analysis, the mice were sacrificed after four weeks using isoflurane followed by carbon dioxide and cervical dislocation. Following explantation, the tissue surrounding the implant area and the polymeric material collected from the animals were fixed in 10 vol% formalin and embedded in paraffin, sliced, dewaxed and stained with hematoxylin and eosin for phase contrast microscopy.

Microscope slides were treated by flaming them on a burner and placing in xylene for 1 h at 50 °C twice to paraffinize the material. The tissue or polymer section was hydrated by passing it through decreasing concentration of alcohol and water baths, for 5 min each (Histol, isopropanol, 96%, 80%, 70%, 50% (v/v) ethanol, distilled water). It was stained with hematoxylin for 30 s. Subsequently, the probe was washed in running tap water twice for 5 min until the sections turned blue and rinsed with distilled water. Then, it was differentiated in 1 vol% acid alcohol (1% HCl in 70% alcohol) for 5 min and washed in running tap water until the sections were again blue by dipping in an alkaline solution followed by a tap water washing. Stained in acidic 0.1 vol% eosin solution (1:10 diluted in distilled water and 1 drop acetic acid per 100 mL) for 5 min. Afterward, washed in distilled water for 2 min. Finally, the probes were dehydrated in increasing concentration of alcohols and cleared in xylene, mounted in mounting media (Roti-Histokit, Carl Roth GmbH) and observed under a phase contrast microscope.

3 Results and discussion

3.1 Polymer characterization

3.1.1 Size exclusion chromatography (SEC)

Size exclusion chromatography was used to determine the average molar mass and molar mass distribution of the polymer backbone. SEC is being used since [142] to separate the molecules based on their hydrodynamic volume or size [143]. By convention, it is also named Gel Permeation Chromatography (GPC). The following equation resumes the features related to the theoretical background of the technique:

$$\bar{M}_n = \frac{\sum M_i N_i}{\sum N_i} \tag{1}$$

Where M_n is the number-average molar mass, M_i is the molar mass of a chain and N_i is the number of chains of that molar mass. The molar mass is determined based on the separation of the molecules through a column packed with porous material (stationary phase), like silica gel. A polymer with a range of known molar masses, such as polystyrene, is used as a standard to determine the molar mass of the sample according to the elution time because SEC is a relative technique. The smaller sample molecules flow more slowly through the column as they get entrapped into the stationary phase, which increases the time they are retained in the system, whereas the bigger ones need less time to elute, due to less interaction with the porous material.

Figure 12 displays representative traces of poly(glycerol adipate) and its oleate grafted variations performed by SEC diluted in THF. PGA with almost Mn = 5,000 g/mol was achieved under mild conditions (50 °C) in the polymer synthesis with a high reaction yield of 88% (Table 1). The system removes side products continuously, shifting the reaction towards ester formation to achieve esterification. The synthesis of PGA was carried out using *Candida antarctica* lipase B as a biocatalyst. The hydroxyl pendant groups of PGA enable further grafting of the polymer with different materials. The grafting was performed with oleoyl chloride for a short period (3 h), with triethylamine as an HCl acceptor in THF

solution. The oleic acid functionalization of PGA occurred without difficulties and enabled the synthesis of polymers with different degrees of grafting.

The enzymatic polymerization of PGA and its use as nanoparticles as a drug release system was first described in 2005 [116]. The use of enzymes offers several advantages over chemical catalysts used in the preparation of polymers for *in situ* forming implants, like its regioselectivity and the decrease of crosslinking reactions [119,144]. One important parameter to be taken into account in the polymerization process is its reproducibility. Several studies have reported the synthesis of poly(glycerol adipate) and proved that controlled conditions result in defined properties [119,128,131]. Although a full range of grafting is possible to be achieved, when using a fluid modifier as oleic acid, a low degree of grafting did not decrease the viscosity of the final polymer sufficiently for a direct injection, which was our aim. Even if the lower degree of grafting was not optimal for this study, its exploration as nanoparticles as drug carrier or other purposes, as demonstrated by Bilal et al. [131], places PGA-*g*-Ox as a versatile platform to be fully investigated. After a preliminary screening, grafting higher than 50 mol% were selected to proceed in the study. To work in the range of applied force considered as clinically acceptable without using any organic solvent, I further selected the graftings with 75 and 100 mol% oleic acid with respect to hydroxyl groups. Besides that, the yield obtained in the first step was considerably high and the decrease in the second reaction, the acylation step, was expected due to the workup of the reaction, requiring several solvent transfers, which led to a material loss despite careful work.

Table 1. Representative data of number-average molar mass (M_n), polydispersity index (M_w/M_n), the yield of PGA, PGA-*g*-O75, *and* PGA-*g*-O100.

Polymer	M_n (g/mol)	PDI	Yield (%)
PGA	4,768	1.8	88
PGA-*g*-O75	9,610*	1.9	62
PGA-*g*-O100	11,140*	2.0	57

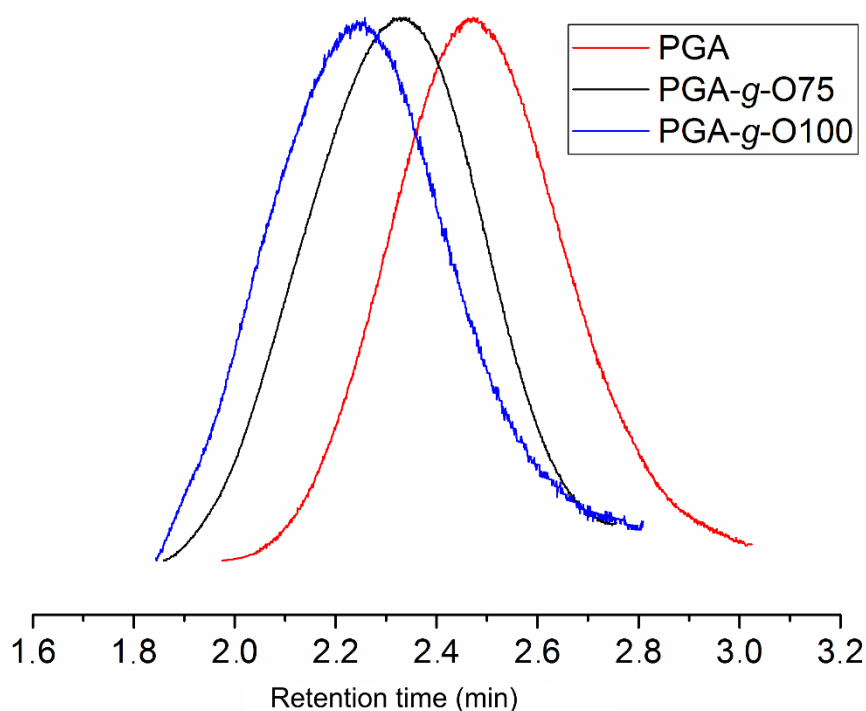** Molar masses of PGA-g-O75 and PGA-g-O100 were calculated from ^{1}H NMR spectra. PDI from GPC.*

Figure 12. Representative SEC chromatograms of PGA (red line), PGA-g-O75 (black line) and PGA-g-O100 (blue line). THF was used as eluent at 30 ºC. Polystyrene standards were used for calibration.

3.1.2 ^{1}H NMR and ^{13}C NMR spectroscopy

Nuclear magnetic resonance spectroscopy is a common and widely non-destructive spectroscopy-based technique used to characterize polymers [145-147]. Its principle relies on the atomic nuclei intramolecular magnetic field around an atom in a molecule changes the resonance frequency, thus giving access to details of the electronic structure of a molecule and its functional groups [89,148]. The calculation of the polymer degree of grafting, *DG,* was made using the following equation:

$$\%DG = \frac{a \ \mathrm{x} \ 1.33}{d - 0.67a} \mathrm{x} \ 100 \tag{2}$$

Where the peak *a* corresponds to terminal CH_3 groups of fatty acid side chains and peak *d* refers to CH_2 groups located in the α-position to carbonyl groups. Table 2 shows the assignments for the peaks found in the ^1H and ^{13}C NMR spectra of the samples.

Table 2. Chemical shifts and assignment for ^1H and ^{13}C NMR.

	Chemical shifts δ		
Carbon	**^1H NMR (ppm)**	**^{13}C NMR (ppm)**	**Assignment**
1	0.9	14	**CH_3**
2	1.35	29	**CH_2**
3	1.42-1.51	22.17 and 22.63	**CH_2**
4	1.42-1.55	29.60 and 29.67	**CH_2**
5	1.42-1.55	33.12 and 33.54	**CH_2**
6	1.6	24	**CH_2**
7	2	26	**CH_2**
8	2.3	32	**C (alpha)**
10	3.37-3.47	61.50 and 62.04	**CH_2**
11	3.5-4.5	62	**CH_2**
12	-	65	**C-O**
13	5.3	68	**C-O**
14	5-5.3	129	**C=C**
15		173	**C=O**
16	7.3	77	**$CDCl_3$**

The results revealed the correspondent assignments seeing in Figure 13 as follows: the peak at 0.8 ppm refers to CH_3, while peaks at 1.15-1.30 ppm, 1.5 and 1.9 ppm represent CH_2, and CH_2 related to the saturated bond, respectively. The peak at 2.2 ppm is related to CH_2 of the fatty acid. Peaks in the region between 3.5 and 4.5 ppm are related to glycerol as previously reported. The peak at 5.3 ppm assigns to the protons of the double bond of the fatty acid [149,150].

The advantage of characterizing (bio)polymers using NMR spectroscopy is that, besides enabling chemical groups assignments and thereby uncovering the chemical structure of molecules, it is possible to determine the molar mass of polymers using the integrals of peaks *a* and *d* to assess the purity of the sample. Such feature is important because it offers a fast

and complementary answer, especially when working with copolymers and block copolymers [146].
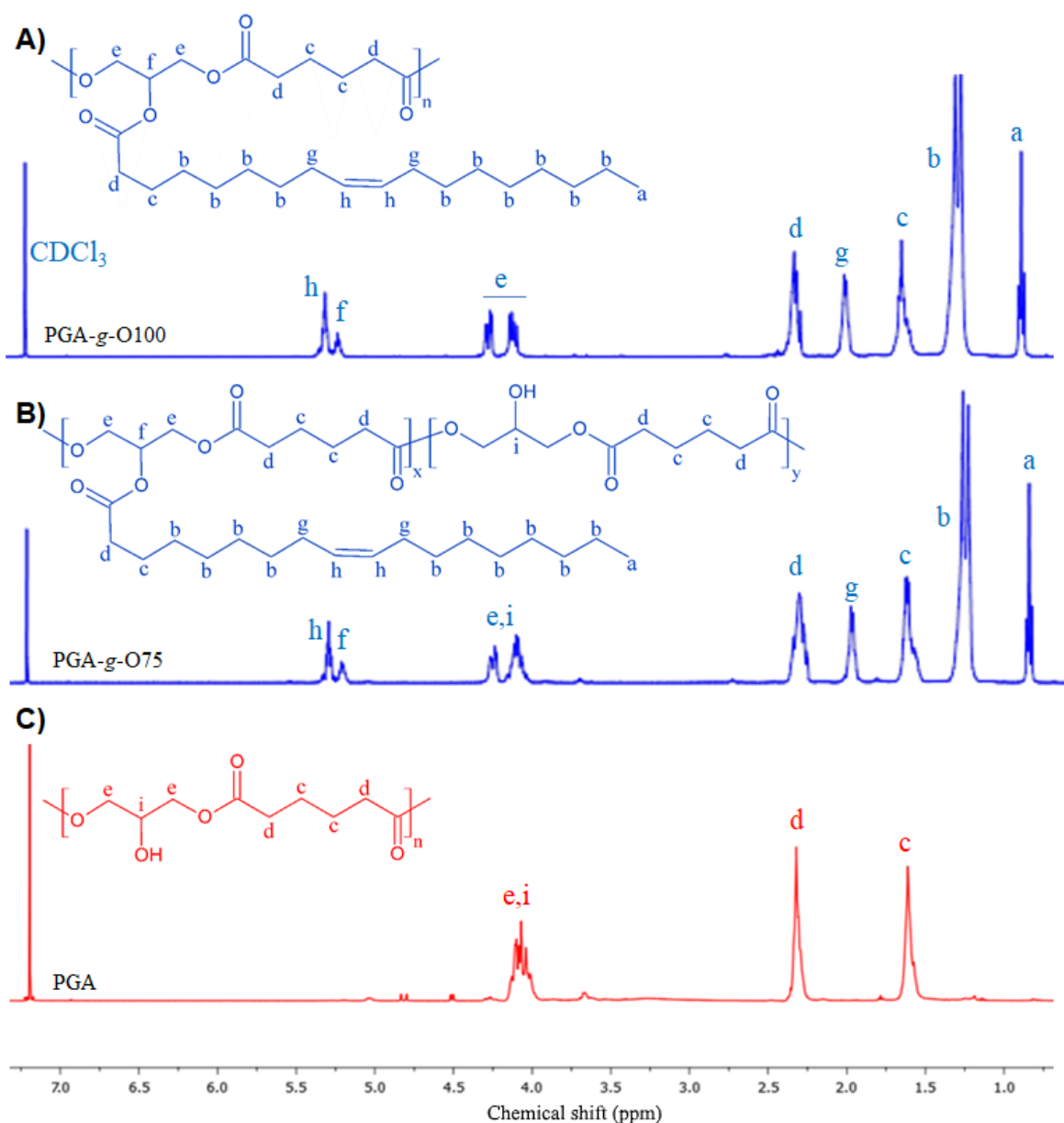

Figure 13. Representative ^1H NMR spectra of PGA-g-O100 (A) PGA-g-O75 (B) and PGA (C) measured at 27 °C in CDCl₃.

^1H NMR spectra reveal the hydrogen environment in a sample, while ^{13}C NMR deals with the position of the carbon atoms and their surroundings in the investigated material [148]. It is less sensitive than its ^1H NMR analogue, however, as it focuses on the carbons of the

molecule, it reveals other aspects that can be difficult to see in the proton NMR spectrum. In carbon NMR, the peaks correspond to different carbons spread in a wider spectrum than in ^{1}H NMR, which makes it easier to identify the atoms. It is then an important complementary technique to assure more accuracy during analysis and for the identification of functional groups without hydrogen, as e.g. C=O groups.

When analyzing the results of PGA from ^{13}C NMR spectroscopy, Figure 14, we see that the peak at 65 ppm is characteristic of carbon bonded to hydroxyl groups. ^{13}C NMR revealed the structure of PGA and its grafted versions. It decreases and disappears when the polymer is highly grafted with a fatty acid.
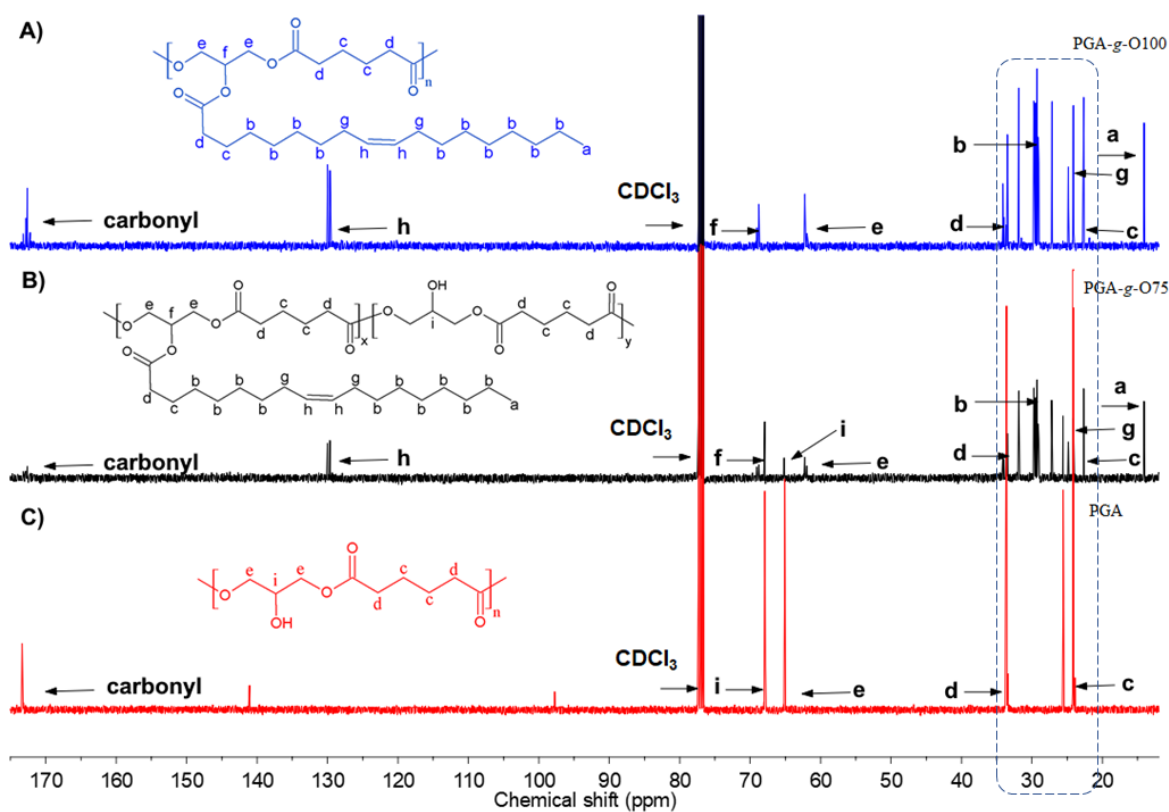
Figure 14. Representative ^{13}C NMR spectra of PGA-g-O100 (A), PGA-g-O75 (B) and PGA (C) with correspondent assignment and structures, in CDCl₃ at 27 ℃. The selected range, in dashed blue, shown in detail below.

In contrast, when the polymer is highly grafted the peak at 65 ppm decreases or disappears while a typical peak at 129-130 ppm relates to the double bond of oleic acid appears. The

presence of this peak in the spectrum of PGA-*g*-O75 (Figure 14 B) indicates the incomplete grafting of the polymer. Figure 14 A shows the ^{13}C spectrum of PGA-*g*-O100 and corroborates the full grafting already seen using infrared spectroscopy and proton NMR. In this case, no peak appears at 65 ppm. As observed in the IR spectrum, the resonance of the carbon attached to the hydroxyl group of glycerol is not present herein. A detailed part of the spectra of figure 14 is shown in figure 15 as the peaks appear close. As it can b noticed, the grafting with oleic acid is evidenced also in the selected spectra region through the peaks at 14, 25, 27, 29-30, 31.7 and 34 ppm. Besides that, the peaks (24 and 33.6 ppm) of PGA decrease in intensity and progressively decrease until disappearance at 25.5 ppm, as the polymer is fully grafted. These data were acquired from the literature and confronted with spectra from the raw material of the polymers as well.
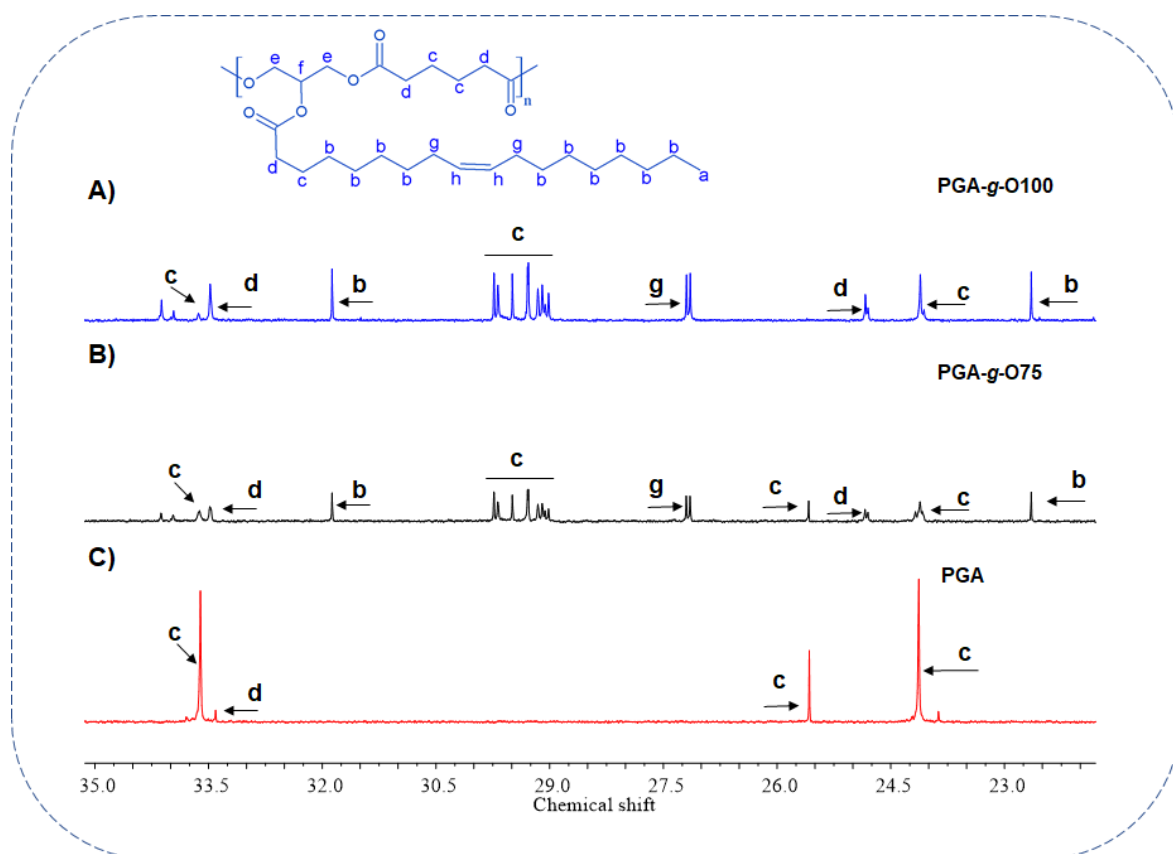

Figure 15. Expanded ^{13}C NMR of PGA-g-O100 (A), PGA-g-O75 (B) and PGA (C) (from figure 14), with the correspondent assignment and PGA-g-O100 structure for comparison purposes, in CDCl₃ at 27 ℃.

3.1.3 2-D (two-dimensional) NMR (COSY and HSQC)

Two-dimensional (2D) NMR spectroscopy techniques are used to confirm molecular chemical structures and help discriminate the resonance, as a complementary to one dimension NMR [151]. Based on that, correlation spectroscopy (COSY) and heteronuclear single-quantum correlation spectroscopy (HSQC) were employed to characterize and assure the peak assignments of grafted PGA. Figure 16 shows the ^{1}H-^{1}H 2D NMR of PGA-*g*-O100. In this case, the ^{1}H-^{1}H spectrum helps to determine the couplings of PGA-*g*-O100, especially the frequency coming from the fatty acid peaks in the grafted backbone.
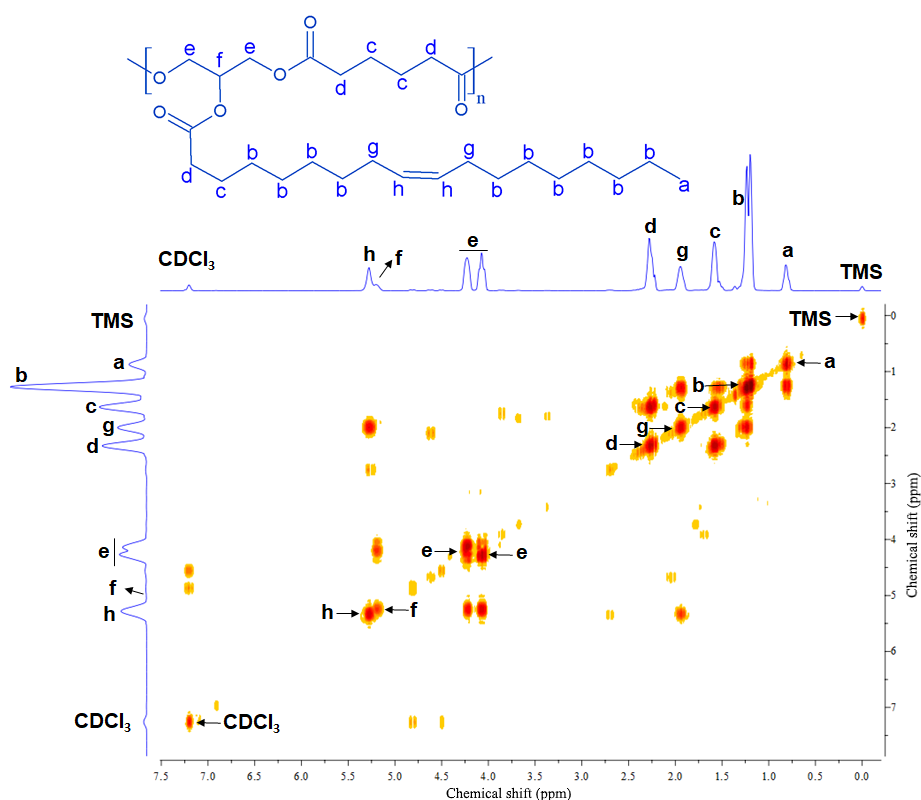
Figure 16. 400 MHz spectrum 2D NMR of PGA-g-O100 at 27 °C in CDCl₃. ^{1}H frequencies are shown in both axes.

In figure 16 the vertical axis corresponds to ^{1}H NMR whereas the ^{13}C NMR spectrum is shown on the horizontal axis. The signals are clearly separated and the assignment is therefore facilitated. The peak of methyl, *a*, correlates to the peak *b* of the fatty acid when comparing the diagonal peaks to the cross peaks. Likewise, peak *b* is coupled with peaks *a*,

c and *g*, while peak *c* is coupled with peak *d*. Peak *g* correlates to the cross peaks *b* and *h* of the CH$_2$ and C=C groups, respectively. Peak *c* is coupled with peak *d* in the fatty acid as well as in the PGA backbone. The peaks of glycerol, *e* and *f*, are coupled with which other, while peaks *g* and *h* correlate, as illustrated in the figure by the assigned chemical structure.

Further analysis of the polymer structures with 2D NMR spectroscopy permitted to assign the peaks with certainty and correlation between the ^{1}H and ^{13}C peaks (Figure 17). These data are consistent with the assignments previously obtained in separated ^{1}H and ^{13}C, as well as with the data collected from the literature. The addition of oleic acid to PGA can be observed by the appearance of peak *h* (downfield) corresponding to C=C and *a* (upfield) to methyl groups, besides peak *f*, when the backbone is grafted. Moreover, the other peaks from the fatty acid further confirm the grafting.
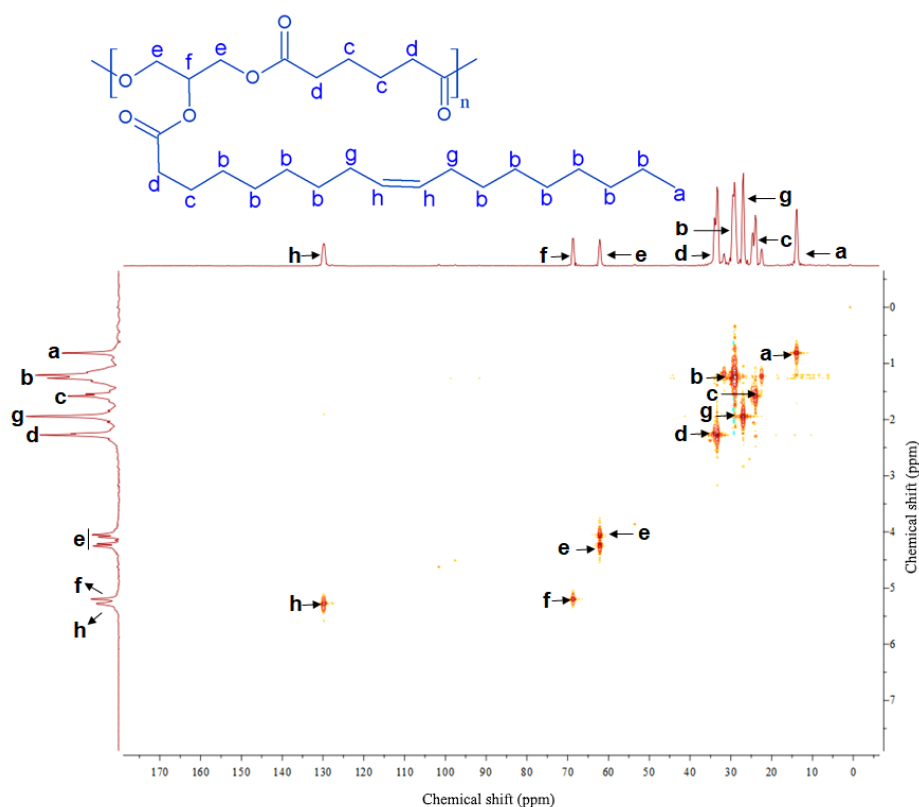

Figure 17. 400 MHz spectrum 2D NMR (^{1}H-^{13}C) of PGA-g-O100 at 27 ºC in CDCl$_3$.

3.1.4 Attenuated total reflectance infrared spectroscopy (ATR-IR)

To further confirm the esterification, ATR-IR measurements were conducted, and the characteristic functional groups were assigned, as a complementary method for NMR.

The infrared spectrum is generated by the absorption of electromagnetic vibrations at determined frequencies of chemical bonds in a molecule. Each molecule has a unique vibrational spectrum. Thus, the infrared spectrum distinguishes molecules, serving as a fingerprint of the chemical entity and can be used to identify chemical substances [152]. The technique permits the identification of a molecule, either by acquiring information from the backbone or functional groups and differentiates between linear and branched polymers. Besides that, further details, such as aromatic rings or unsaturation, can be detected [152]. Equation 3 represents the components of the vibration concerning the energy of the system:

$$E = h\nu \tag{3}$$

Where energy E, equals Planck's constant times the frequency. Commonly, the spectrum starts at 4000 cm^{-1} down to 500 cm^{-1}. An important aspect of infrared interpretation is that the identification of a compound is related to a characteristic band present and absent in the spectrum [152]. Table 3 shows the main IR functional groups.

Table 3. Infrared assignments based on information obtained from published group frequency data [152]*, shows the functional groups present in the polymer along with their frequency and assignments.*

Origin	Frequency, Wave number (cm^{-1})	Assignment
C=O	1750–1700	Ester
C=C	1620-1680	Alkenyl stretch
C–H$_2$	2935–2915/2865–2845	Methylene C–H asym./sym. stretch
–CH$_3$	2970–2950/2880–2860	Methyl C–H asym./sym. stretch
O–H	3570–3200	Hydroxy group, H-bonded OH stretch
C–C	1300–700	Skeletal vibration

Figure 18 shows the infrared spectra of PGA with different functionalization degrees. The characteristic hydroxyl stretching (1) in the region of 3470 cm^{-1} is decreased as the degree of grafting with oleic acid increases, corroborating the data acquired from NMR spectroscopy. These data were used as a qualitative measure, by which one can have a fair impression of the grafting occurring. Typical ester bands at 3003 cm^{-1} (2), 2920 cm^{-1} (3) and 2850 cm^{-1} (4) have their absorption increased correspondingly. As it is a common assignment for oleic acid, these C-H stretch vibrations of aliphatic groups increase considerably with increasing the grafting. The vibrations of the correspondent stretches appear at 1450 cm^{-1}, 1240 cm^{-1} and 720 cm^{-1}, respectively. The band at 3003 cm^{-1} reveals the presence of unsaturated C-H bonds. At 1740 cm^{-1} the presence of the carbonyl group is evident by a strong absorption in the grafted as well as in the polymer backbone.
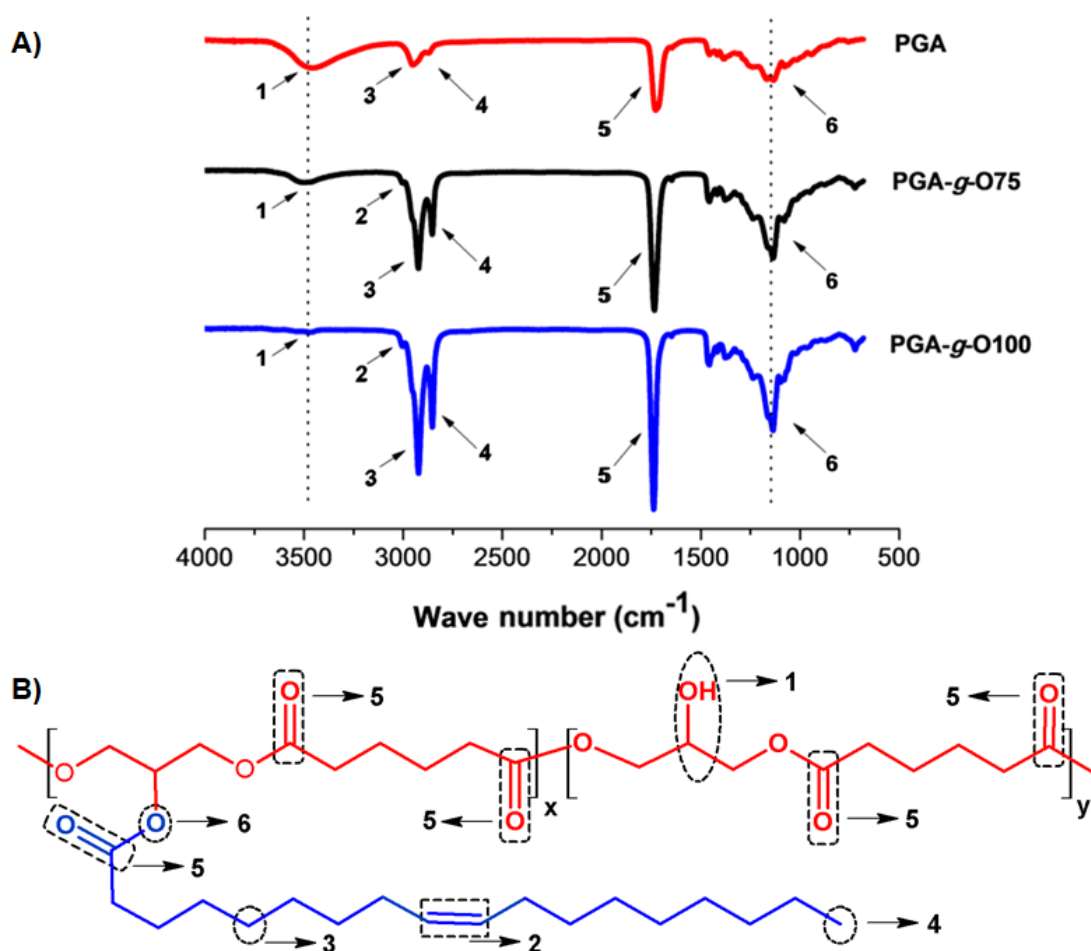
Figure 18. ATR-IR spectra of PGA (A), PGA-g-O75 and PGA-g-O100 and their structure with assigned functional groups (B).

3.1.5 Differential scanning calorimetry (DSC)

Differential Scanning Calorimetry is a classical method to characterize polymers. It is a thermoanalytical technique based on the measurement of the heat necessary to cause a physical transformation (or phase change) in a sample [153]. One of these phenomena is the glass transition temperature (T_g) [154]. It is a temperature range, in which the mobility of the polymer changes as the material undergoes a phase transition. The glass transition temperatures reported here are then the midpoint temperature found to be the range corresponding to the glass transition temperature.

According to DSC results, the polymer possesses T_g in the range of -36 to -64 ºC (Figures 19 and 20). As PGA is amorphous [120], the modification with unsaturated fatty acid as side chains were expected to lead to a lower T_g, contrary to the case of stearic acid [127], for which increasing the grafting led to an increase in T_g. This result agrees with the broad band observed in IR spectra at 3450 cm^{-1}, characteristic of an amorphous material. Taresco et al. observed a decrease in T_g as the carbon length and amount of fatty acid side chain increased, as it is known that this behavior appears in alkyl side chain polymers [155]. The same behavior was observed in this study. In the case of PGA-g-O75 and PGA-g-O100 an artefact is observed in the measurement as no cooling is expected to take place.
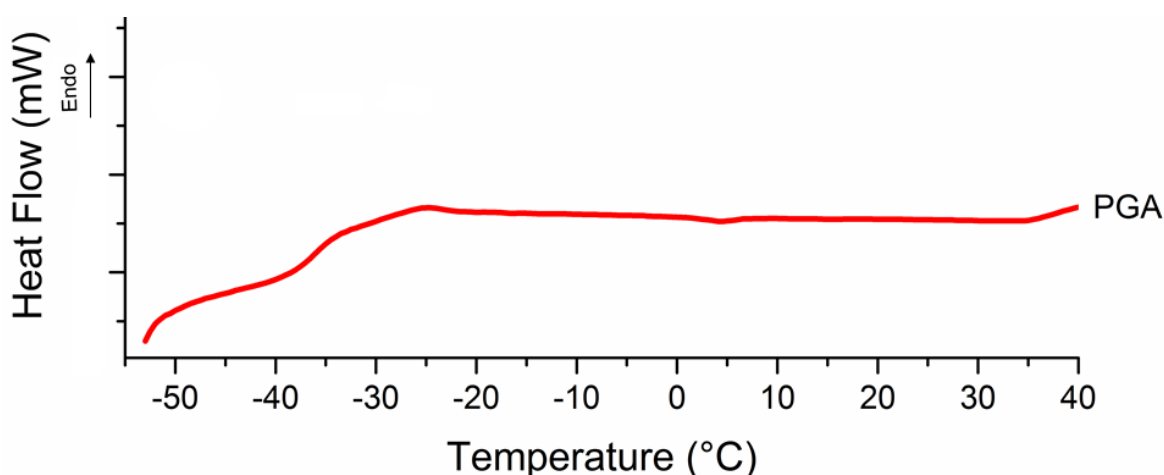

Figure 19. Differential Scanning Calorimetry (DSC) thermogram of PGA measured with a heating rate of 5 Cº/min. The second heating curve is shown.
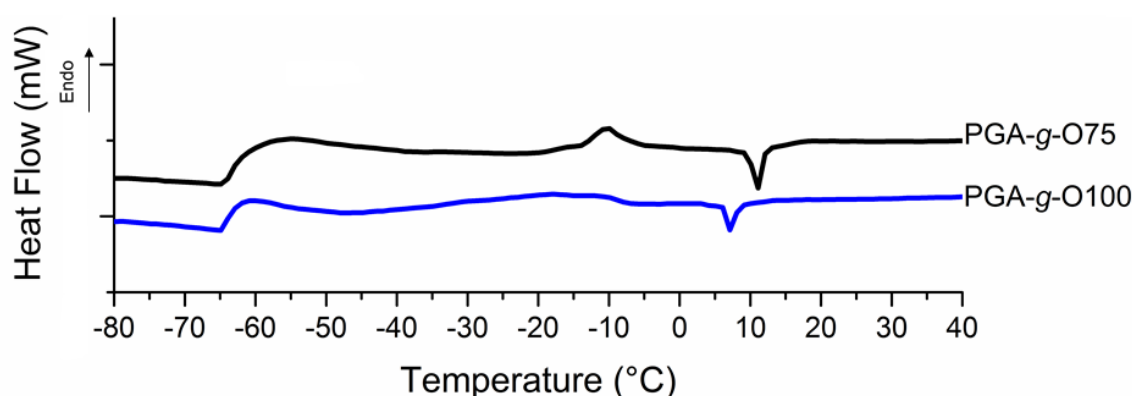
Figure 20. Differential Scanning Calorimetry thermograms PGA-g-O75 and PGA-g-O100 with a heating rate of 5 Cº/min. The second heating curve is shown.

3.1.6 Thermogravimetric analysis (TGA)

Thermogravimetric analysis is a classical method to study the thermal degradation stability profiles of polyesters [156]. To learn about the thermal characteristics of the polymers PGA and of its modified versions, we carried out TGA measurements at a heating rate of 10 ºC min^{-1} in a nitrogen atmosphere. Figure 21 depicts the TG and the corresponding derivative curves (DTG).

The results of TGA showed that the polymers are quite stable until 300 ºC. The onset of the degradation is more pronounced at *ca*. 350 ºC and applies to PGA as well as to PGA-*g*-O75 and PGA-*g*-O100. The mass loss was slightly greater for the polymer backbone, and PGA-*g*-O75 version whereas the highly grafted PGA-*g*-O100 presented a slightly higher thermal stability. Nevertheless, all polymers had a drastic degradation between 350-450 ºC. The derivatives show the thermal events are consistent and happen at once, within the same temperature range.

These results show that the polymer is highly stable at the intended temperature range. The grafting with oleic acid did not alter the thermal decomposition profile of poly(glycerol adipate) significantly. The polymer chains probably remain intact over 300 ºC, regardless of the existence of a grafting of the hydroxyl group of PGA, or its degree of grafting. After 450 ºC, both linear backbone and its comb-like varieties have suffered thermal decomposition.
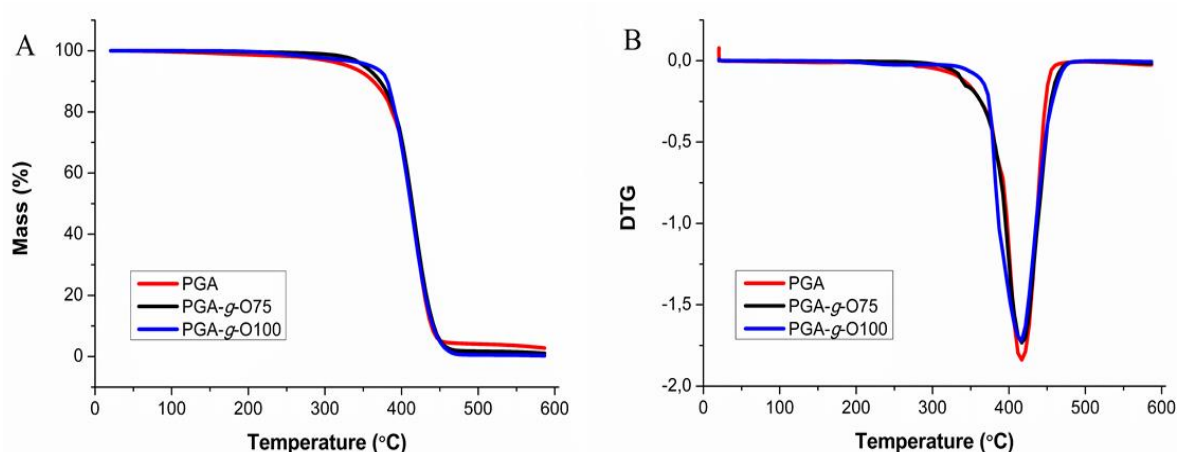
Figure 21. A) TGA Mass (%) and B) Derivative mass (DTG) versus temperature with a heating rate of 10 ºC/min of PGA, PGA-g-O75, and PGA-g-O100.

3.2 Characterization for Pharmaceutical applications

3.2.1 Contact angle measurements

The contact angle is the angle, conventionally measured through the liquid, where a liquid-vapor interface meets a solid surface. It quantifies the wettability of a solid surface by a liquid via Young`s equation. A given system of solid, liquid, and vapor at a given temperature and pressure has a unique equilibrium contact angle.

Implantable biomaterials in contact with tissue may react to the surroundings according to the surface characteristics [157]. The degree of hydrophobicity may trigger the response of the tissue in contact with the biomaterial and determine which cells will interact with the implant. Therefore, knowing the surface characteristics of the implant is important to gain previous insight into how it may behave *in vivo* and modulate, if necessary, these properties to obtain adequate responses [158]. As the biomaterial surface wettability may alter the protein absorption that is known to occur after implantation (from minutes to hours after the procedure), contact angle measurements were performed [159]. In this manner, more information about the parameters that affect the host response can be acquired and help understand the host-biomaterial interaction.

The Young's equation described in figure 22 shows the interfaces related to the contact of a liquid with a solid:

Young's equation

$$\gamma^{sv} = \gamma^{sl} + \gamma^{lv}\cos\theta$$
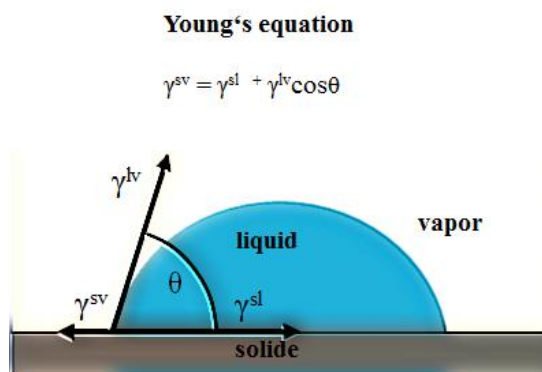
θ = contact angle

γ^{sl} = solid-liquid interfacial free energy

γ^{sv} = solid interface free energy

γ^{lv} = liquid interface free energy

Figure 22. Representation of different phases and interphases forming the contact angle.

According to the literature, the least concentration solution should provide the more appropriate polymer film [160]. Different concentrations were tested and examined under the light microscope. The solution with THF resulted in a less ordered film when compared to toluene in the same concentration and presented irregular coating, with wider uncovered surfaces [Figure 23]. Finally, solutions of 3 mg/mL were used as it showed better results regarding the surface covered and uniformity.
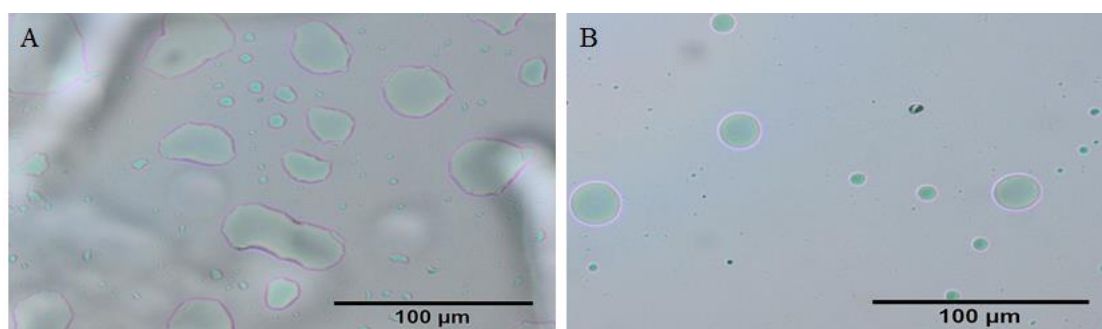

Figure 23. A) Representative glass slides spin-coated with the polymer solution in THF and B) glass slides spin-coated with the polymer solution in toluene at RT (3mg/mL).

The contact angle of the PGA/water did not exceed 90 ° regardless the amount of fatty acid used in its grafting (Figure 24). However, it has a contact angle ranging from 48.38±0.82 (PGA backbone) until 78.70±1.08 °, according to the degree of grafting.

Contact angle measurements can determine the wettability of biomaterials. Materials that present contact angle until 90 ° are regarded as hydrophilic, while hydrophobic materials are considered to have a contact angle higher than 90 °, and when this value is higher than 150 °, the material is called superhydrophobic.

They are therefore categorized as hydrophilic, or not hydrophobic, although in different degrees. Differences in hydrophobicity can be related to a different response in living cells and proteins aggregation. Biomaterials with a more hydrophobic surface tend to have a high affinity for different types of protein, such as albumin and fibrinogen [161].
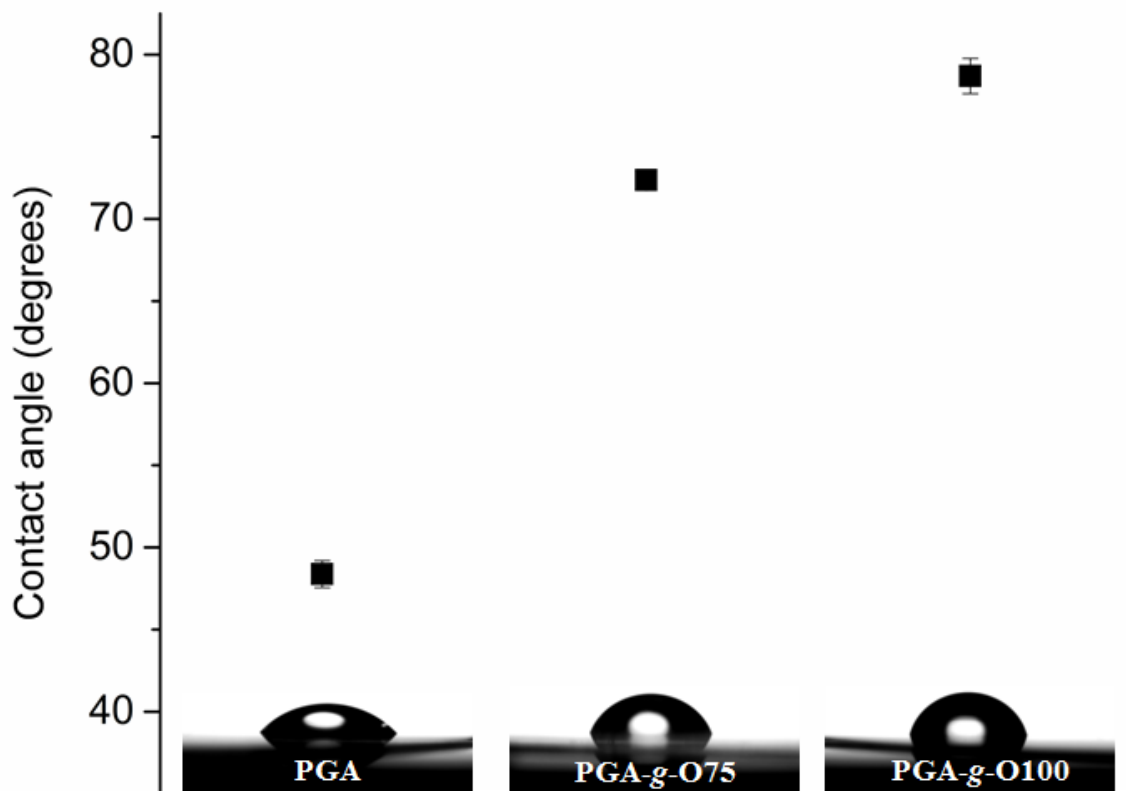

Figure 24. Representative contact angle images of PGA, PGA-g-O75, and PGA-g-O100 at 25 ºC. n = 5.

3.2.2 Magnetic resonance imaging (MRI)

MRI imaging is a powerful technique to access the water penetration/interaction with a system and has been used in the pharmaceutical field to characterize tablets [162]. Another use of MRI is in the investigation of the process that dosage forms, such as *in situ* forming implants, assume after implantation and how this behavior can influence therapeutic aspects [163]. MRI machines are expensive and require a large operation facility. Conversely, benchtop equipment is attractive since it can provide valuable information, occupies a smaller space and reduces the operating costs.

The ability to detect the proton mobility in different macromolecular environments enable to construct an image that depicts the relaxation times (T_1 and T_2) of a given sample after a radio frequency is applied. The proton is sensitive to its environment, and this difference in relaxation time permits the monitoring and mapping of the tissue or physical state of the material under investigation. While T_1 relaxation reflects the relaxation in the longitudinal axis (z), T_2 relaxation denotes the time the protons go out of phase.

Figure 25 depicts the process of water uptake for seven days in phosphate buffer solution. The MRI signal was measured. A minimal amount of water approached the surface of the polymer for seven days. The boundaries of the sample interact with the buffer and therefore have a higher mobility than the center, which contains the polymer with no water and less mobile structures. The relaxation time is faster in the center while the boundaries present a slower relaxation time, resulting from its free bounded protons. It can be seen that PGA-*g*-O100 suffers a slow water penetration, leading at least to a medium-term degradation as observed later *in vivo*. Unfortunately, the experiment had to be interrupted due to a floating of the polymer on the seventh day, as the closing of the glass vial (as using a net on the surface) would prevent part of contact with water, no further attempt was made to tackle this issue due to the time limit.
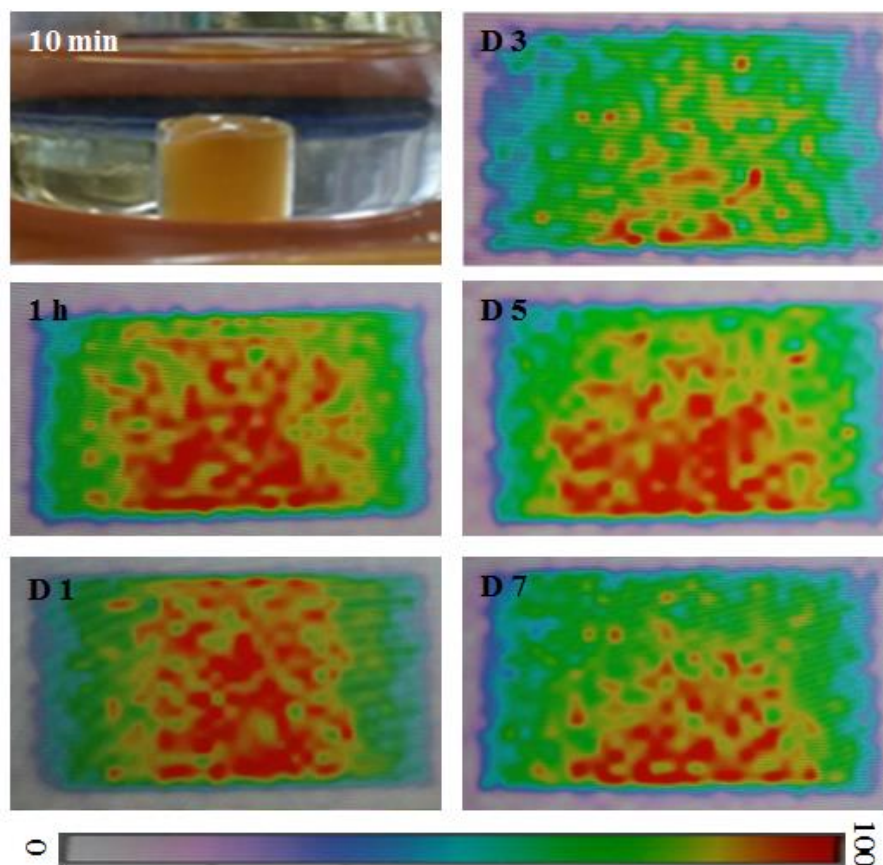
Figure 25. Representative MRI images of PGA-g-O100 in PBS at 37 ºC for seven days. Photo immediate after incubation (top left) and MRI images at 1 h, as well as on days 1, 3, 5 and 7. The blue outline corresponds to the buffer in contact with the polymer.

3.2.3 Electron-beam sterilization

Sterilization is an important part of pharmaceutical formulation development. As a material intended for parenteral use, polymers must be sterile before use. The strategies to achieve such requirement are limited to aseptic production or terminal sterilization. Ionizing irradiation may still cause changes in polymers, such as chain scission leading to a decrease in molar mass or cross-link, with increased molar mass as a result [164].

The choices of sterilization, in this case, fall in the irradiation. Gamma irradiation is known to affect more polymers when compared to beta rays [165]. To access the behavior of fatty acid grafted PGA, we decided in favor of beta irradiation at 25 kGy following the EMEA decision-tree guidelines. The polymers were irradiated at RT and under liquid nitrogen to know whether the temperature would influence the samples.

Concerning the sterilization, no significant impact on molar mass was observed after irradiation at RT or under liquid nitrogen (Figure 26).
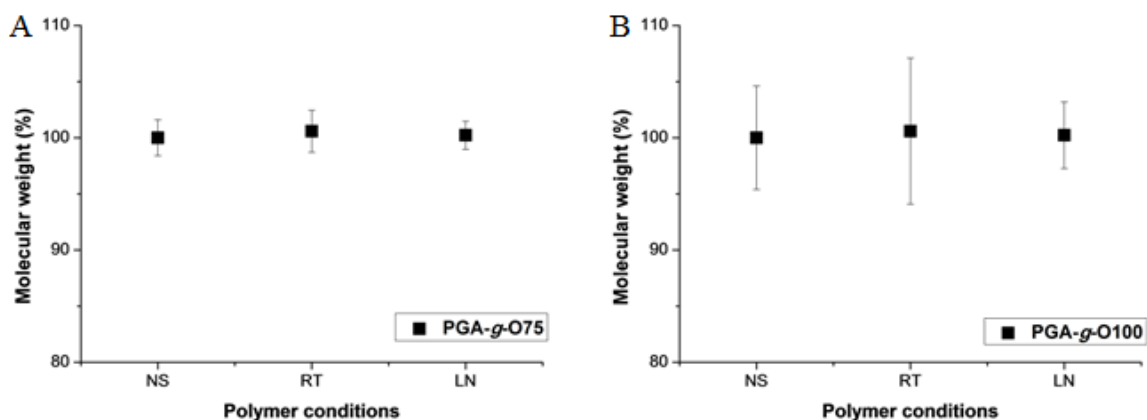

Figure 26. The molar mass of PGA-g-O75 (A) and PGA-g-O100 (B) non-sterilized (NS) and sterilized at room temperature (RT) and sterilized under liquid nitrogen (LN), with e-beam irradiation at 25 kGy doses. (n=3).

The proton NMR spectra of the irradiated polymer presented only slight changes regarding the polymer peaks (Figures 27 and 28). The spectra still show the decrease of the solvent peaks, tetrahydrofuran in both polymers and toluene in PGA-*g*-O100. In this case, as the effect on the spectra is minimal, I can assume that the molecule structure has not been substantially affected.
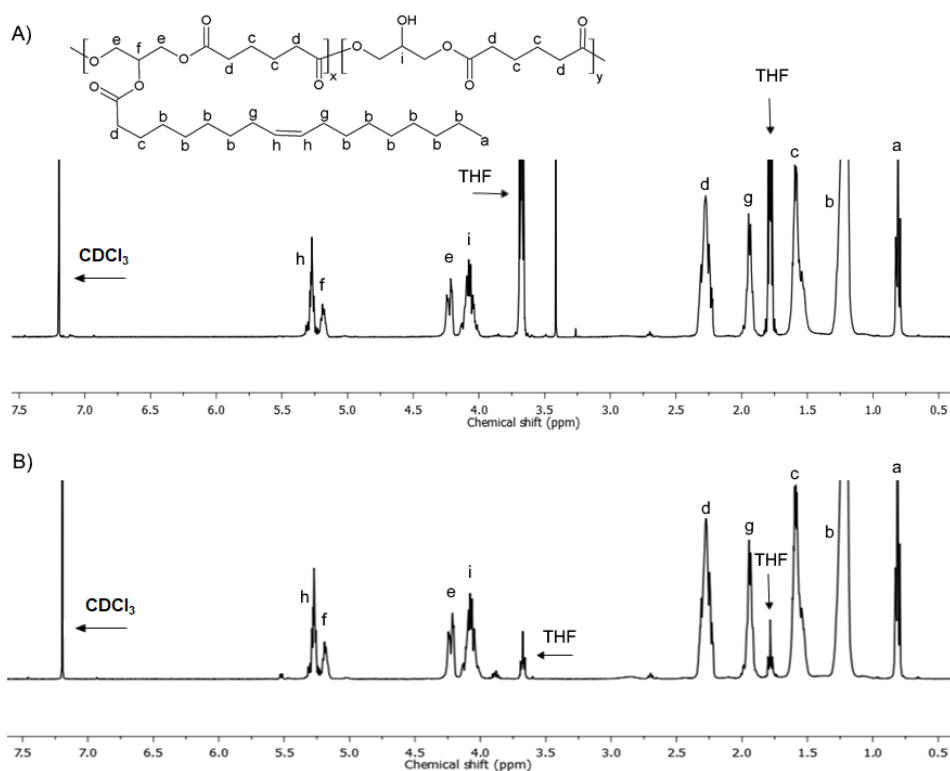
Figure 27. ¹H NMR spectra of PGA-g-O75 non-sterilized (A) and sterilized at RT (B) irradiation at 25 kGy.
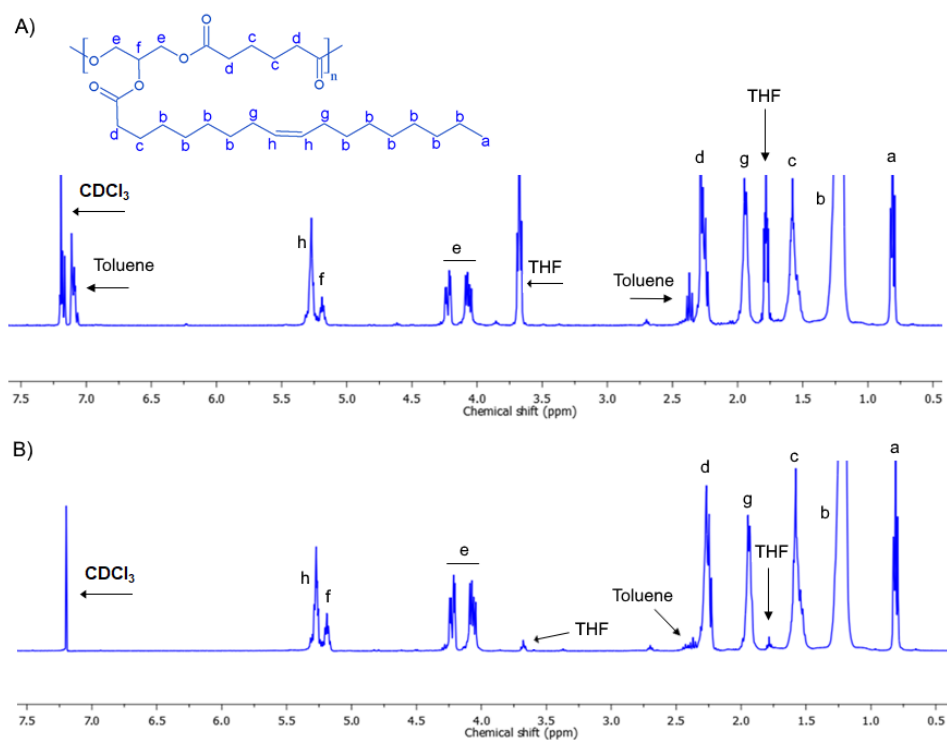

Figure 28. ¹H NMR spectra of PGA-g-O100 non-sterilized (A) and sterilized at RT (B) irradiation at 25 kGy.

3.2.4 *In vitro* toxicity

Different chemical entities, such as polymers, compound biomaterials, and different substances, including chemical organic solvents used during sample preparation. Biocompatibility tests must be conducted to ensure that the sample does not exhibit toxicity in the targeted tissue. Following subcutaneous implantation, the foreign body response takes place and fibrous tissue forms around the applied sample.

In this study, we used 3T3 mouse fibroblasts to explore the reaction of the extractable materials on the sample. The cell layer showed no significant deviations from the negative control (FCS-supplemented MEM) after cultivation with extracts of the sample for 48 h. The cell layer was dense, and changes in cell morphology and cell lysis were only rarely observed (see Figure 29). Accordingly, using the scoring scheme given by the DIN EN ISO 10993-5, no evidence of a cytotoxic effect of the samples was detected (cytotoxicity graded as 0), based on the cell morphology.

In the cells cultured with extracts of the sample, the lactate dehydrogenase release and the activity of the intracellular dehydrogenases were comparable with the corresponding activities in the cells cultured with extracts of the negative control (no significant differences were observed). MTS is a procedure by which tetrazolium salt undergoes oxidation in the mitochondria of living cells. The cell metabolism in thus assessed by the change in light absorbance, which is proportional to the number of viable cells. LDH relates the amount of enzyme that extravagates after membrane disruption and is also monitored by light absorbance. Accordingly, the LDH and MTS tests did not reveal toxic effects of the samples, indicating no cytotoxic effects of the sample (Figure 30).
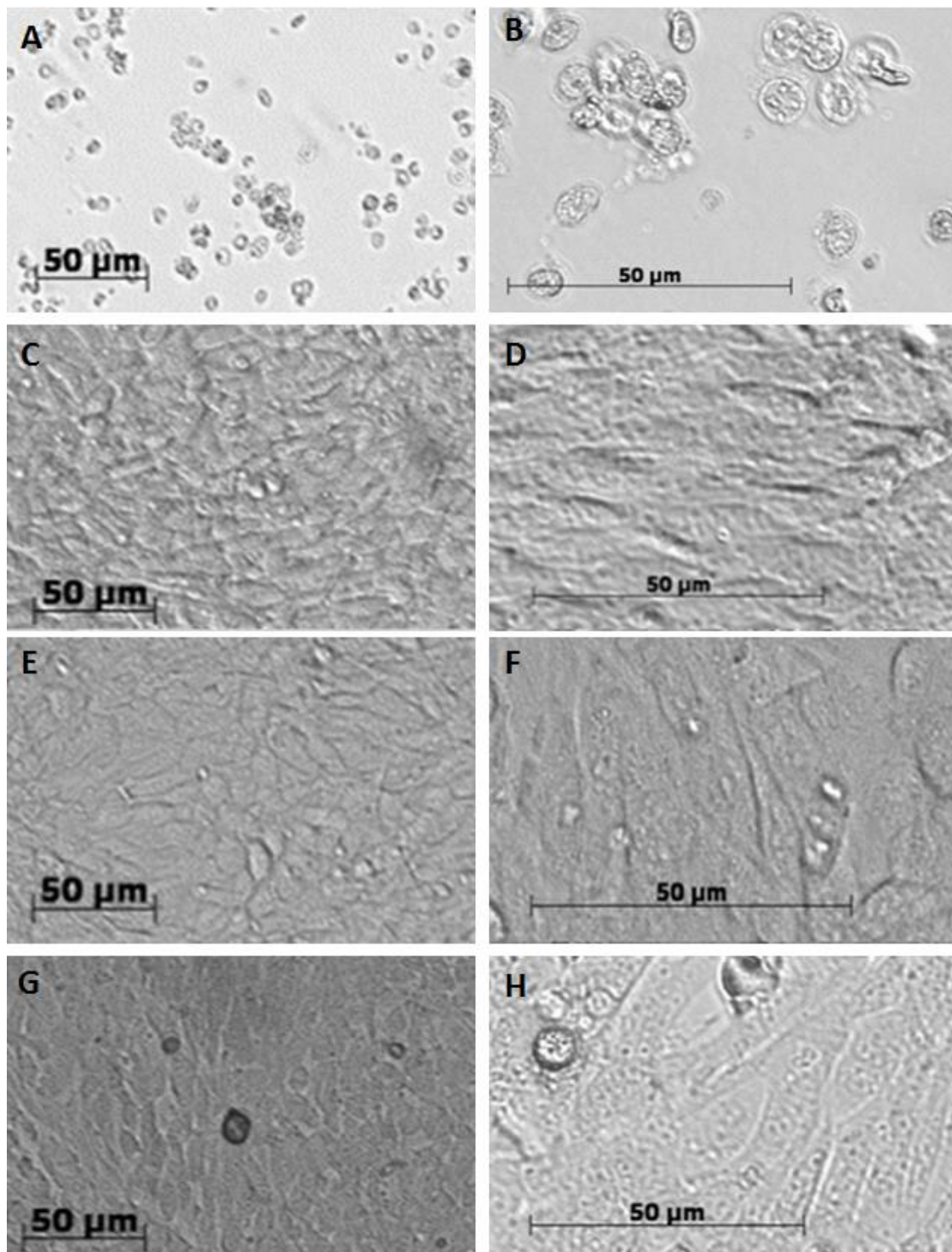
Figure 29. 3T3 cells 48 h after cultivation in cell culture medium (negative control), in cell culture medium with 1 mM CuCl₂ (positive control) and after cultivation in the sample extract (24 h extract); Transmitted light phase contrast microscopy, primary magnification 20 ×.
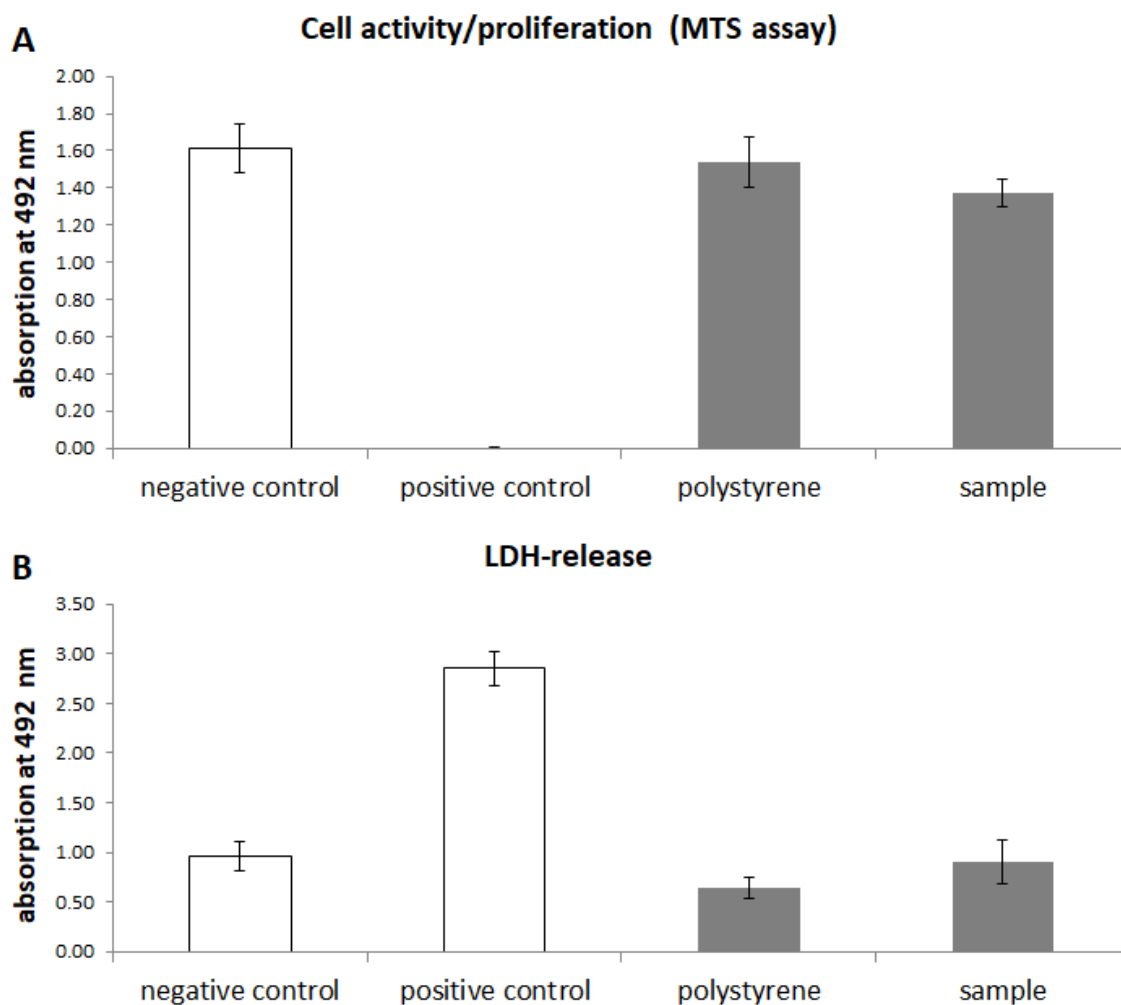
Figure 30. Biocompatibility of PGA-g-Ox. A) Activity of intracellular dehydrogenases and B) Lactate dehydrogenase release after cultivation of 3T3 cells with extracts of the sample, mean values ± sd, n = 8. 3T3 cells after growth in 24 h extract.

3.2.5 Parenteral injection

Over 10 billion injections are performed a year worldwide [166,167]. This outstanding number demonstrates the importance of parenteral formulations. In this regard, formulations that allow to injection forming a depot offer considerable advantages and are of great interest [168].

When injecting a substance through a syringe, several parameters contribute to the resultant force that must be applied to expel such liquid. The plunger exerts this force while the area of the syringe and the needle internal diameter and length limit the force applied. According to Newton's second law (equation 4), force corresponds to the variation of pressure against acceleration.

$$\vec{F} = m \bullet \vec{a} \qquad (4)$$

Where the force F (in Newtons), equals the mass m (in kg) times the acceleration a (m/s^2). According to fluid dynamics, the resistance of the flow will be higher where the substance has contact with the surface of the container and lower in the middle. The intersection between different cross-sectional areas, represented in figure 31 by the contact of the plunger and the needle, will influence the force necessary to expel the substance.

The Hagen-Poiseuille equation (5) represents:

$$\Delta P = \frac{8Q\eta L R^2}{R^4} \qquad (5)$$

where:

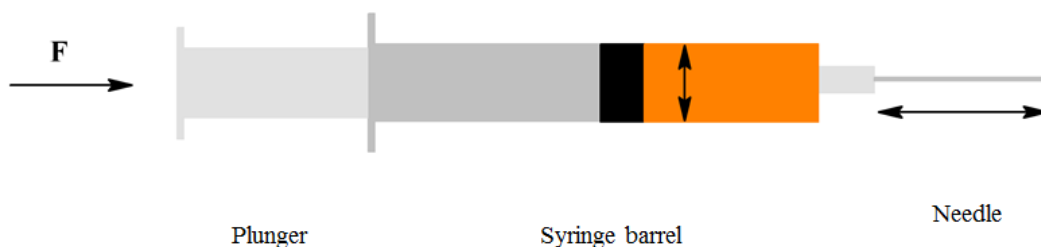|		
ΔP	=	pressure difference
Q	=	volumetric flow rate
L	=	length of the plunger
R^4	=	needle internal diameter
η	=	dynamic viscosity
R^2	=	plunger radius

Figure 31. Syringe with its parts, namely, the plunger, syringe barrel and the needle.

3.2.6 Syringeability

Syringeability and injectability are key product performance attributes for parenteral formulations. Syringeability is the ability of a solution or a suspension to pass through a hypodermic needle at an injection rate and determined needle gauge and length. Injectability refers to its performance during injection. Texture analyzer can be used to measure syringeability and injectability regarding force required to pull a liquid into the syringe barrel and push out the liquid from the syringe barrel. While the syringeability can be measured by expelling the formulation into the air, the injectability requires a material that should mimic the target tissue and may be tested by using chicken meat [169] or a subcutaneous tissue model [170].

Subcutaneous injection is an important route of drug administration and the route of choice for *in situ* forming implants. Formulations used in prefilled syringes have several advantages [171]. However, prefilled syringes require a designed procedure to measure and predict the ease of injectability of parenteral formulations [172]. As demonstrated by Burkburchler et al. [173], the addition of the API influences the formulation viscosity. The pressure the tissue exercises on the implant influences the properties of the system and its performance [174]. Another aspect that plays a role in defining the force required to a given system inside the syringe is the nature of the formulation. In this regard, being it of hydrophilic or hydrophobic characteristic impacts the results [175]. These characteristics, together with the syringe material properties and the strength of the individual (applicator), are responsible for the final force needed to inject a formulation [176]. Moreover, the stability of the drug must be comprehensibly assessed to ensure the optimal choices at an early stage of the development [177].

With the highest grafting (100 mol%) the polymer showed a quite good syringeability with less than 30 N to displace the plunger using a needle of 25 G. The least force of less than 10 N with a needle of 21 G (Figure 32), exhibiting a good performance with a needle used in the clinic (172). This property can still be tuned according to the desired formulation and the characteristics of the drug and drug load. In case the desired formulation requires less grafting for use, one last alternative could be the use of small amount of organic solvents as an enhancer.

In parenteral injections, it is important to obtain a formulation with acceptable injectability, thereby allowing the medication to reach the target area in a minimally invasive manner. One way to change this property in the case of PGA-*g*-Ox is by manipulating the polymer molecular mass. As the molar mass decreases the viscosity tends to decrease, however, in this case, it is necessary to consider an interplay between the molecular mass and the amount of fatty acid added to the polymer. The fatty acid here, being liquid, can modify the rheological properties of PGA and contribute to tailoring the flow of the polymer in the desired manner. That means a higher modified backbone will be less viscous, thus, requiring less injection force.
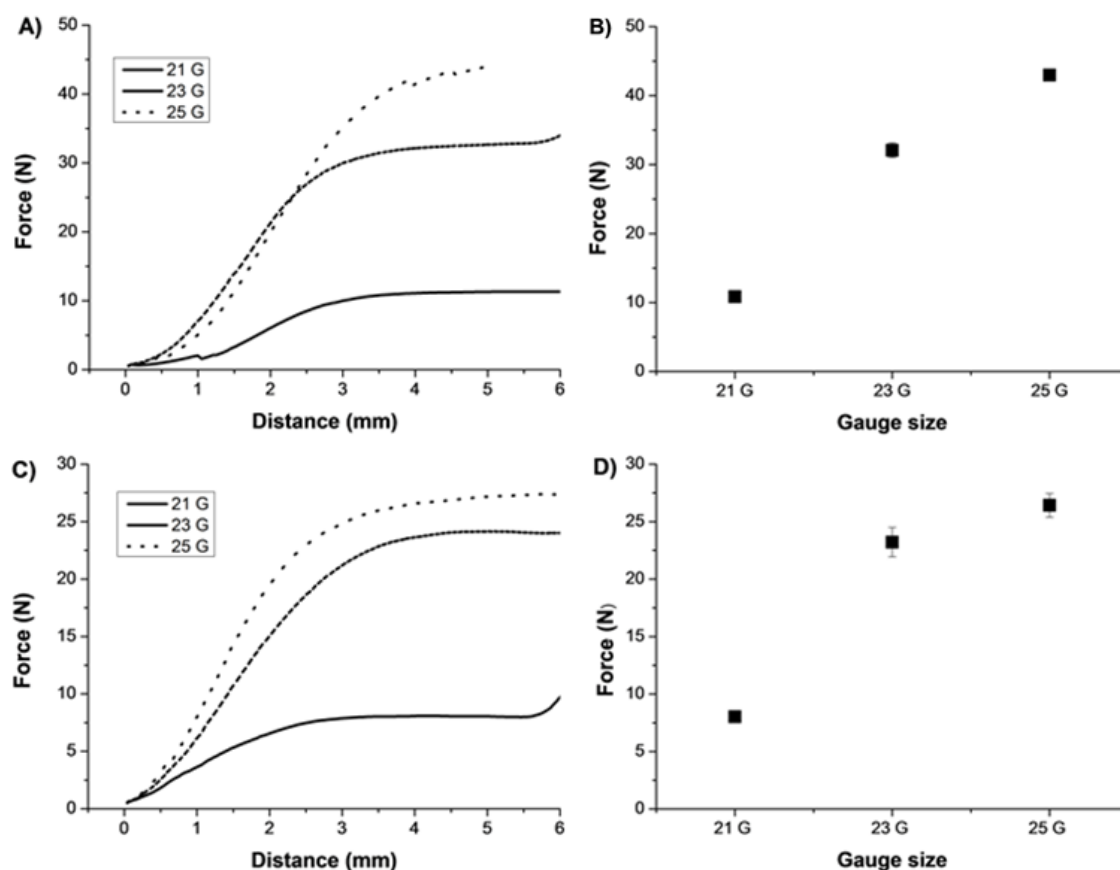

Figure 32. Syringeability of PGA-g-Ox. Mean values (n=3) of injection of PGA-g-O75 with 1 mL syringe using needles of 21, 23 and 25 G (A and B). Mean values (n=3) of injection of PGA-g-O100 with 1 mL syringe using needles of 21, 23 and 25 G of grafted PGA (C and D), under the same conditions.

3.2.7 Peptide formulation

The formulation of peptides is an important and challenging task that influences the performance of the product. In a broad view, considering practical and economical aspects, it should be well designed and oriented [178]. Peptides are fragile molecules that need careful manipulation, and the formulation must accommodate the drug without causing stress or degradation.

Various techniques can be applied to formulate leuprolide acetate, such as mixing the drug solubilized in a solvent and the polymer in another syringe in a back and forward movement [179], cryo-milling the drug together with a viscous polymer [180], or covalent linkage of the peptide to polymeric micelles [181]. Apart from that, the concentration of leuprolide in the formulation has shown to influence its release [182]. Ion-pairing is an approach by which a hydrophilic substance is paired, becoming more lipophilic [183,184] and has been employed successfully to formulate leuprolide [139,185].

The principle by which photon correlation spectroscopy calculates particle size lies in the Stokes-Einstein equation:

$$D = \frac{kT}{6\pi\eta R} \tag{6}$$

where the diffusion coefficient, D, equals the Boltzmann constant, *k,* times absolute temperature, *T*, divided by the viscosity of the medium, *η,* times the radius of a spherical particle *R*.

Upon the dropwise addition of sodium oleate solution into the leuprolide solution, a milky turbid one was formed. The particles resulted from ion pairing measured by PCS had a size under 465 ± 8 nm with PDI of 0.065 and zeta potential of -40.2, with a narrow distribution and indicating good stability (Figures 33 and 34).
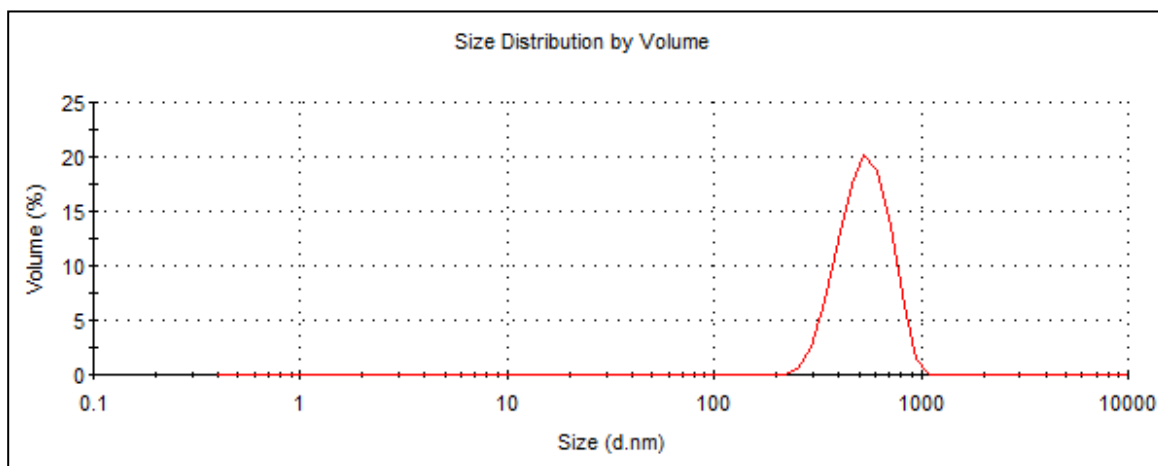
Figure 33. Representative measurement of Leuprolide-Sodium oleate paired particles size at 25 ºC.
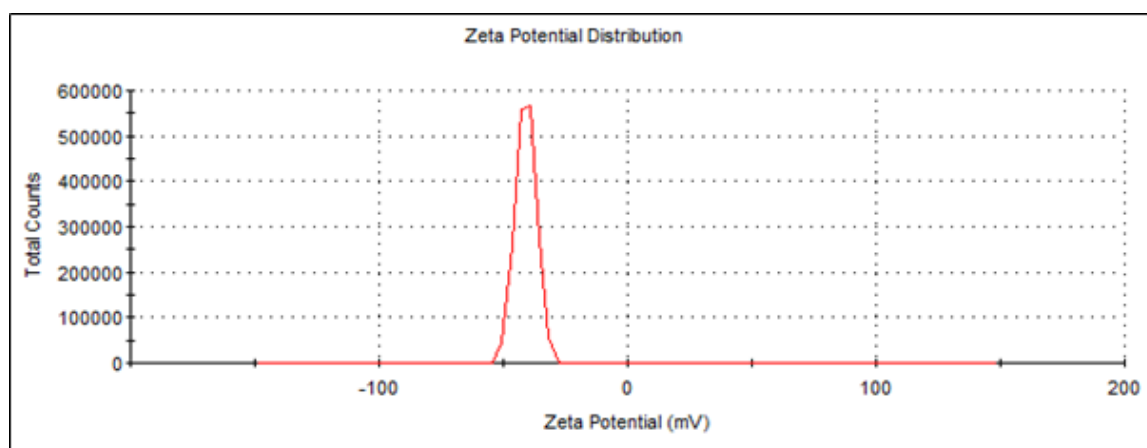

Figure 34. Representative image of the zeta potential of Leuprolide-Sodium oleate paired particles at 25 ºC.

The presented approach to formulating the peptide drug, without the use of organic solvent and based on the semi-solid nature of the polymer, is advantageous as the formulation may be affected by the type of solvent and the drug-polymer interaction, as investigated with PLGA [50]. Moreover, it was possible to achieve a homogeneous suspension (Figure 35).
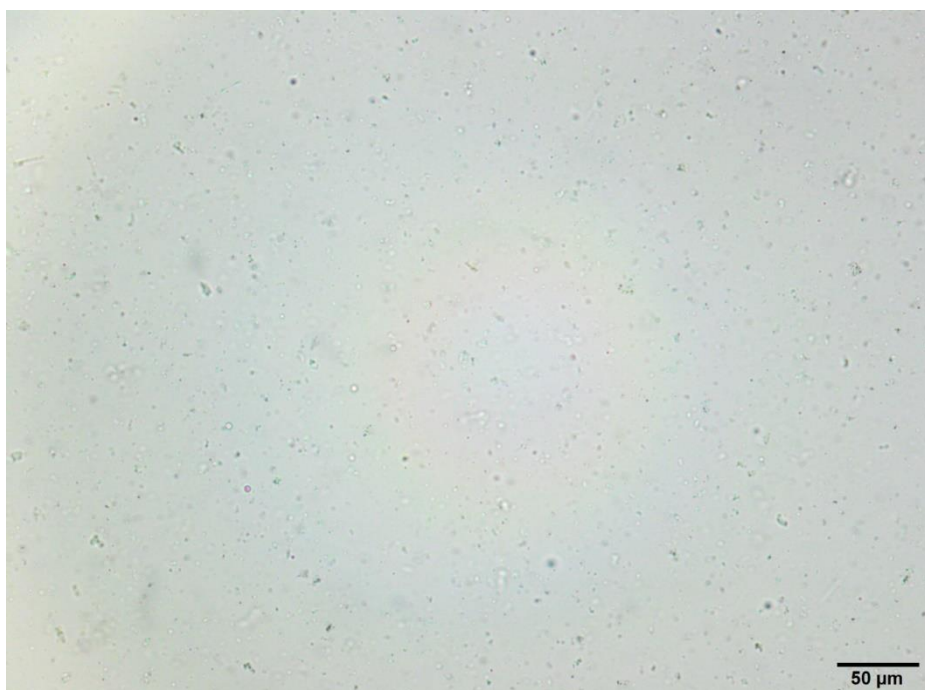
Figure 35. Leuprolide ion-paired particles suspended in pre-warmed PGA-g-Ox.

The release device was previously developed in-house for the delivery of drugs from semi-solid preparations [186]. It consists of a polymeric frame with three cavities. Each cavity has a size of 8 x 4 mm resulting in a volume of 200 mm^3, and it is closed using a poly(ethylene terephthalate) (PET) net to function as a barrier and avoid the leaking of the material in the buffer solution.

3.2.8 *In vitro* drug release

Leuprolide acetate is a synthetic nonpeptide hormone analog used to treat prostate and breast cancer, endometriosis and precocious puberty [187,188]. It was discovered during the 1970s and decreases the level of testosterone in the body, thereby, regulating the diseases by modulating the concentration of hypothalamic-pituitary-gonadal (HPG) hormone [188,189].

Prostate and breast cancer are among the leading types of cancer not only in Europe, where the incidence number of cases is approaching 1 million cases and with over 200,000 deaths were computed in 2012 [190], but also in the world. Over 8 million cases of prostate and breast cancer were reported in 2008 [191]. Prostate cancer is prevalent in males over 65

years old and accounts for 3 million cases of cancer. It is responsible for nearly 30,000 men deaths in the USA. The common detection of prostate cancer is through prostate-specific antigen (PSA) detection. Following that, a biopsy is carried out to confirm the case. Other methods, such as MRI have been used as diagnostic tools [192]. As a treatment, the cancer is removed by surgery (castration) and the patient receives agonists hormones as a palliative alternative. The administration of agonist hormones suppresses the level of testosterone, which is the cause of prostate cancer. Then a chemical castration level is achieved, leading to a control of hormonal level and the disease.

Endometriosis is a chronic disease characterized by endometrial-like tissue outside the uterine lining [187]. It is a chronic inflammatory disease that affects 10% of women of reproductive age and characteristically presents endometrial tissue outside the uterus [193]. Likewise, precocious puberty is a hormone related disease [194]. The premature activation of the hypothalamic-pituitary-gonadal axis results in early sexual maturation [195].

The goal of treatments of hormonal disbalance and inhibition of tumor growth with repeated injections of hormone agonists (e.g., luteinizing hormone-releasing hormone (LH-RH) is to lower plasma testosterone levels, which leads to a hormone suppression and control of the condition. When the pharmaceutical ingredient is fragile, daily injections may be required to sustain drug levels within the therapeutic range. Injectable delivery systems play this role, providing extended release of the active agent while protecting the unreleased labile payload [12].

Several factors can influence drug release from a system, such as a polymer molar mass [196]. The release of the peptide over the period planned was not optimal. The polymer with higher fatty acid grafting exhibited a slower release, reaching 5% whereas the more hydrophilic polymer released nearly 20% of the drug. Although the release profile is not as expected, it is important to highlight that the burst released was successfully avoided in both cases with a steady release during the period of the experiment. The polymer with a lower degree of grafting and freer hydroxyl groups exhibited a higher drug release.

The drug release profile of leuprolide as seen in figure 36, is influenced by the fatty acid amount in the polymer. The higher the amount of fatty acid grafted in the polymer backbone, the more hindered the drug release. The relation of the polymer hydrophobicity and its

effect on drug release has been demonstrated by other authors as well [197-199]. The addition or variation of the oil phase using PLGA also demonstrated a slower drug release [182,200,201]. Formulations of peptides in oily systems offer advantages, such as enhancing the drug permeation and mask the hydrophilic surface of the molecule [202].

Another factor that may impact the release of a given formulation is the vehicle porosity. As demonstrated by Luan and Bodmeier [203], a higher polymer porosity leads to a higher water penetration, thus resulting in a faster release of the drug due to interaction with the medium. Regarding this aspect, the polymer version with less modification in the present study, PGA-*g*-O75, had hydroxyl groups available to interact with the medium, as opposed to the fully grafted version. This characteristic probably was fundamental to distinguish the difference in the release profile observed. The variation of the drug concentration in the system may impact the porosity [204] when developing the delivery formulation one should also investigate how the structure changes according to its composition.

The properties of the polymer combined with the design of the formulation was responsible for the control over the release behavior. We can expect that due to the lipid content, the polymers formed a low degree of porosity, making it difficult for water penetration. Ion pairing had been demonstrated to be beneficial as a tool to modulate hydrophilic drug release [205]. As shown in other studies, the complexation was effective in suppressing the initial burst release of the drug in both formulations. It demonstrates that the release can also be tuned to last for different periods of time, according to the desired goals of the therapy. Although the release was slowed down, in this case, it is important to remind that only one side of the sample holder was open to interacting with the buffer. The drug release would be faster if the formulation were subcutaneously injected, among other factors, due to the larger surface area of the implant exposed to the tissue in comparison with the present experiment.
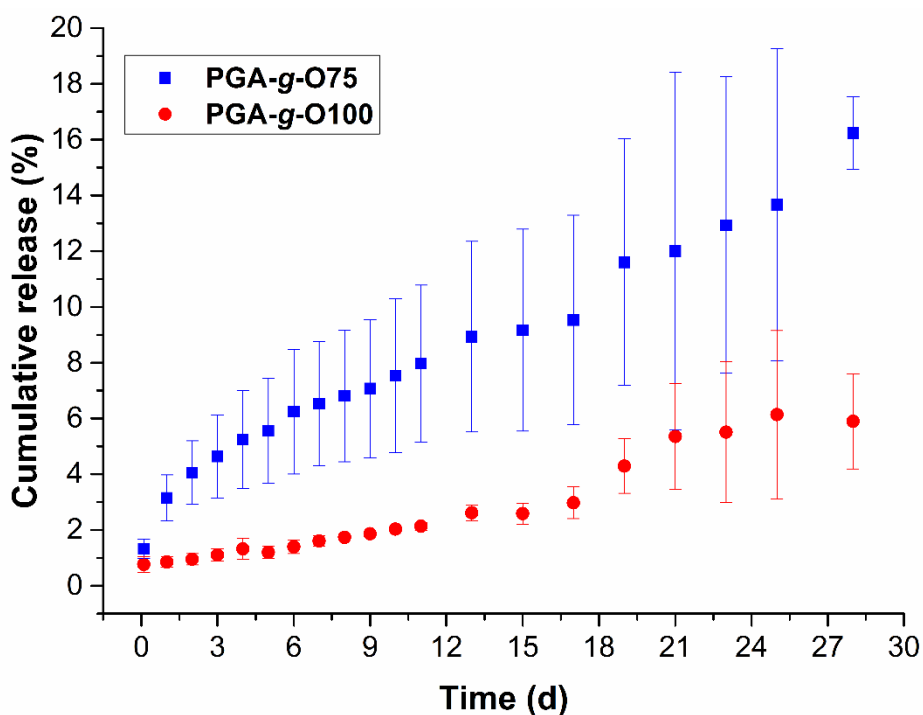
Figure 36. In vitro release of leuprolide from PGA-g-O75 and PGA-g-O100 in triethylamine buffer, pH 7.4, at 37 ºC over a period of 28 days determined by HPLC.

Another aspect that has been under investigation by some research groups is the medium in which the *in vitro* experiments are performed. Ye et al. [206], studied the release of piroxicam from oil into agarose gel as a matrix with the intention to mimic the subcutaneous tissue. This approach is interesting because it intends to mimic the subcutaneous tissue.

3.2.9 Subcutaneous administration of implants and *in vivo* imaging

Fluorescence microscopy is based on the property of an electron to become excited by a light source, which leads the matter to absorb photons (electromagnetic radiation). Following an energy loss due to the return to its relaxed electronic state, photons are emitted as fluorescence. As the energy source is light, it is then a type of photoluminescence [207]. As it can be found in the Jablonski diagram, the energy transitions generate and emit fluorescence. The fluorescence frequency is lower than the absorption frequency, giving rise to a shift of energy. This is called the Stoke's shift and is depicted in figure 37.
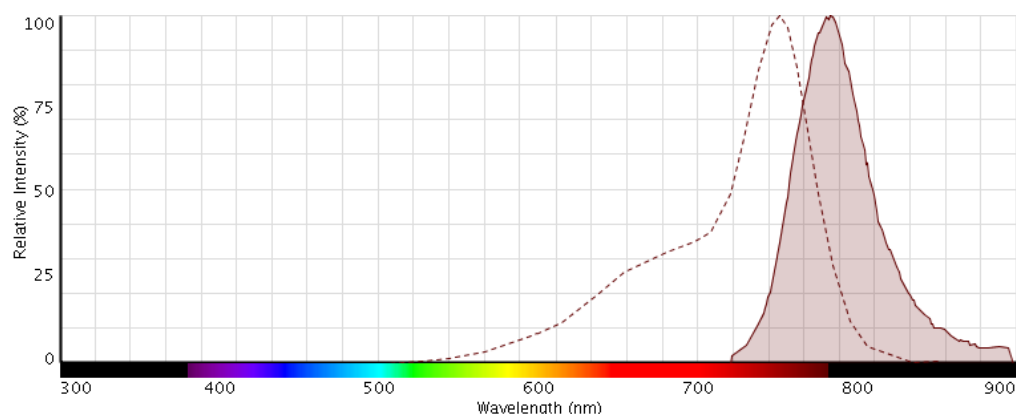
Figure 37. Absorption (dotted line) and emission (full line) spectra of DiR (208).

Dyes that are adequate for *in vivo* imaging are those that emit fluorescence in the near- or far-infrared regions (NIR and FIR, respectively), diminishing the chance of autofluorescence from the skin. The Stoke's shift shows that a photon is emitted at a higher wavelength than that where it is absorbed. As observed in figure 37, the absorption and emission energy of DiR lies in the near-infrared region. It means there is less chance that the autofluorescence properties of the tissue will interfere with the fluorescence detection. A preliminary experiment was performed using syringes as probe holders with different concentrations to determine the *in vivo* working conditions, to ensure that the dye concentration would be enough in the formulation (Figure 38). As a good detection was found, an optimal concentration was set for the *in vivo* experimentation.
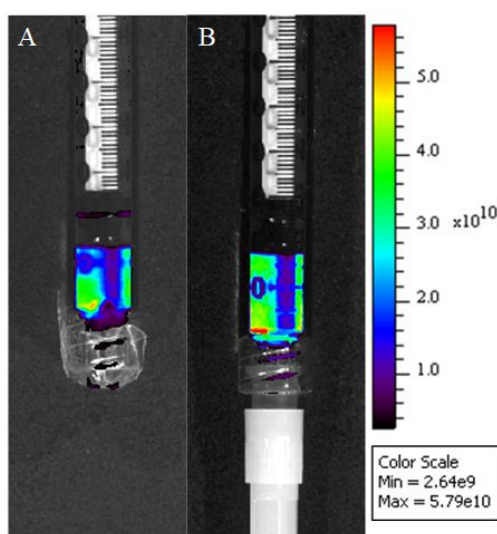

Figure 38. Syringes containing DiR formulation with peanut oil (A) and PGA-g-Ox (B).

Arachnis (peanut) oil was used in this study as a reference vehicle due to its similar properties and recorded use in the pharmaceutical field [209]. It has been used in animal experimentation and also reported in the formulation of peptide analogs [210]. Figure 39 shows a mouse implanted with the formulation of PGA-*g*-Ox and DiR (A) and a control mouse (B) without implantation. As it is seen, the dye fluorescence is strong enough to inhibit autofluorescence coming from the animal tissue, enabling the detection of the dye through the skin.
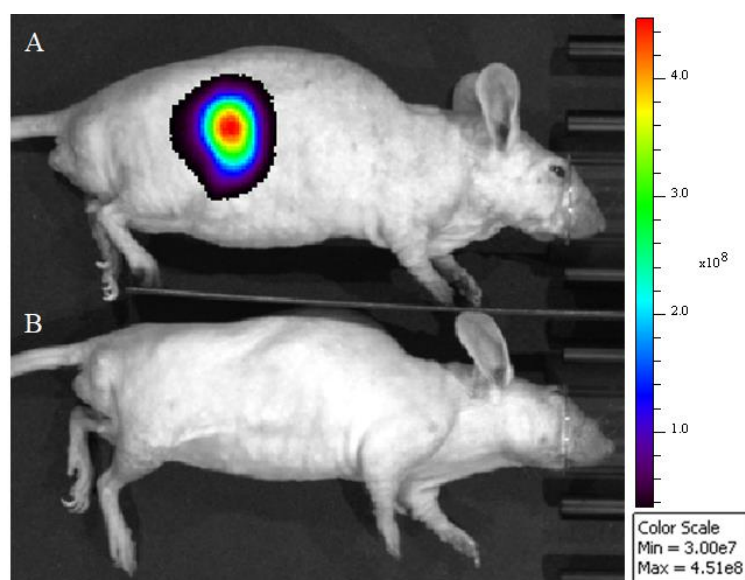

Figure 39. Mouse with the implanted polymer (A) and control mouse without implant (B).

Non-invasive methods are preferred for *in vivo* studies because fewer animals may be used to acquire reliable data and monitor *in vivo* processes whereas the animal suffering is minimized. This is in compliance with the ethics in scientific experimentation required by the public through regulatory agencies. Along with other methods, *in vivo* fluorescence imaging has evolved and enables studies to be conducted with minimal intervention and optimized results [93]. The mice in this study were monitored during the experiment concerning any harm symptoms and body weight fluctuations. While no visual signal of inflammation or other limiting condition was observed, the body weight varied to a minimum level ($< 10 \%$) and all animals remained healthy.

The results from the *in vivo* fluorescence showed that the signal of the lipophilic dye was

markedly lost after 48 h in all groups under investigation. As the dye was not covalently attached to the tested systems, it there was expected that the signal would not last for a too long time. There was although, a difference mainly among the more hydrophilic polymer and the other systems. The peanut oil formulation virtually completely lost the signal within two days while a weak signal (about 2%) could be detected in the highly grafted polymer and just over 10% remained in the group with less grafted implanted polymer (PGA-*g*-O75) (Figure 40).
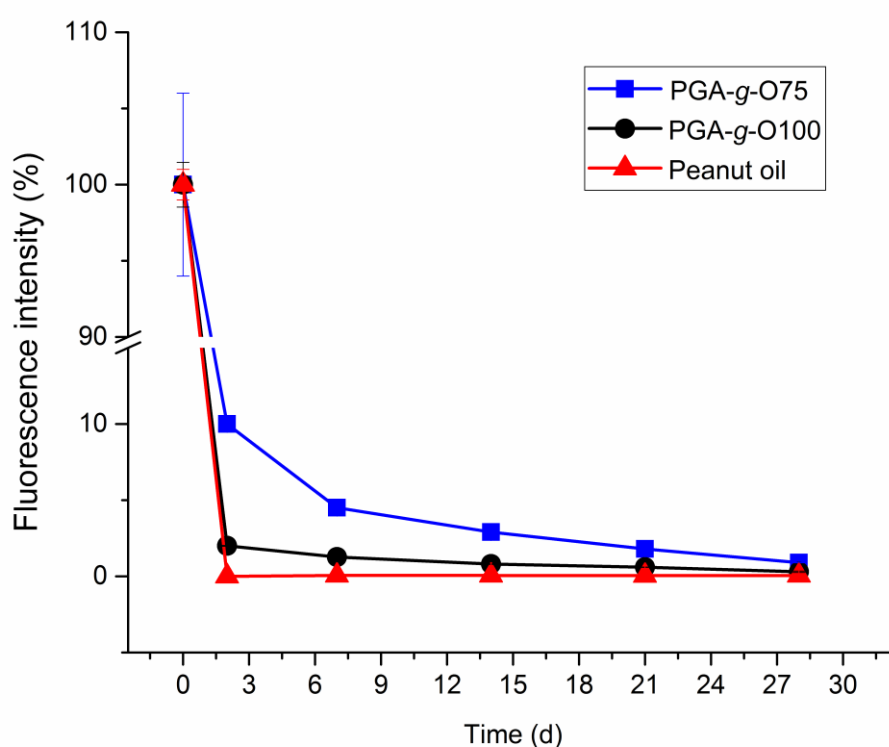

Figure 40. Relative fluorescence intensities of three mice groups implanted with DiR in peanut oil, PGA-g-O75, and PGA-g-O100 over a period of 28 days.

As briefly cited before, the shape of the implant influences the release pattern of a drug from a delivery system [11,68]. In the present study, the mice with peanut oil had a flattering shape compared to the polymeric implants. The polymer with higher oleic acid content was clearly flatter than poly(glycerol adipate)-*g*-O75. That implies the model drug would travel a shorter distance to interact with the surrounding tissue, being released faster.

The subcutaneous tissue is composed of elastin and collagen [211]. The role of oleic acid as a permeation enhancer is an important and known property. This set of characteristics permits to conclude that the drug release can be modulated by a combination of several factors cited here, in addition to the nature and form of the target pharmaceutical ingredient. The subcutaneous tissue is suitable for the administration of parenteral formulations for long-term and self-administered. The subcutaneous injection volume is a key point to be considered because of the restrictions it represents [212]. The volume of injection used has been between 1.5–2.5 mL, with injections of 2 mL being associated with pain. Besides that, the demand for high drug load implies further challenges for the formulator, as viscosity may increase significantly.

The needle gauge is important, as smaller gauge means a larger needle internal diameter and can cause pain at a level the patient may be not willing to bear, considering the factors affecting the formulation performance and patient compliance. In this respect, researchers have tried to establish *in vitro* evaluations that permit a prediction of the force necessary to administer a given formulation at a determined speed rate. It has been proposed that a force of 50 N would be acceptable for clinical purposes [175].

The injection site has been another issue of discussion regarding the possibilities and limitation for subcutaneous injection, as the hypodermis has a variety in structure depending on the considered location. Given that, new *in vitro* models have also been proposed to simulate the injection site and conditions more accurately and realistically, while trying to improve the bioavailability in humans in the subcutaneous site [213]. Upon on that, the patient's preferences should be taken into account as this can drive the decisions about formulation development [214,215].

As shown in figure 41, the release of DiR from the control group (Group 1) was complete in the first 48 h after injection. The decrease in the fluorescence dye intensity increased the autofluorescence. The shorter release from Arachnis oil was no surprise since its behavior has been reported [216]. The second group was implanted with the highest oleic acid contend PGA. Although the injectability was better than a less modified backbone, the release of the dye from PGA-*g*-O100 was more comparable with the peanut oil formulation. The quick release may be because of the less viscous character presented by this polymer variant, resulting in a flattering shape, which increases the surface area whereas diminishing the path the dye has to diffuse to reach the subcutaneous tissue. A preliminary study in our group

with PGA esterified with stearic acid also observed the same pattern, in which the implant bearing more hydrophobic characteristics released the lipophilic dye at a shorter time [129].
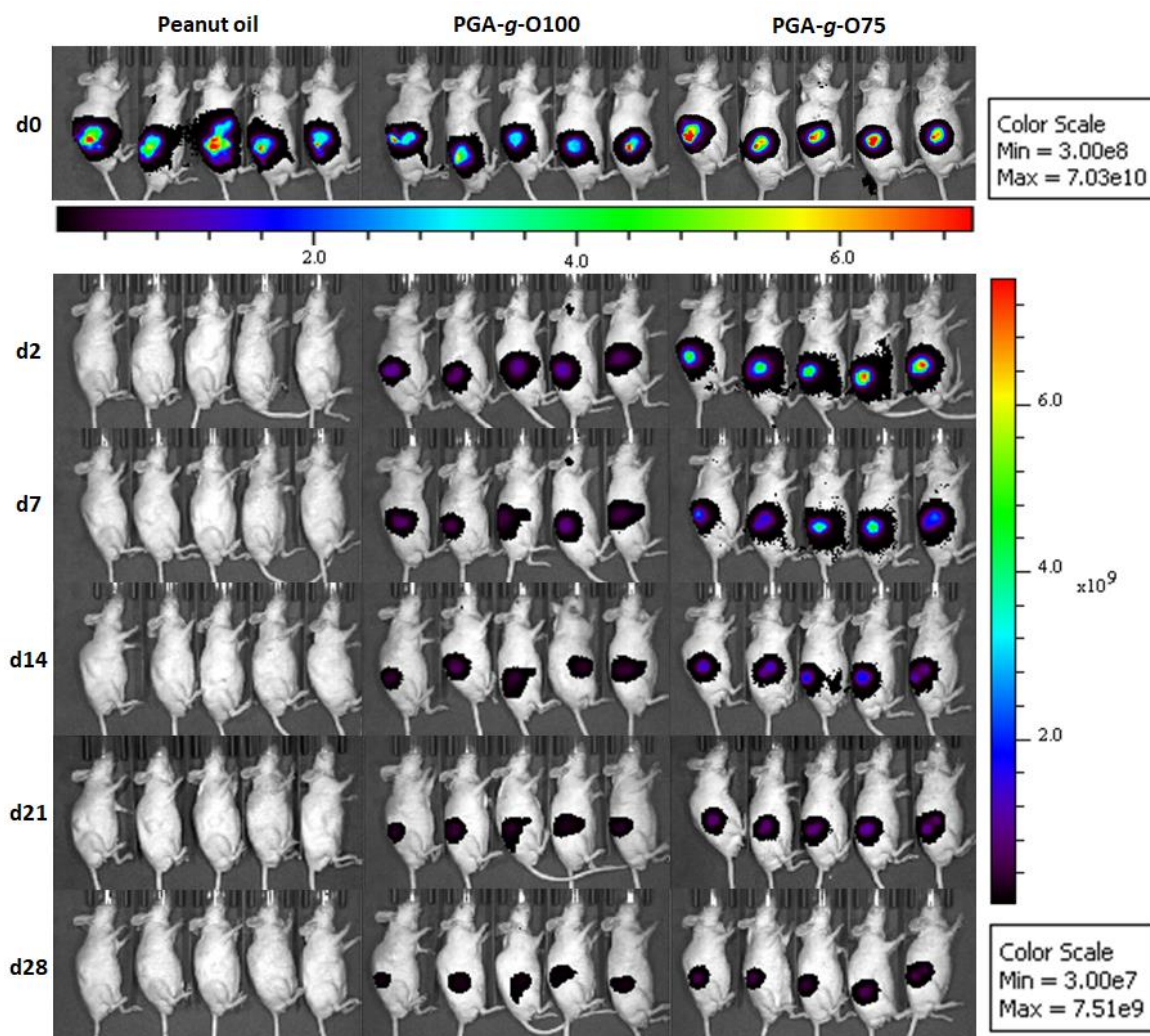

Figure 41. Fluorescence image of SKH1 mice implanted with peanut oil and DiR formulation (Group 1), PGA-g-O100 (Group 2) and PGA-g-O75 (Group 3) during 28 days of the experiment.

The last formulation consisted of PGA backbone 75 mol% grafted with oleic acid. This variant provided a polymer with a higher force to be injected. Nevertheless, the polymer was injected as conceptualized, without the aid of organic solvents. The consistent shape of PGA-*g*-O75 may have aided the release of the dye to be completed within the stipulated period. The transport of substances to the membranes and its relation to the chemical nature of these substances may provide support to this idea [217]. In figure 42, the reader can

observe a detailed image of a mouse from each experimental group as well as the clear fluorescence loss within 28 days.
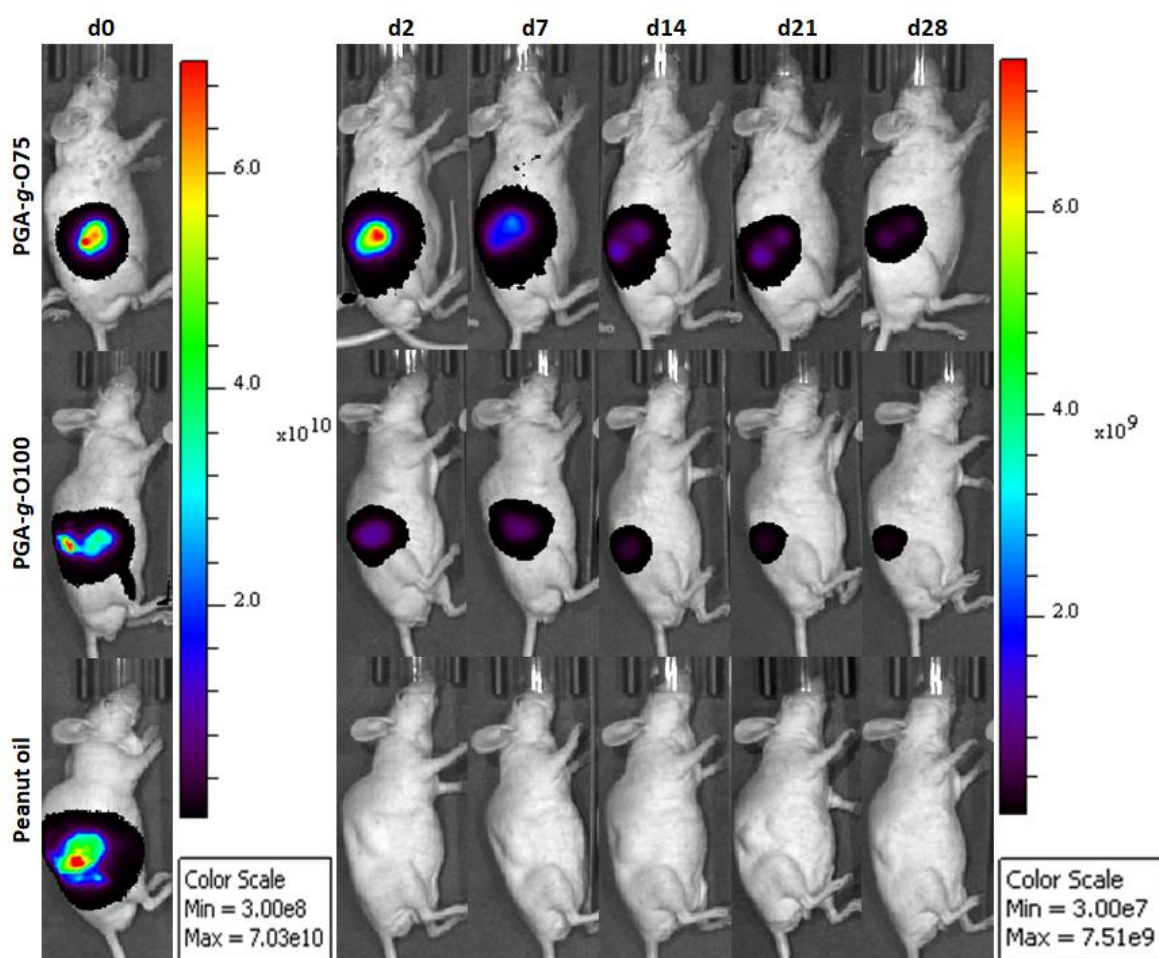

Figure 42. Fluorescence imaging of 3 mice groups over a period of 28 days. Group 1 (oil formulation), Group 2, PGA-g-O100 and Group 3 mice with PGA-g-O75. MFI = maximum fluorescence intensity signal.

As commented above, the less grafted polymer (PGA-*g*-O75), kept its shape almost unchanged while the formulations with peanut oil and PGA-*g*-O100 exhibited a more flattering shape as the time progressed. Similar results were obtained by Chytil et al. [218]. Thus, the dye diffused faster in these cases than for the polymer with a higher distance to be crossed. Although promising results were achieved, the system may be further studied to offer more efficient outcomes. Despite not being covalently conjugated, the fluorescent imaging allowed to track the re-shaping of the polymer *in vivo*. As can be observed in figure 42 (first row), as the polymer moved under the skin, dividing itself into smaller parts, the

correspondent fluorescent signal permitted visualization of the process. As depicted, the method is adequate to track the *in vivo* process in a non-invasive manner throughout the experimentation plan.

At the third week a second group, implanted with PGA-*g*-O100, started showing signals of skin autofluorescence (not shown). As it can be seen in figure 43, the implant, in the lateral position, can be distinguished from the animal autofluorescence in different perspectives when the fluorescence signal is appropriately adjusted.
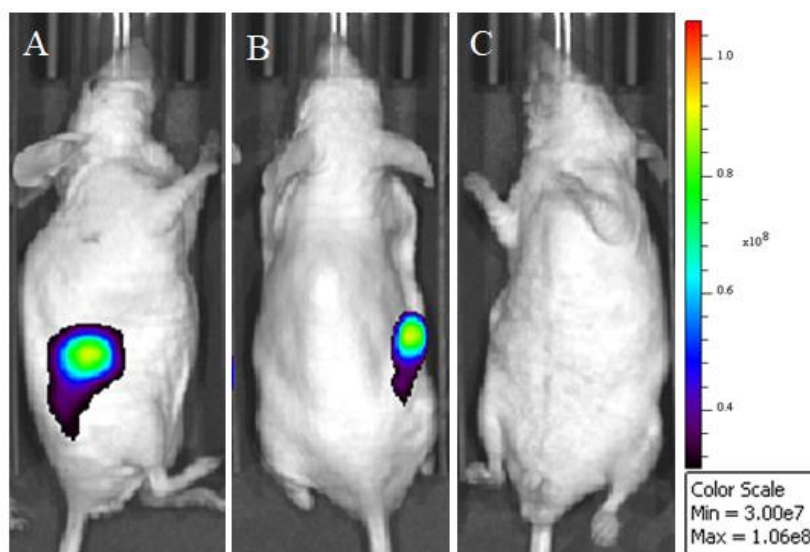

Figure 43. In vivo images of a mouse implanted with PGA-g-O100 in different positions (A, B and C).

3.2.10 *Ex vivo* study of the surrounding tissue and implanted polymers

Ex vivo studies are related to the material after completion of *in vivo* experiments. After sacrificing the mice, the polymeric material was excised and preserved for further analysis. Investigators must evaluate every biomaterial employed in subcutaneous implantation regarding the risks it may pose to the host. In the case of polymers, as it undergoes several steps of the interaction of chemicals during its synthesis, it is important to assure that no leachable substances are present and there exists tissue compatibility. This, however, has to be assessed through *in vivo* experiments to obtain more reliable and broad response [219].

The shape of the polymer, shown in figure 44 injected in the buffer, was expected to be similar when injected *in vivo*. As the material is soft, it would suffer deformation and

accommodate itself according to the force exercised from the tissue. This is indeed, a topic of research itself because of the many aspects it relates to the formulation and the patient, as well as to the performance of the therapy [176]. As reported by Allmendinger et al. [176], the tissue pressure increased linearly when different injection rate and volume were applied to Göttingen minipigs. Besides that, the injection site stiffness is connected to the formulation characteristics and the material performance [220].
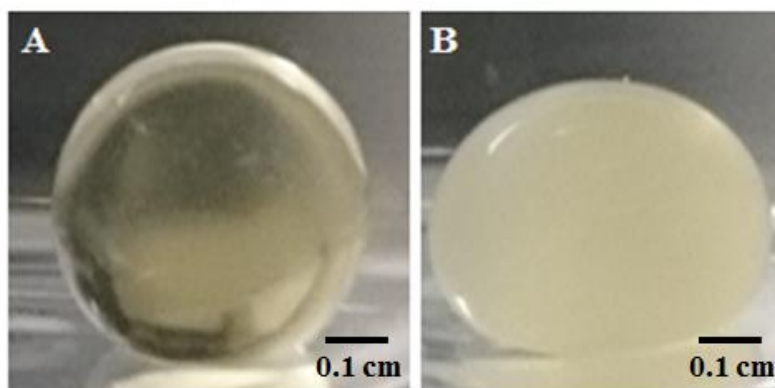

Figure 44. Photograph of in vitro injection of PGA-g-Ox into PBS after 10 min and 24 h.

As it is shown in figure 45, the implanted polymer formed a semi-solid depot, without causing a strong inflammatory reaction or any visual disturbance to the animals. From a macroscopic evaluation, the implant did not harm the animals on the implantation site nor to adjacent tissues (Figure 46). The polymers did not present a swelling behavior *in vivo*, which may be attributed to its lipid content. Thus, the pressure in the subcutaneous tissue is not expected to have increased over time. The pressure at the subcutaneous site is an important factor to be further investigated as the swelling behavior is hydrogels is known to compromise those materials, leading to an increased pressure that can trigger inflammatory reactions and prevent their use [221]. Furthermore, as opposed to systems like hydrogels, PGA-*g*-Ox requires neither solvent exchange nor gelation time, leading to a depot formation shortly after injection as observed in figure 44. The quick depot formation may contribute to an easier controlled release, as the rate of solvents exchange in other systems influence the drug release [11,39], and improve the chances for biocompatibility, as the system is solvent-free. Further investigations should include the drug-polymer interaction and whether this can affect *in vivo* reaction and to which extent, as observed in the literature [222].
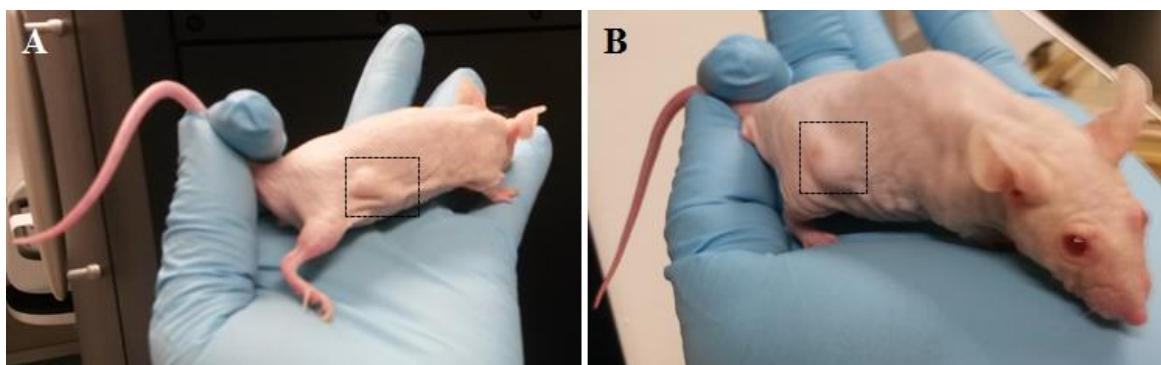
Figure 45. Mice with polymers implanted subcutaneously during the experiments.

When the animals were sacrificed, it was possible to carefully excise most of the polymeric depots and a few of the oil depots. A part of the surrounding skin was taken together to avoid leaking of the viscous polymer. During the experimental period, no macroscopic signal of inflammation was visible on the tissue surrounding the formulations, either the sample nor the controls. Moreover, the behavior no sign of disturbance to the animals was noticed, with all animal's behavior being classified as no harmful. This is an excellent signal of biocompatibility, although care has to be taken when concluding in this direction. After four weeks of the experiment, remaining of the polymer was still present (Figure 46). Showing that the degradation *in vivo* was not complete in this period. This may be achieved by several means, such as modulating the hydrophilic-lipophilic ratio as well as the molar mass of the polymer.
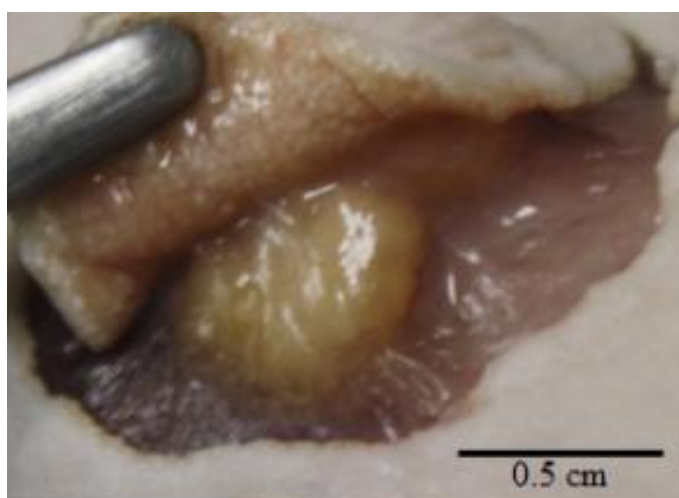

Figure 46. Macroscopic findings of polymers explantation after 28 days.

The removed tissue was embedded in paraffin and stained with eosin-hematoxylin, to stain the nuclei [223]. The fibrous capsule formation must be taken into consideration when analyzing the *in vivo* performance of biomaterials [224]. The fluorescence method showed successful in tracking the distribution of the polymer.

The organs were imaged, however, as it can be seen that the fluorescence was restricted to the implant site. The mobility of the polymer can be tracked over a different time depending on the nature of the implant. As shown in figure 47 it is that the material spreads in the subcutaneous tissue and it can be traced safely until the third week. As the dye quenches, its intensity drops down, and the weakest signal around the main portion of the implant emits a fluorescence signal that is already at the level of autofluorescence (not shown). In this regard, the viscosity of the formulation influences on the mobility and absorption of the polymer more strongly than in the case of PGA-*g*-O75. It requires a careful interpretation to see the outcomes correctly in such cases.
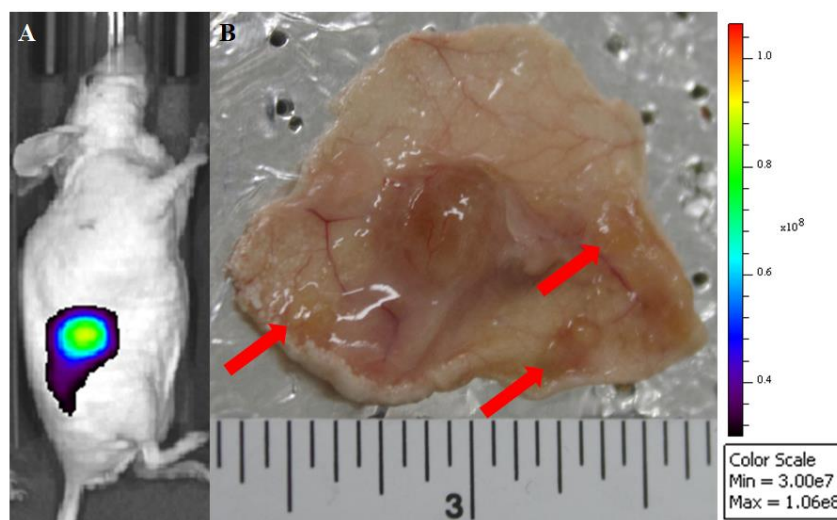

Figure 47. Mouse from the group implanted with PGA-g-O100 (A) section of the skin containing the remaining polymeric material (B), red arrows indicate the locations where the polymer spread to, corresponding to the in vivo fluorescence image.

In the section below (Figure 48), it is possible to see that the fluorescence comes from the polymeric formulation and, as it reaches a low intensity the fragmented parts of the implant contribute to the signal intensity. It is also possible to conclude that the polymer is not spreading further than shown by the *in vivo* fluorescence imaging.
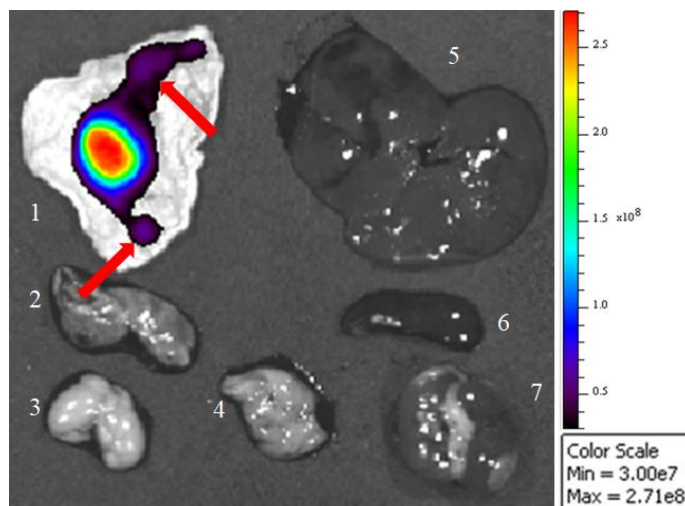
Figure 48. Organs under fluorescence microscopy. It contains the skin (1) section placed with lungs (2), testis (3), pancreas (4), liver (5), spleen (6) and kidneys (7). The red arrows indicate the spread of the polymer to side locations.

The organs were displayed and examined regarding their fluorescence emission compared to the polymer, to ensure that no further movement of the polymer occurred. The organs were placed on the imaging system and recorded together with the polymer to assess a possible fluorescence signal to any part of the animal body. As expected, no signal was detected rather than a strong signal coming from the dye in the polymer. The weak fluorescence signal from the stomach is not likely to be related to the dye signal (Figure 49).
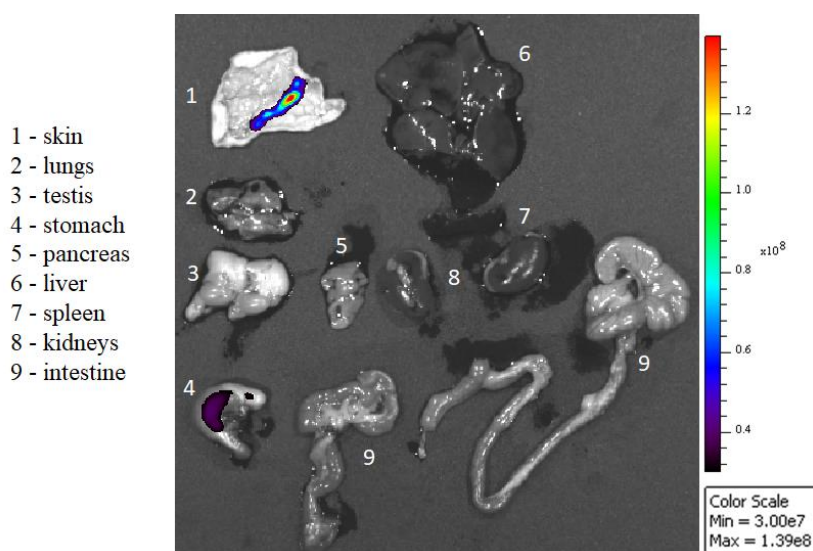

Figure 49. Ex vivo image of skin (1) containing depot material and organs (2-9) displayed. The fluorescence of the dye inside the polymer shows that no leaking of the dye occurred.

3.2.11 Histological results

Figure 50 (A) and (B) displays, the subcutaneous tissue of a mouse without implantation normal structures can be identified. The adipose tissue was not altered, and the cells do not present any reaction. The tissue of mice bearing the peanut oil formulation presents a similar pattern, although in this case, it is noticeable a slightly higher presence of inflammatory cells. As found in the subcutaneous space [225], the typical structures are fairly found in our data.

The body responses to an implanted material are regarded as inflammation, wound healing and foreign body responses as part of tissue and cellular reaction [226]. After implantation, the body will respond through humoral and cellular mechanisms. The response will be specific in the tissue, organ and species levels. Also, the implant characteristics will contribute to the type and extent of the reaction. These characteristics include the physical aspects such as size and shape as well as its chemical properties) [226].

The common reactions may be classified as acute and chronic. They are time and intensity dependents. In the beginning, neutrophils will be present at the injury site. This is part of the inflammation process and composes the phase of the acute response. Following that, macrophages should appear, and neovascularization may accompany. Next, foreign giant body cells are observed. After this stage, fibroblasts start coming, and later fibrosis is placed. In this phase, granulation is being developed, and the foreign body reaction is taking place. Through these processes, mononuclear leucocytes are present [226].

At this stage of four weeks, the initial body reactions, as inflammatory responses, should be finished. However, and even though according to the observations made, no inflammatory reaction was observed at naked eye, a minimal response is expected to have taken place. The recovery and treatment of the *ex vivo* material posed a challenging task to obtain relevant evidence. The lipophilic nature of the polymer and its semi-solid property limit the obtaining of the same after the necessary treatment the material has to undergo during the histology sample preparation. Therefore, the histological material does not contain polymeric remaining.

After undergoing a breakdown, the material should be subjected to macrophage phagocytosis. Following that, giant cells should be present in the tissue. Another important

characteristic to pay attention is that the presence of a drug in the formulation and is pharmacological characteristics may influence the host tissue response. Therefore, performing *in vivo* studies with the vehicle loaded with and without the drug is important to evaluate specific responses.

Similarly, to the tissue from a non-implanted mouse, the mouse with peanut oil depot exhibits the major parts of its structures (Figure 50 C and D). In figure 50 E and F, it is possible to identify the region once probably occupied by the implant. As observed in other subcutaneous implantations [227-229], the surrounding of the cavity displays a concentration of cellular response.

The tissue recovered from the polymer implant was challenging due to the semi-solid nature of the polymer it vanished from the site was the tissue preparation was performed. Here, it is not possible to identify a comprehensive structure, as in the case of the sample from the mouse without an implant. One reason for this is that the tissue sectioned was in contact with the polymeric material and thus its recovery was not an easy task. On the other hand, the material may have some effect when in contact with the subcutaneous tissue, as it is also known that more lipophilic biomaterial surfaces interact more with cells.

In comparison with the peanut oil formulation, the polymer did not differ regarding reaction and effect on the surrounding tissue (see Figure 50 G and H). As found in other studies [230,231], due to the time of implantation, a higher inflammatory response would have occurred during the first days of the experiment. Therefore, we can see only a mild reaction in the tissue once in contact with the implants after 28 days. Figure 51 presents other areas of the same material. The response is fairly similar to all cases, except the tissue with no implant. A higher cell concentration is found especially in the area around the implant site.
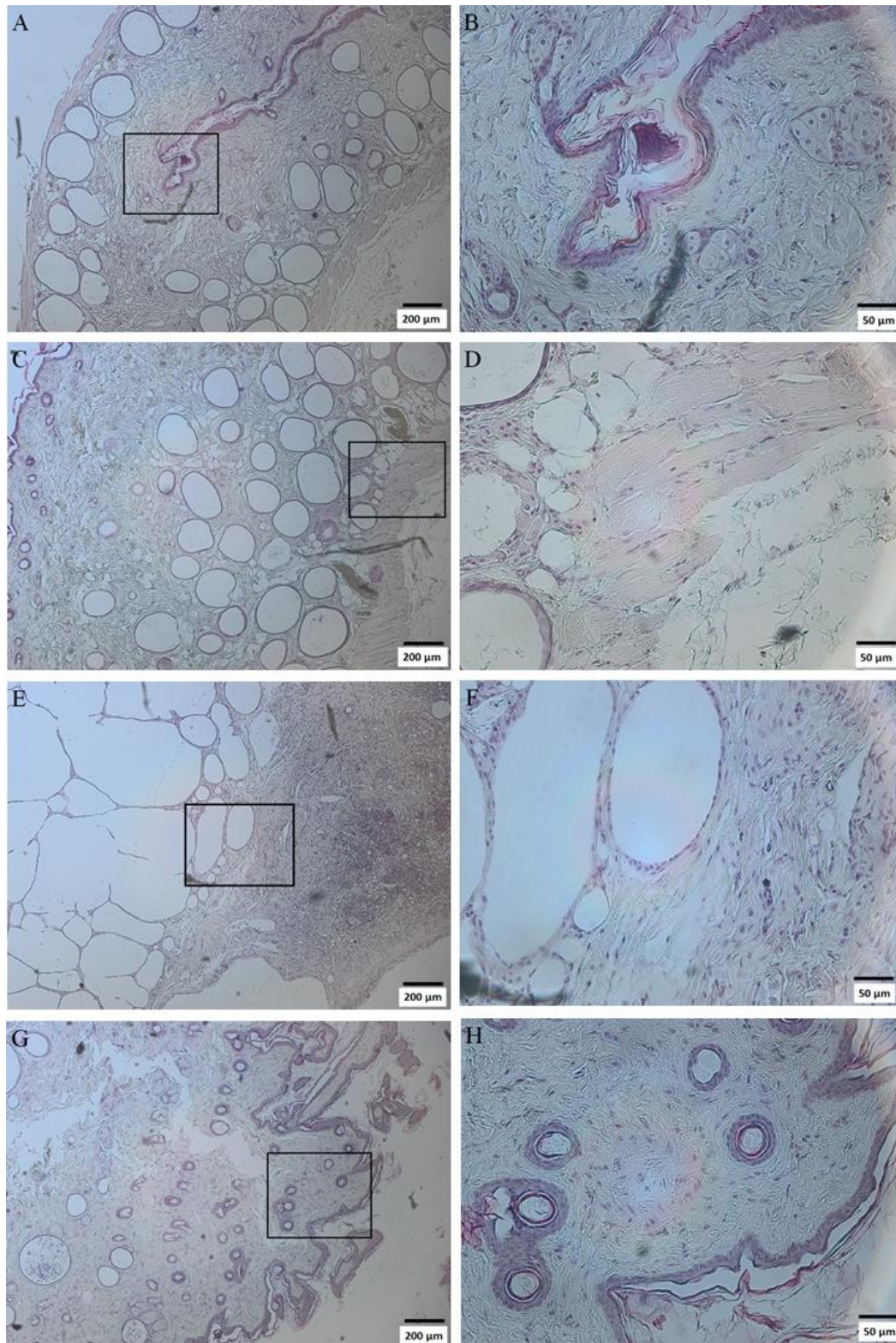
Figure 50. Eosin-Hematoxylin staining images of mice after four weeks. Images (A + B) show the tissue of mice without implantation; (C + D) mice implanted with peanut oil; (E + F) PGA-g-O75 and (G + H) PGA-g-O100 formulations containing DiR.
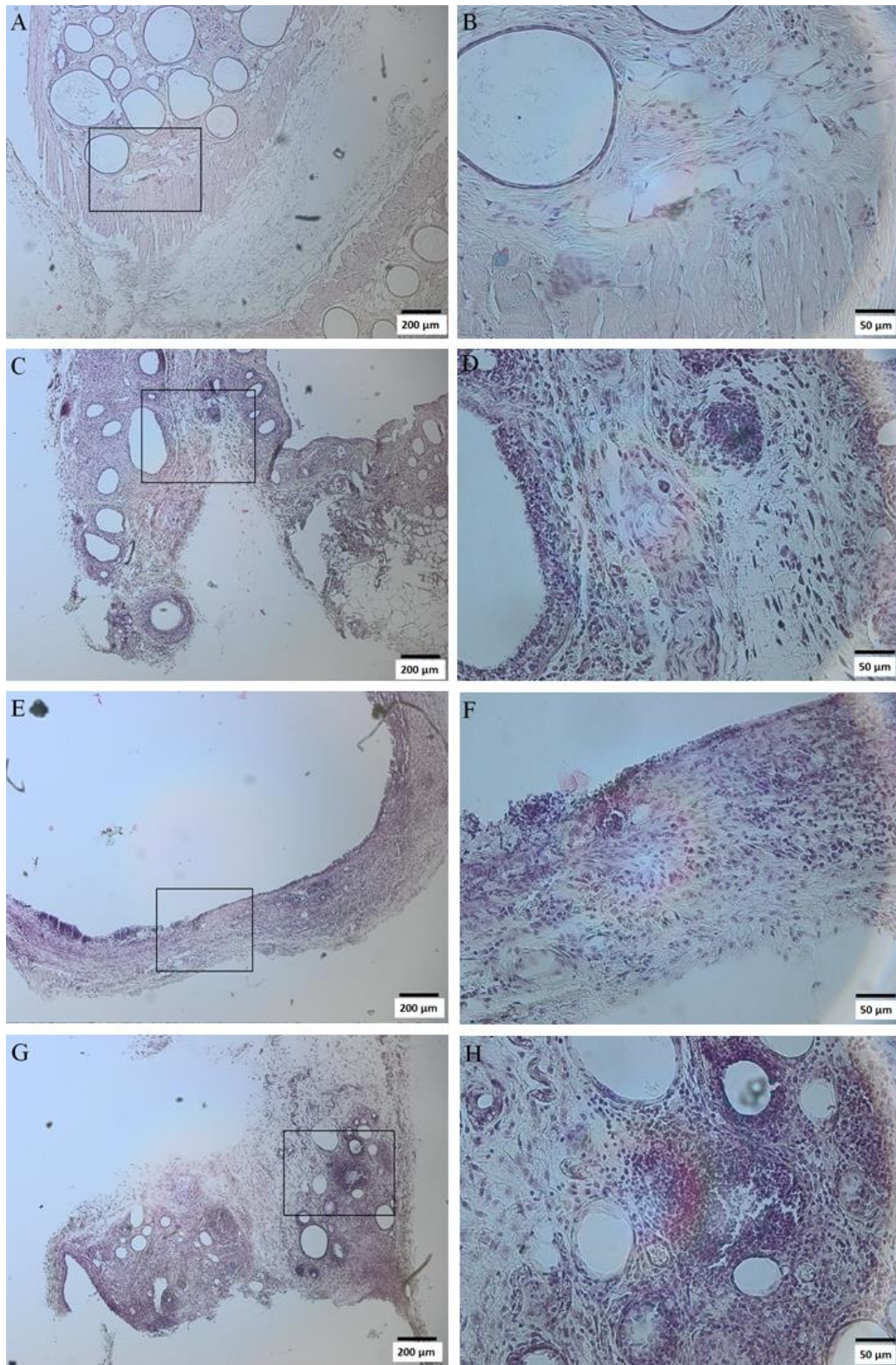
Figure 51. Eosin-Hematoxylin staining images of mice after four weeks. Images (A + B) show the tissue of mice without implantation; (C + D) mice implanted with peanut oil; (E + F) PGA-g-O75 and (G + H) PGA-g-O100 formulations containing DiR.

4 Conclusions

The synthesis and characterization of a polymer, poly(glycerol adipate) (PGA) grafted with a fatty acid has been presented, with interesting formulation properties as an alternative to overcome existing challenges in the parenteral delivery of hydrophilic and lipophilic drugs, especially proteins and peptides.

The synthesis has been performed via enzymatic polycondensation, and the backbone has been further grafted with oleic acid in different variations, named PGA-*g*-Ox. The preparation of poly(glycerol adipate) has been described, and much work has been done regarding its characterization and several studies on nanoparticles for drug release have been published. PGA grafted with fatty acids, such as stearic and oleic acid, has been reported. However, no study has been done using PGA-*g*-Ox as an *in situ* forming implant. PGA-*g*-Ox is interesting as a depot because the properties of this polymer can be modulated according to the experimental setup, due to the hydroxyl pendant group. Comparatively, PLGA, the polymer used in most marketed products does not possess such characteristic and lack the versatility PGA-*g*-Ox offers. In view of that, the grafting with lipophilic molecules allows for a system less vulnerable to an acidic environment and assists in the formulation process.

For its characterization, several techniques have been employed such as SEC, NMR, TGA, contact angle, and ATR-IR. These techniques have confirmed the polymer chemical and physical structure variation with different properties depending on the target polymer while the syringeability was performed by texture analyzer to screen and determine its profile. The grafted versions of the polymer with the highest content of fatty acid allowed for direct injection with no use of organic solvents using a needle size commonly used in the clinics. Solvent-free systems are important because they represent an advance concerning available systems on the market that use up to 60% or organic solvent. It also ensures that no harm to the patients will occur due to the presence of organic solvent in the formulation. Because of its versatility, PGA-*g*-Ox can be used for parenteral delivery, as it requires a force under 30 N using a 25 G needle, which aids to enhance patient acceptance and compliance since the skin is less affected by this needle size when compared to wider

inner diameters used in other systems. The formulation has been injected through a small gauge syringe compatible with clinical requirements.

Other aspects have also been assessed, such as the polymer sterilization with e-beam irradiation and it's *in vitro* toxicity, in which minimal and not compromising effects have been observed. Due to a positive profile from these tests, the material underwent further investigations. The formulation of the semisolid polymer with leuprolide, a peptide used in several diseases, such as and breast cancer, has been carried out and during the *in vitro* studies presented a favorable profile with the controlled release and no burst release. After ion pairing the drug with sodium oleate, its incorporation in the polymer was carried out by simply mixing the two components under 50 ℃. Due to its biodegradable characteristics and solvent-free nature, this polyester in promising for delivering biomolecules and can be used as a tunable platform for drug delivery. Considering that most of the systems investigated for ISFI present a challenging release profile with a burst effect, the presented system can be optimized to deliver peptides for a short as well as a long-term therapy.

To gain insight about the *in vivo* behavior of the polymers, SKH1-Elite nude mice have been injected with different PGA-*g*-Ox formulations and arachnis oil as a control containing a fluorescent lipophilic dye, DiR, as a drug model. The experiment has been carried out for 28 days. The fate of the dye has presented a different fate according to which formulation was tested and, as already discussed for other polymers, the shape and viscosity of the systems influenced the dye release and distribution.

Based on the findings, I believe that this material has a potential to be employed as a depot formulation. It can modulate the release of a drug, can be injected without organic solvents and can be monitored *in vivo* by non-invasive methods. The *ex vivo* experiments showed a good compatibility in comparison with the control group. The histological analysis revealed a mild inflammation. However, no further effect was detected, and the mice have not shown any signal of discomfort when implanted. Macroscopically no harm has been detected during a daily monitoring throughout the whole experiment. Therefore, it may conclude that polymer presents promising characteristics as *in situ* implant and can also be used in different applications in the pharmaceutical field

5 Summary and perspectives

The development of drug delivery systems took place just a few decades ago, and its evolution has brought about considerable therapeutic and economic impact. The progress from preformed implants to *in situ* forming implants has opened new avenues of possibilities to the patients and the healthcare providers. Procedures there were once not convenient and exposed patients with possible complications can be done nowadays by the patients through a syringe in the safety of their home.

The products on the market have aided the patients to combat difficult health conditions so far and will still play an important role in the future. Nevertheless, the continuation of science and technology allow us to look for further improved products. In this regard, an implant that can cause minimal damage to the patients and put them at least risk is not available yet. However, with the progress being made, this will not take a long time until it becomes a reality.

The work with nanoparticles made of PGA has been covered before in our research group and others. Further study in our group has dealt with new possibilities to work with poly(glycerol adipate) as a drug conjugate. This work has contributed to explore and widen the application spectrum PGA offers as a drug delivery vehicle by designing, synthesizing and studying PGA-*g*-Ox from synthesis to preclinical experiments. In this case, the polymer was used as an implant rather than particles. Thereby, we have gained many insights about how an *in situ* forming implant behaves and what it needs to be an optimal system. The results brought by this study have been a step further in the search for an optimal injectable implant. It has provided us with knowledge about the important parameters and composition of polymers and their interaction as part of a formulation and experiments *in vivo*.

However, there are still tasks that should be improved to have a system that works in different setups and as complete as possible. Every new material has to be tested exhaustively to provide safe information and assure the end user does not suffer from careless handling or incomplete development phase. The further search and development process must comply with legal and ethical norms to be fully accepted.

As a continuation of the present research project, the optimization of several parameters and determination of other aspects are still to be performed. The *in vitro*/*in vivo* correlation should be obtained. A systematic *in vivo* study should be carried out with the drug to evaluate the clinical results of the system. Moreover, the optimization and timing of degradability and drug release, as well as a detailed pathway of the degradation products, can be performed, and gain valuable knowledge on the mechanisms governing the fate of PGA-*g*-Ox.

Based on that, the future developments should focus on the clinical aspects of the PGA-*g*-Ox and its performance in small and medium-size animals. This work helped to advance the current knowledge about *in situ* forming implants with an advantageous concept. The expectations are that, through further studies, the material may fulfill its potential and reach clinical use.

6 References

[1] T. Uhlig, T. Kyprianou, F.G. Martinelli, C.A. Oppici, D. Heiligers, D. Hills, X.R. Calvo, P. Verhaert, The emergence of peptides in the pharmaceutical business: From exploration to exploitation, EuPA Open Proteomics 4 (2014) 58-69.

[2] M. Witting, K. Obst, W. Friess, S. Hedtrich, Recent advances in topical delivery of proteins and peptides mediated by soft matter nanocarriers, Biotechnology Advances 6 (2015) 1355-1369.

[3] P. Vlieghe, V. Lisowski, J. Martinez, M. Khrestchatisky, Synthetic therapeutic peptides: science and market, Drug Discovery Today 1-2 (2010) 40-56.

[4] S. Mitragotri, P.A. Burke, R. Langer, Overcoming the challenges in administering biopharmaceuticals: formulation and delivery strategies, Nature Reviews Drug Discovery 13 (2014) 655-672.

[5] K. Fosgerau, T. Hoffmann, Peptide therapeutics: Current status and future directions, Drug Discovery Today 1 (2015) 122-128.

[6] R.P. Evens, Pharma success in product development-Does biotechnology change the paradigm in product development and attrition, American Association of Pharmaceutical Scientists Journal 1 (2016) 281-285.

[7] A.W. Du, M.H. Stenzel, Drug carriers for the delivery of therapeutic peptides, Biomacromolecules 4 (2014) 1097-1114.

[8] C. Wischke, S.P. Schwendeman, Principles of encapsulating hydrophobic drugs in PLA/PLGA microparticles, International Journal of Pharmaceutics 364 (2008) 298-327.

[9] A. Mc Gillicuddy, M. Kelly, C. Sweeney, A. Carmichael, A.M. Crean, L.J. Sahm, Modification of oral dosage forms for the older adult: An Irish prevalence study, International Journal of Pharmaceutics 510 (2016) 386-93.

[10] M. Parent, C. Nouvel, M. Koerber, A. Sapin, P. Maincent, A. Boudier, PLGA in situ implants formed by phase inversion: Critical physicochemical parameters to modulate drug release, Journal of Controlled Release 172 (2013) 292-304.

[11] S. Kempe, K. Mäder, In situ forming implants - an attractive formulation principle for parenteral depot formulations, Journal of Controlled Release 161 (2012) 668-679.

[12] A. Exner, G.M. Saidel, Drug-eluting polymer implants in cancer therapy, Expert Opinion on Drug Delivery 5 (2008) 775-788.

[13] R.J.C. Bose, S.H. Lee, H. Park, Biofunctionalized nanoparticles: an emerging drug delivery platform for various disease treatments, Drug Discovery Today 8 (2016)

1303-1312.

[14] B.S. Pattni, V.V. Chupin, V.P. Torchilin, New developments in liposomal drug delivery, Chemical Reviews 115 (2015) 10938-10966.

[15] J. Gong, R. Jaiswal, P. Dalla, F. Luk, M. Bebawy, Microparticles in cancer: A review of recent developments and the potential for clinical application, Seminars in Cell and Development Biology 40 (2015) 35-40.

[16] J. Li, D.J. Mooney, Designing hydrogels for controlled drug delivery, Nature Reviews Materials 1 (2016) 1-17.

[17] P. Agarwal, I.D. Rupenthal, Injectable implants for the sustained release of protein and peptide drugs, Drug Discovery Today 7-8 (2013) 337-349.

[18] Y. Zhang, H.F. Chan, K.W. Leong, Advanced materials and processing for drug delivery: The past and the future, Advanced Drug Delivery Reviews 65 (2013) 104-120.

[19] B.J. Bruno, G.D. Miller, C.S. Lim, Basics and recent advances in peptide and protein drug delivery, Therapeutic Delivery 11 (2014) 1443-1467.

[20] M. Parent, I. Clarot, S. Gibot, M. Derive, P. Maincent, P. Leroy, A. Boudier, One-week in vivo sustained release of a peptide formulated into in situ forming implants, International Journal of Pharmaceutics 521 (2017) 357-360.

[21] F. Plourde, A. Motulsky, A.C. Couffin-Hoarau, D. Hoarau, H. Ong, J.C. Leroux, First report on the efficacy of L-alanine-based in situ-forming implants for the long-term parenteral delivery of drugs, Journal of Controlled Release 108 (2005) 433-441.

[22] O. Sartor, Eligard: Leuprolide acetate in a novel sustained-release delivery system, Urology 61 (2003) 25-31.

[23] O. Peralta, S. Diaz, H. Croxatto, Subdermal contraceptive implants, The Journal of Steroid Biochemistry and Molecular Biology 53 (1995) 223-226.

[24] H.P. Merkle, Drug delivery's quest for polymers: Where are the frontiers? Dedicated to Robert Gurny on the occasion of his 70th birthday, European Journal of Pharmaceutics and Biopharmaceutics 97 (2015) 293-303.

[25] J. Folkman, D.M. Long, The use of silicone rubber as a carrier for prolonged drug therapy, Journal of Surgical Research 3 (1964) 139-142.

[26] T.M. Rudlang, K. Brasso, Efficacy and tolerability of the histrelin implant, Austin Journal of Urology 2 (2016) 2-4.

[27] E.L. Weber, Cerebral edema associated with Gliadel wafers: Two case studies, Neuro Oncology 1 (2005) 84-89.

[28] R.L. Dunn, J.P. English, D.R. Cowsar, D.P. Vanderbilt, inventors; Atrix Laboratories, Inc., Fort Collins, CO assignee, Biodegradable in situ forming implants and methods of producing the same, US Patent No. 4938 763. July 3, 1990.

[29] S. Kempe, H. Metz, K. Mäder, Do in situ forming PLG/NMP implants behave similar in vitro and in vivo? A non-invasive and quantitative EPR investigation on the mechanisms of the implant formation process, Journal of Controlled Release 3 (2008) 220-225.

[30] L. Yuan, Y. Wu, Q-S. Gu, H. El-Hamshary, M. El-Newehy, X. Mo, Injectable photo crosslinked enhanced double-network hydrogels from modified sodium alginate and gelatin, International Journal of Biological Macromolecules 96 (2016) 569-577.

[31] J. Qu, X. Zhao, P.X. Ma, B. Guo, pH-responsive self-healing injectable hydrogel based on N-carboxyethyl chitosan for hepatocellular carcinoma therapy, Acta Biomaterialia 58 (2017) 168-180.

[32] R.A.A. Muzzarelli, Genipin-crosslinked chitosan hydrogels as biomedical and pharmaceutical aids, Carbohydrate Polymers 1 (2009) 1-9.

[33] L. Liu, Q. Gao, X. Lu, H. Zhou, In situ forming hydrogels based on chitosan for drug delivery and tissue regeneration, Asian Journal of Pharmaceutical Sciences 6 (2016) 673-683.

[34] E. Ruel-Gariépy, J.C. Leroux, In situ-forming hydrogels - Review of temperature-sensitive systems, European Journal of Pharmacy and Biopharmacy 2 (2004) 409-426.

[35] C. Wischke, C. Schneider, A.T. Neffe, A. Lendlein, Polyalkylcyanoacrylates as in situ formed diffusion barriers in multimaterial drug carriers, Journal of Controlled Release 3 (2013) 321-328.

[36] A. Vintiloiu, J-C. Leroux, Organogels and their use in drug delivery - A review, Journal of Controlled Release 3 (2008) 179-192.

[37] R.R.S. Thakur, H.L. McMillan, D.S. Jones, Solvent induced phase inversion-based in situ forming controlled release drug delivery implants, Journal of Controlled Release 1 (2014) 8-23.

[38] X. Zhang, J.K. Jackson, W. Wong, W. Min, T. Cruz, W.L. Hunter, H.M. Burt, Development of biodegradable polymeric paste formulations for taxol: An in vitro and in vivo study, International Journal of Pharmaceutics 2 (1996) 199-208.

[39] S. Supper, N. Anton, J. Boisclair, N. Seidel, M. Riemenschnitter, C. Curdy, T. Vandamme, Chitosan/glucose 1-phosphate as new stable in situ forming depot system for controlled drug delivery, European Journal of Pharmacy and Biopharmacy 2 (2014) 361-373.

[40] K.Y. Lee, D.J. Mooney, Alginate: properties and biomedical applications, Progress in Polymer Science 1 (2013) 106-126.

[41] N. Nasongkla, A. Boongird, S. Hongeng, C. Manaspon, N. Larbcharoensub, Preparation and biocompatibility study of in situ forming polymer implants in rat brains, Journal of Materials Science Materials Medicine 2 (2012) 497-505.

[42] M.P. Do, C. Neut, H. Metz, E. Delcourt, K. Mäder, J. Siepmann, In-situ forming composite implants for periodontitis treatment: How the formulation determines system performance, Internation Journal of Pharmaceutics 1-2 (2015) 38-51.

[43] N.H. Stoller, L.R. Johnson, S. Trapnell, C.Q. Harrold, S. Garrett, The pharmacokinetic profile of a biodegradable controlled-release delivery system containing doxycycline compared to systemically delivered doxycycline in gingival crevicular fluid, saliva, and serum, Journal of Periodontology 10 (1998) 1085-1091.

[44] A. Büchter, U. Meyer, B. Kruse-Lösler, U. Joos, J. Kleinheinz, Sustained release of doxycycline for the treatment of peri-implantitis: Randomised controlled trial, British Journal of Oral Maxillofacial Surgery 5 (2004) 439-444.

[45] K. Mäder, B. Gallez, K.J. Liu, H.M. Swartz, Non-invasive in vivo characterization of release processes in biodegradable polymers by low-frequency electron paramagnetic resonance spectroscopy, Biomaterials 4 (1996) 457-461.

[46] A. Shenderova, A.G. Ding, S.P. Schwendeman, Potentiometric method for determination of microclimate pH in poly(lactic-co-glycolic acid) films, Macromolecules 37 (2004) 10052-10058.

[47] L. Li, S.P. Schwendeman, Mapping neutral microclimate pH in PLGA microspheres, Journal of Controlled Release 1-3 (2005) 163-173.

[48] A. Schädlich, S. Kempe, K. Mäder, Non-invasive in vivo characterization of microclimate pH inside in situ forming PLGA implants using multispectral fluorescence imaging, Journal of Controlled Release 1 (2014) 52-62.

[49] Y. Tang, J. Singh, Biodegradable and biocompatible thermosensitive polymer based injectable implant for controlled release of protein, International Journal of Pharmaceutics 1-2 (2009) 34-43.

[50] W.Y. Dong, M. Körber, V.L. Esguerra, R. Bodmeier, Stability of poly(d,l-lactide-co-glycolide) and leuprolide acetate in in-situ forming drug delivery systems, Journal of Controlled Release 2 (2006) 158-167.

[51] L. Wang, A. Wang, X. Zhao, X. Liu, D. Wang, F. Sun, Y. Li, Design of a long-term antipsychotic in situ forming implant and its release control method and mechanism, International Journal of Pharmaceutics 2 (2012) 284-292.

[52] K. Schoenhammer, H. Petersen, F. Guethlein, A. Goepferich, Injectable in situ forming depot systems: PEG-DAE as novel solvent for improved PLGA storage stability, International Journal of Pharmaceutics 1-2 (2009) 33-39.

[53] K. Agossa, M. Lizambard, T. Rongthong, E. Delcourt-Debruyne, J. Siepmann, F. Siepmann, Physical key properties of antibiotic-free, PLGA/HPMC-based in-situ forming implants for local periodontitis treatment, International Journal of Pharmaceutics 1-2 (2017) 282-293.

[54] L.R. Asmus, R. Gurny, M. Möller, Solutions as solutions – Synthesis and use of a liquid polyester excipient to dissolve lipophilic drugs and formulate sustained-release

parenterals, European Journal of Pharmaceutics and Biopharmaceutics 3 (2011) 584-591.

[55]   L.R. Asmus, J.C. Tille, B. Kaufmann, L. Melander, T. Weiss, K. Vessman, W. Koechling, G. Schwach, R. Gurny, M. Möller, In vivo biocompatibility, sustained-release and stability of triptorelin formulations based on a liquid, degradable polymer, Journal of Controlled Release 3 (2013) 199-206.

[56]   M-H. Ki, J-L. Lim, J-Y. Ko, S-H. Park, J-E. Kim, H-J. Cho, E-S. Park, D-D. Kim, A new injectable liquid crystal system for one month delivery of leuprolide, Journal of Controlled Release 185 (2014) 62-70.

[57]   Y. Wu, L. Wang, X. Zhao, S. Hou, B. Guo, P.X. Ma, Self-healing supramolecular bioelastomers with shape memory property as a multifunctional platform for biomedical applications via modular assembly, Biomaterials 104 (2016) 18-31.

[58]   A. Nadim, S.N. Khorasani, M. Kharaziha, S.M. Davoodi, Design and characterization of dexamethasone-loaded poly(glycerol sebacate)-poly caprolactone/gelatin scaffold by coaxial electro spinning for soft tissue engineering, Materials Science and Engineering: C 78 (2017) 47-58.

[59]   Á. Conejero-García, H.R. Gimeno, Y.M. Sáez, G. Vilariño-Feltrer, I. Ortuño-lizarán, A. Vallés-lluch, Correlating synthesis parameters with physicochemical properties of poly(glycerol sebacate), European Polymer Journal 87 (2017) 406-419.

[60]   S.H. Zaky, K.W. Lee, J. Gao, A. Jensen, K. Verdelis, Y. Wang, A.J. Almarza, C. Sfeir, Poly(glycerol sebacate) elastomer supports bone regeneration by its mechanical properties being closer to osteoid tissue rather than to mature bone, Acta Biomaterialia 54 (2017) 95-106.

[61]   L. Gustini, B.A.J. Noordover, C. Gehrels, C. Dietz, C.E. Koning, Enzymatic synthesis and preliminary evaluation as coating of sorbitol-based, hydroxy-functional polyesters with controlled molecular weights, European Polymer Journal 67 (2015) 459-475.

[62]   S. Selvam, M.V. Pithapuram, S.P. Victor, J. Muthu, Injectable in situ forming xylitol – PEG-based hydrogels for cell encapsulation and delivery, Colloids and Surfaces B: Biointerfaces 126 (2015) 35-43.

[63]   N. Babanejad, A. Farhadian, I. Omrani, M.R. Nabid, Design, characterization and in vitro evaluation of novel amphiphilic block sunflower oil-based polyol nanocarrier as a potential delivery system: Raloxifene-hydrochloride as a model, Materials Science and Engineering: C 78 (2017) 59-68.

[64]   Y. Zhang, S. Spinella, W. Xie, J. Cai, Y. Yang, Y. Wang, Y-Z. Wang, R.A. Gross, Polymeric triglyceride analogs prepared by enzyme-catalyzed condensation polymerization, European Polymer Journal 4 (2013) 793-803.

[65]   T. Chongcharoenchaikul, P. Thamyongkit, S. Poompradub, Synthesis, characterization and properties of a bio-based poly(glycerol azelate) polyester, Materials Chemistry and Physics 177 (2016) 485-495.

[66]   J. Natarajan, S. Movva, G. Madras, K. Chatterjee, Biodegradable galactitol based crosslinked polyesters for controlled release and bone tissue engineering, Materials Science Engineering: C 77 (2017) 534-547.

[67]   T. Debuissy, E. Pollet, L. Avérous, Synthesis and characterization of biobased poly (butylene succinate- ran -butylene adipate). Analysis of the composition- dependent physicochemical properties, European Polymer Journal 87 (2016) 84-98.

[68]   R.B. Patel, L. Solorio, H. Wu, T. Krupka, A.A. Exner, Effect of injection site on in situ implant formation and drug release in vivo, Journal of Controlled Release 3 (2010) 350-358.

[69]   M.J. Rodriguez, J. Brown, J. Giordano, S.J. Lin, G. Fiorenzo, D.L. Kaplan, Silk based bioinks for soft tissue reconstruction using 3-dimensional (3D) printing with in vitro and in vivo assessments, Biomaterials 117 (2016) 105-115.

[70]   K.J.A. Kairemo, PET/Computed Tomography for radiation therapy planning of prostate cancer, Positron Emission Tomography 2 (2017) 257-267.

[71]   J. Hickson, In vivo optical imaging: Preclinical applications and considerations, Urologic Oncology: Seminars and Original Investigations 3 (2009) 295-297.

[72]   K. Lei, Y. Chen, J. Wang, X. Peng, L. Yu, J. Ding, Non-invasive monitoring of in vivo degradation of a radiopaque thermoreversible hydrogel and its efficacy in preventing post-operative adhesions, Acta Materialia 55 (2017) 396-409.

[73]   L. Solorio, B.M. Babin, R.B. Patel, J. Mach, N. Azar, A.A. Exner, Noninvasive characterization of in situ forming implants using diagnostic ultrasound, Journal of Controlled Release 2 (2010) 183-190.

[74]   L. Solorio, A.M. Olear, J.I. Hamilton, R.B. Patel, A.C. Beiswenger, J.E. Wallace, H. Zhou, A.A. Exner, Noninvasive characterization of the effect of varying PLGA molecular weight blends on in situ forming implant behavior using ultrasound imaging, Theranostics 11 (2012) 1064-1077.

[75]   X. Leng, B. Liu, B. Su, M. Liang, L. Shi, S. Li, S. Qu, X. Fu, Y. Liu, M. Yao, D.L. Kaplan, Y. Wang, X. Wang, In situ ultrasound imaging of silk hydrogel degradation and neovascularization, Journal of Tissue Engineering and Regenerative Medicine 3 (2015) 822-830.

[76]   K. Mäder, G. Bacic, A. Domb, O. Elmalak, R. Langer, H.M. Swartz, Noninvasive in vivo monitoring of drug release and polymer erosion from biodegradable polymers by EPR spectroscopy and NMR imaging, Journal of Pharmaceutical Sciences 1 (1997) 126-134.

[77]   H. Metz, K. Mäder, Benchtop-NMR and MRI-A new analytical tool in drug delivery research, International Journal of Pharmaceutics 2 (2008) 170-175.

[78]   R. López-Cebral, M. Martín-Pastor, B. Seijo, A. Sanchez, Progress in the characterization of bio-functionalized nanoparticles using NMR methods and their applications as MRI contrast agents, Progress in Nuclear Magnetic Resonance

Spectroscopy 79 (2014) 1-13.

[79] B. Madhu, I. Elmroth, A. Lundgren, B. Abrahamsson, B. Soussi, B. Group, A novel evaluation of subcutaneous formulations by in vivo magnetic resonance imaging (MRI), Pharmacological Research 3 (2002) 3-8.

[80] A.S. Mikhail, A. Partanen, P. Yarmolenko, A.M. Venkatesan, B.J. Wood, Magnetic resonance-guided drug delivery, Magnetic Resonance Imaging Clinics of North America 2 (2015) 643-655.

[81] J.P.M. van Duynhoven, Food and Nutritional Science, Applications of Magnetic Resonance, (2010) 663-670. In: Encyclopedia of Spectroscopy and Spectrometry (Second Edition), Ed. J.C. Lindon, Elsevier, Oxford (2010) 3312.

[82] H. Nitzsche, H. Metz, A. Lochmann, A. Bernstein, G. Hause, T. Groth, K. Mäder, Characterization of scaffolds for tissue engineering by benchtop-magnetic resonance imaging, Tissue Engineering: Part C Methods 3 (2009) 513-521.

[83] A. Besheer, H. Caysa, H. Metz, T. Mueller, J. Kressler, K. Mäder, Benchtop-MRI for in vivo imaging using a macromolecular contrast agent based on hydroxyethyl starch (HES), International Journal of Pharmaceutics 1-2 (2011) 196-203.

[84] A. Belete, H. Metz, T. Mueller, K. Mäder, Benchtop MRI for pharmacokinetic evaluation of two aqueous-based nano-scaled formulations of oleic acid stabilized magnetite nanocrystals, Drug Development and Industrial Pharmacy 3 (2013) 1-9.

[85] H. Caysa, H. Metz, K. Mäder, T. Mueller, Application of benchtop-magnetic resonance imaging in a nude mouse tumor model, Journal of Experimental and Clinical Cancer Research 30 (2011) 1-7.

[86] S. Kempe, H. Metz, P.G.C. Pereira, Mäder K, Non-invasive in vivo evaluation of in situ forming PLGA implants by benchtop magnetic resonance imaging (BT-MRI) and EPR spectroscopy, European Journal Pharmaceutics and Biopharmaceutics 1 (2010) 102-108.

[87] J. Walldorf, M. Hermann, M. Porzner, S. Pohl, H. Metz, K. Mäder, In-vivo monitoring of acute DSS-colitis using colonoscopy, high resolution ultrasound and bench-top magnetic resonance imaging in mice, European Radiology 10 (2015) 2984-2991.

[88] M.V.S. Elipe, R.R. Milburn, Monitoring chemical reactions by low-field benchtop NMR at 45MHz: pros and cons, Magnetic Resonance in Chemistry 6 (2015) 437-443.

[89] S.D. Riegel, G.M. Leskowitz, Benchtop NMR spectrometers in academic teaching, Trends in Analytical Chemistry 83 (2016) 29-38.

[90] G.G. Stokes, On the change refrangibility of light, Philosophical Transactions of the Royal Society of London, 463 (1852) 463-562.

[91] F. Leblond, S.C. Davis, P.A. Valdés, B.W. Pogue, Pre-clinical whole-body fluorescence imaging: Review of instruments, methods and applications, Journal Photochemistry and Photobiology B: Biology 1 (2010) 77-94.

[92]   T. Etrych, H. Lucas, O. Janoušková, P. Chytil, T. Mueller, K. Mäder, Fluorescence optical imaging in anticancer drug delivery, Journal of Controlled Release 226 (2016) 168-181.

[93]   M. Gumbleton, D.J. Stephens, Coming out of the dark: The evolving role of fluorescence imaging in drug delivery research, Advanced Drug Delivery Reviews 1 (2005) 5-15.

[94]   H. Cho, C.S. Cho, G.L. Indig, A. Lavasanifar, M.R. Vakili, G.S. Kwon, Polymeric micelles for apoptosis-targeted optical imaging of cancer and intraoperative surgical guidance, PLoS ONE 2 (2014a) e89968.

[95]   M. Grossi, M. Morgunova, S. Cheung, D. Scholz, E. Conroy, M. Terrile, A. Panarella, J.C. Simpson, W.M. Galagher, D.F. O'Shea, Lysosome triggered near-infrared fluorescence imaging of cellular trafficking processes in real time, Nature Communications 7 (2016) 1-13.

[96]   S. Luo, E. Zhang, Y. Su, T. Cheng, C. Shi, A review of NIR dyes in cancer targeting and imaging, Biomaterials 29 (2011) 7127-7138.

[97]   Y. Chen, W. Zhang, Y. Huang, F. Gao, X. Fang, In vivo biodistribution and anti-tumor efficacy evaluation of doxorubicin and paclitaxel-loaded pluronic micelles decorated with c (RGDyK) peptide, PLoS ONE 3 (2016) e0149952.

[98]   Z. Lin, S. Xu, W. Gao, H. Hu, M. Chen, Y. Wang, B. He, W. Dai, H. Zhang, X. Wang, A. Dong, Y. Yin, O. Uhang, A comparative investigation between paclitaxel nanoparticle- and nanocrystal-loaded thermosensitive PECT hydrogels for peri-tumoural administration, Nanoscale 8 (2016) 18782-18791.

[99]   B. Aghabarari, M. Ghiaci, S. Ghaed, Esterification of fatty acids by new ionic liquids as acid catalysts, Journal of the Taiwan Institute of Chemical Engineers 45 (2014) 431-435.

[100] Y. Yu, D. Wu, C. Liu, Z. Zhao, Y. Yang, Q. Li, Lipase/esterase-catalyzed synthesis of aliphatic polyesters via polycondensation : A review, Process Biochemistry 7 (2012) 1027-1036.

[101] E.M. Anderson, K.M. Larsson, O. Kirk, One biocatalyst - many applications: The use of Candida antarctica B-lipase in organic synthesis, Biocatalysis Biotransformation 16 (1998) 181-204.

[102] S. Kobayashi, Review Lipase-catalyzed polyester synthesis - A green polymer chemistry, Proceedings of the Japan Academy. Series B, Physical and Biological Sciences 4 (2010) 338-365.

[103] A. Idris, A. Bukhari, Immobilized Candida antarctica lipase B : Hydration, stripping off and application in ring opening polyester synthesis, Biotechnology Advances 3 (2012) 550-563.

[104] J. Uppenberg, M.T. Hansen, S. Patkar, T.A. Jones, The sequence, crystal structure determination and refinement of two crystal forms of lipase B from Candida

antarctica, Structure 4 (1994) 293-308.

[105] Y. Poojari, S.J. Clarson, Biocatalysis and agricultural biotechnology thermal stability of Candida antarctica lipase B immobilized on macroporous acrylic resin particles in organic media, Biocatalysis and Agricultural Biotechnology 1 (2013) 7-11.

[106] M.R. Ganjalikhany, B. Ranjbar, A.H. Taghavi, T.T. Moghadam, Functional Motions of Candida antarctica Lipase B: A Survey through open-close conformations, PloS one 7 (2012) 1-11.

[107] M. Jbeily, T. Naolou, M.H. Bilal, E. Amado, J. Kressler, Enzymatically synthesized polyesters with pendent OH groups as macroinitiators for the preparation of well-defined graft copolymers by atom transfer radical polymerization, Polymer International 63 (2014) 894-901.

[108] T. Tsujimoto, H. Uyama, S. Kobayashi, Enzymatic synthesis of cross-linkable polyesters from renewable resources, Biomacromolecules 2 (2001) 29-31.

[109] P.B. Juhl, K. Doderer, F. Hollmann, O. Thum, J. Pleiss, Engineering of Candida antarctica lipase B for hydrolysis of bulky carboxylic acid esters, Journal of Biotechnology 4 (2010) 474-480.

[110] B.J. Kline, E.J. Beckman, A.J. Russell, One-step biocatalytic synthesis of linear polyesters with pendant hydroxyl groups, Journal of the American Chemical Society, 120 (1998) 9475-9480.

[111] C.A.G. Quispe, C.J.R. Coronado, J.A. Carvalho, Glycerol: Production, consumption, prices, characterization and new trends in combustion, Renewable and Sustainable Energy Reviews 27 (2013) 475-493.

[112] V.M. Weiss, T. Naolou, G. Hause, J. Kuntsche, J. Kreßler, K. Mäder, Poly(glycerol adipate)-fatty acid esters as versatile nanocarriers: From nanocubes over ellipsoids to nanospheres, Journal of Controlled Release 1 (2012) 156-164.

[113] S. Dai, L. Xue, M. Zinn, Z. Li, Enzyme-catalyzed polycondensation of polyester macrodiols with divinyl adipate: A green method for the preparation of thermoplastic block copolyesters, Biomacromolecules 10 (2009) 3176-3181.

[114] U. Edlund, A-C. Albertsson, Polyesters based on diacid monomers, Advanced Drug Delivery Reviews 4 (2003) 585-609.

[115] W.H. Carothers, An introduction to the general theory of condensation polymers, Journal of the American Chemical Society, 51 (1929) 2548-2559.

[116] P. Kallinteri, S. Higgins, G.A. Hutcheon, C.B. St. Pourçain, M.C. Garnett, Novel functionalized biodegradable polymers for nanoparticle drug delivery systems, Biomacromolecules 6 (2005) 1885-1894.

[117] S. Puri, P. Kallinteri, S. Higgins, G.A. Hutcheon, M.C. Garnett, Drug incorporation and release of water soluble drugs from novel functionalised poly(glycerol adipate) nanoparticles, Journal of Controlled Release 125 (2008) 59-67.

[118] T. Naolou, M. Jbeily, P. Scholtysek, J. Kressler, Synthesis and characterization of

stearoyl modified poly(glycerol adipate) containing ATRP initiator on its backbone, Advanced Materials Research 812 (2013) 1-11.

[119] V. Taresco, R.G. Creasey, J. Kennon, G. Mantovani, C. Alexander, J.C. Burley, M.C. Garnett, Variation in structure and properties of poly(glycerol adipate) via control of chain branching during enzymatic synthesis, Polymer 89 (2016) 41-49.

[120] D. Pfefferkorn, M. Pulst, T. Naolou, K. Busse, J. Balko, J. Kressler, Crystallization and melting of poly(glycerol adipate)-based graft copolymers with single and double crystallizable side chains, Journal of Polymer Science: Part B Polymer Physics 21 (2013) 1581-1591.

[121] C. Korupp, R. Weberskirch, J.J. Müller, A. Liese, L. Hilterhaus, Scaleup of lipase-catalyzed polyester synthesis, Organic Process Research and Development 14 (2010) 1118-1124.

[122] V.M. Weiss, T. Naolou, E. Amado, K. Busse, K. Mäder, J. Kressler, Formation of structured polygonal nanoparticles by phase-separated comb-like polymers, Macromolecular Rapid Communications 33 (2012) 35-40.

[123] W. Meng, T.L. Parker, P. Kallinteri, D.A. Walker, S. Higgins, G.A. Hutcheon, M.C. Garnett, Uptake and metabolism of novel biodegradable poly(glycerol-adipate) nanoparticles in DAOY monolayer, Journal of Controlled Release 3 (2006) 314-321.

[124] D.R. Vardon, M.A. Franden, C. W. Johnson, E.M. Karp, M.T. Guarnieri, J.G., Linger, M.J. Salm, T.J. Strathmann, G.T. Beckham, Adipic acid production from lignin, Energy and Environmental Science 8 (2015) 617-628.

[125] Z. Gholami, A. Zuhairi, K. Lee, Dealing with the surplus of glycerol production from biodiesel industry through catalytic upgrading to polyglycerols and other value-added products, Renewable and Sustainable Energy Reviews 39 (2014) 327-341.

[126] T. Polen, M. Spelberg, M. Bott, Toward biotechnological production of adipic acid and precursors from biorenewables, Journal of Biotechnology 2 (2013) 75-84.

[127] V. Taresco, J. Suksiriworapong, R. Creasey, J.C. Burley, G. Mantovani, C. Alexander, K. Treacher, J. Booth, M.C. Garnett, Properties of acyl modified poly(glycerol-adipate) comb-like polymers and their self-assembly into nanoparticles, Journal of Polymer Science: Part A Polymer Chemistry 20 (2016) 3267-3278.

[128] T. Wersig, M.C. Hacker, J. Kressler, K. Mäder, Poly(glycerol adipate)- indomethacin drug conjugates - synthesis and in vitro characterization, International Journal of Pharmaceutics 1 (2017) 225-234.

[129] V. Weiss, "Parenteral drug delivery systems based on fatty acid modified poly(glycerol adipate ", Martin Luther University Halle-Wittenberg, 2015.

[130] K. Mäder, V. Weiss, T. Naolou, J. Kressler, Injectable and implantable carrier systems based on modified poly(dicarboxylic acid multi-oil esters) for the controlled release of active ingredient, 20170151334, 2015.

[131] M.H. Bilal, H. Hussain, M. Prehm, U. Baumeister, A. Meister, G. Hauser, K. Busse,

K. Mäder, J. Kreßler, Synthesis of poly(glycerol adipate)-*g*-oleate and its ternary phase diagram with glycerolmonooleate and water, European Polymer Journal 91 (2017) 162-175.

[132] A.C. Rustan, C.A. Drevon, Fatty acids: Structures and properties, Encyclopedia Life Science (2005) 1-7.

[133] K.J. Bowen, P.M. Kris-Etherton, G.C. Shearer, S.G. West, L. Reddivari, P.J.H. Jones, Oleic acid-derived oleoylethanolamide: A nutritional science perspective, Progress in Lipid Research 67 (2017) 1-15.

[134] N. Kolb, M. Winkler, C. Syldatk, M.A.R. Meier, Long-chain polyesters and polyamides from biochemically derived fatty acids, European Polymer Journal 1 (2014) 159-166.

[135] A. Lauterbach, C.C. Müller-Goymann, Design of lipid microparticle dispersions based on the physicochemical properties of the lipid and aqueous phase, International Journal of Pharmaceutics 1 (2015) 445-452.

[136] M.C. Teixeira, C. Carbone, E.B. Souto, Beyond liposomes: Recent advances on lipid based nanostructures for poorly soluble/poorly permeable drug delivery, Progress in Lipid Research 68 (2017) 1-11.

[137] F. Kreye, F. Siepmann, J.F. Willart, M. Descamps, J. Siepmann, Drug release mechanisms of cast lipid implants, European Journal of Pharmaceutics and Biopharmaceutics 3 (2011) 394-400.

[138] K. Lewis, A.K. Goldyn, K.W. West, E. Eugster, A single histrelin implant is effective for 2 years for treatment of central precocious puberty, Journal of Pediatrics 163 (2013) 1214-1216.

[139] S.H. Choi, T.G. Park, Hydrophobic ion pair formation between leuprolide and sodium oleate for sustained release from biodegradable polymeric microspheres, International Journal of Pharmaceutics 1-2 (2000) 193-202.

[140] Promega, Celltiter 96® AQ Non-Radioactive Cell Proliferation Assay, (2012) 1-15. Available: https://www.promega.de/resources/protocols/technical-bulletins/0/celltiter-96-aqueous-nonradioactive-cell-proliferation-assay-protocol/

[141] Roche, Cytotoxicity Detection Kit (LDH), (2016) 1-24. Available: http://netdocs.roche.com/DDM/Effective/00000000000001004022000793_000_06_005_Native.pdf

[142] J.C. Moore, Gel Permeation Chromatography. I. A new method for molecular weight distribution of high polymers, Journal of Polymer Science 2 (1964) 835-843.

[143] M. Gaborieau, P. Castignolles, Size-exclusion chromatography (SEC) of branched polymers and polysaccharides, Analytical and Bioanalytical Chemistry 4 (2011) 1413-1423.

[144] M.B. Frampton, P.M. Zelisko, Enzyme and microbial technology chain length selectivity during the polycondensation of siloxane-containing esters and alcohols by immobilized Candida antarctica lipase B, Enzyme and Microbial Technology 58-59

(2014) 87-92.

[145] H.W. Spiess, 50th anniversary perspective: The Importance of NMR spectroscopy to macromolecular science, Macromolecules 5 (2017) 1761-1777.

[146] J.U. Izunobi, C.L. Higginbotham, Polymer molecular weight analysis by 1H NMR spectroscopy, Journal of Chemical Education 88 (2011) 1098-1104.

[147] K. Saalwächter, D. Reichert, Magnetic Resonance: Polymer Applications of NMR, in: J. Lindon, G. Tranter, D. Koppendaal (Eds), Encyclopedia of Spectroscopy and Spectrometry, 2nd Edition, Academic Press: Elsevier, Oxford (2009) 1-16.

[148] B. Diehl, Principles in NMR Spectroscopy, 3-41. In: NMR Spectroscopy in Pharmaceutical Analysis, Ed. U. Holzgrabe, I. Wawer, B. Diehl, Elsevier, Oxford (2008) 528.

[149] A. Barison, C.W. da Silva, F.R. Campos, F. Simonelli, C.A. Lenz, A.G. Ferreira, A simple methodology for the determination of fatty acid composition in edible oils through 1H NMR spectroscopy, Magnetic Resonance in Chemistry 8 (2010) 642-650.

[150] M. Jebrane, N. Terziev, I. Heinmaa, Biobased and sustainable alternative route to long-chain cellulose esters, Biomacromolecules 2 (2017) 498-504.

[151] E. Martineau, K.E. Khantache, M. Pupier, P. Sepulcri, S. Akoka, P. Giraudeau, Non-linear effects in quantitative 2D NMR of polysaccharides : Pitfalls and how to avoid them, Journal of Pharmaceutical and Biomedical Analysis 108 (2015) 78-85.

[152] J. Coates, Interpretation of Infrared Spectra, A Practical Approach, Encyclopedia of Analytical Chemistry, John Wiley & Sons, Ltd, Chichester, (2000) 10815.

[153] PerkinElmer, Differential Scanning Calorimetry (DSC) A Beginner's Guide, (2014) 1-9. Available: http://www.perkinelmer.com/CMSResources/Images/46-74542GDE_DSCBeginnersGuide.pdf

[154] E.D. Zanotto, J.C. Mauro, The glassy state of matter : Its definition and ultimate fate, Journal of Non-Cristalline Solids 1 (2017) 490-495.

[155] H. Kunisada, Y. Yuki, S. Kondo, J. Miyatake, C. Maeda, Synthesis and side-chain crystalization of new comb-like polymers from 2-amino-4-(*N*-alkilanilino)-6-isopropenyl-1,3,5-triazines, Polymer Journal 7 (1990) 559-566.

[156] B.A.A. Basma, M.I. Zaki, Thermal decomposition course of $Eu(CH_3COO)_3.4H_2O$ and the reactivity at the gas/solid interface thus established, Journal of Analytical and Applied Pyrolysis 1 (2011) 123-130.

[157] M.D. Young, N. Tran, P.A. Tran, J.D. Jarrell, R.A. Hayda, C.T. Born, Niobium oxide-polydimethylsiloxane hybrid composite coatings for tuning primary fibroblast functions, Journal of Biomedical Materials Research - Part A 5 (2014) 1478-1485.

[158] K. Yu, Y. Mei, N. Hadjesfandiari, J.N. Kizhakkedathu, Engineering biomaterials surfaces to modulate the host response, Colloids and Surfaces B : Biointerfaces 124 (2014) 69-79.

[159] P. Thevenot, W. Hu, L. Tang, Surface chemistry influence implant, Current Topics in Medicinal Chemistry 4 (2011) 270-280.

[160] D.B. Hall, P. Underhill, J.M. Torkelson, Spin coating of thin and ultrathin polymer films, Polymer Engineering and Science 12 (1998) 2039-2045.

[161] S. Spriano, V.S. Chandra, A. Cochis, F. Uberti, L. Rimondini, E. Bertone, A. Vitale, C. Scolaro, M. Ferrari, F. Cirisano, G. Gautier di Confiengo, S. Ferraris, How do wettability, zeta potential and hydroxylation degree affect the biological response of biomaterials?, Material Science and Engineering: C 1 (2016) 542-555.

[162] S. Kikuchi, Y. Onuki, H. Kuribayashi, K. Takayama, Relationship between diffusivity of water molecules inside hydrating tablets and their drug release behavior elucidated by magnetic resonance imaging, Chemical and Pharmaceutical Bulletin 4 (2012) 536-542.

[163] M. Probst, J.P. Kühn, E. Scheuch, A. Seidlitz, S. Hadlich, K. Evert, S. Oswald, W. Siegmund, W. Weitschies, Simultaneous magnetic resonance imaging and pharmacokinetic analysis of intramuscular depots, Journal of Controlled Release 227 (2016) 1-12.

[164] R. Dorati, C. Colonna, M. Serra, I. Genta, T. Modena, F. Pavanetto, P. Perugini, B. Conti, Gamma-irradiation of PEGd, lPLA and PEG-PLGA multiblock copolymers. I. Effect of irradiation doses, American Association of Pharmaceutical Scientists 2 (2008) 718-725.

[165] B. Sintzel, K. Schwach-Abdellaoui, J. Heller, C. Tabatabay, Influence of irradiation sterilization poly(ortho ester) on a semi-solid, International Journal of Pharmaceutics 2 (1998) 165-176.

[166] M. Kermode, Unsafe injections in low-income country health settings : need for injection safety promotion to prevent the spread of blood-borne viruses, Health Promotion International 1 (2004) 95-103.

[167] A.C. Anselmo, S. Mitragotri, An overview of clinical and commercial impact of drug delivery systems, Journal of Controlled Release 190 (2014) 15-28.

[168] A. Hatefi, B. Amsden, Biodegradable injectable in situ forming drug delivery systems - Review, Journal of Controlled Release 1-3 (2002) 9-28.

[169] R.W. Kalicharan, P. Baron, C. Oussoren, L.W. Bartels, Vromans H, Spatial distribution of oil depots monitored in human muscle using MRI, International Journal of Pharmaceutics 1-2 (2016) 52-60.

[170] R.W. Kalicharan, M.R. Bout, C. Oussoren, H. Vromans, Where does hydrolysis of nandrolone decanoate occur in the human body after release from an oil depot ?, International Journal of Pharmaceutics 1-2 (2016) 721-728.

[171] A. Badkar, A. Wolf, L. Bohack, P. Kolhe, Development of biotechnology products in pre-filled syringes: technical considerations and approaches, American Association of Pharmaceutical Scientists 2 (2011) 564-572.

[172] F. Cilurzo, F. Selmin, P. Minghetti, M. Adami, E. Bertoni, S. Lauria, L. Montanari, Injectability Evaluation: An Open Issue, American Association of Pharmaceutical Scientists 2 (2011) 604-609.

[173] V. Burckbuchler, G. Mekhloufi, A.P. Giteau, J.L. Grossiord, S. Huille, F. Agnely, Rheological and syringeability properties of highly concentrated human polyclonal immunoglobulin solutions, European Journal of Pharmaceutics and Biopharmaceutics 3 (2010) 351-356.

[174] A. Allmendinger, S. Fischer, J. Huwyler, H-C. Mahler, E. Schwarb, I.E. Zarraga, R. Müller, Rheological characterization and injection forces of concentrated protein formulations: An alternative predictive model for non-Newtonian solutions, European Journal of Pharmaceutics and Biopharmaceutics 2 (2014) 318-328.

[175] W. Rungseevijitprapa, R. Bodmeier, Injectability of biodegradable in situ forming microparticle systems (ISM), European Journal of Pharmaceutical Sciences 4-5 (2009) 524-531.

[176] A. Allmendinger, R. Mueller, E. Schwarb, M. Chipperfield, J. Huwyler, H.C. Mahler, S. Fischer, Measuring tissue back-pressure - In vivo injection forces during subcutaneous injection, Pharmaceutical Research 7 (2015) 2229-2240.

[177] J. Jezek, N.J. Darton, B.K. Derham, N. Royle, I. Simpson, Biopharmaceutical formulations for pre-filled delivery devices, Expert Opinion on Drug Delivery 6 (2013) 811-828.

[178] J. Wex, M. Sidhu, I. Odeyemi, A.M. Abou-Setta, P. Retsa, B. Tombal, Leuprolide acetate 1-, 3-and 6-monthly depot formulations in androgen deprivation therapy for prostate cancer in nine European countries: evidence review and economic evaluation, ClinicoEconomics and Outcomes Research 5 (2013) 257-269.

[179] H.B. Ravivarapu, K.L. Moyer, R.L. Dunn, Sustained activity and release of leuprolide acetate from an in situ forming polymeric implant, American Association of Pharmaceutical Scientists 1 (2000) 1-8.

[180] L.R. Asmus, B. Kaufmann, L. Melander, T. Weiss, G. Schwach, R. Gurny, M. Möller, Single processing step toward injectable sustained-release formulations of Triptorelin based on a novel degradable semi-solid polymer, European Journal of Pharmaceutics and Biopharmaceutics 3 (2012) 591-599.

[181] Q. Hu, E.V.B. van Gaal, P. Brundel, H. Ippel, T. Hackeng, C.J.F. Rijcken, G. Storm, W.E. Heninnk, J. Prakash, A novel approach for the intravenous delivery of leuprolide using core-cross-linked polymeric micelles, Journal of Controlled Release 205 (2015) 98-108.

[182] X. Luan, R. Bodmeier, In situ forming microparticle system for controlled delivery of leuprolide acetate: Influence of the formulation and processing parameters, European Journal of Pharmaceutical Sciences 2-2 (2006) 143-149.

[183] D. Quintanar-Guerrero, E. Allémann, E.D.H. Fessi, Applications of the ion-pair

concept to hydrophilic substances with special emphasis on peptides, Pharmaceutical Research 2 (1997) 119-127.

[184] T.S. Wiedmann, A. Naqwi, Pharmaceutical salts: Theory, use in solid dosage forms and in situ preparation in an aerosol, Asian Journal of Pharmaceutical Sciences 6 (2016) 722-734.

[185] A. Adjei, S. Rao, J. Garren, G. Menon, M. Vadnere, Effect of ion-pairing on 1-octanol-water partitioning of peptide drugs. I: The nonapeptide leuprolide acetate, International Journal of Pharmaceutics 2 (1993) 141-149.

[186] J. Kutza, "Entwicklung und charakterisierung von subkutanen gelimplantaten zur kontrollierten proteinfreisetzung", Martin Luther University Halle-Wittenberg, 2015.

[187] W.D. Schlaff, S.A. Carson, A. Luciano, D. Ross, A. Bergqvist, Subcutaneous injection of depot medroxyprogesterone acetate compared with leuprolide acetate in the treatment of endometriosis-associated pain, Fertility and Sterility 2 (2006) 314-325.

[188] A.C. Wilson, S.V. Meethal, R.L. Bowen, C.S. Atwood, Leuprolide acetate: a drug of diverse clinical applications, Expert Opinion on Investigational Drugs 11 (2007) 1851-1863.

[189] D. Teutonico, S. Montanari, G. Ponchel, Leuprolide acetate: pharmaceutical use and delivery potentials, Expert Opinion on Drug Delivery 3 (2012) 343-354.

[190] J. Ferlay, E. Steliarova-Foucher, J. Lortet-Tieulent, S. Rosso, J.W.W. Coebergh, H. Comber, D. Forman, F. Bray, Cancer incidence and mortality patterns in Europe: Estimates for 40 countries in 2012, European Journal of Cancer 6 (2013) 1374-1403.

[191] F. Bray, J.S. Ren, E. Masuyer, J. Ferlay, Global estimates of cancer prevalence for 27 sites in the adult population in 2008, International Journal of Cancer 5 (2013) 1133-1145.

[192] A. Petrillo, R. Fusco, S.V. Setola, F.M. Ronza, V. Granata, M. Petrillo, G. Carone, M. Sansone, R. Franco, F. Fulciniti, S. Perdonà, Multiparametric MRI for prostate cancer detection : Performance in patients with prostate-specific antigen values between 2.5 and 10 ng/mL, Journal of Magnetic Resonance Imaging 5 (2014) 1206-1212.

[193] E.M.M. Yamaguti, M.B. Brito, R.A. Ferriani, A.A. Garcia, J.C. Rosa-E-Silva, C.S. Vieira, Comparison of the hemostatic effects of a levonorgestrel -releasing intrauterine system and leuprolide acetate in women with endometriosis: A randomized clinical trial, Thrombosis Research 6 (2014) 1193-1197.

[194] F.R. Junqueira, L.A. Lara, W.P. Martins, R.A. Ferriani, A.C. Rosa-E-Silva, M.F. de Sá, R.M Reis, Gonadotropin and Estradiol Levels after Leuprolide Stimulation Tests in Brazilian Girls with Precocious Puberty, Journal of Pediatric and Adolescent Gynecology 5 (2015) 313-316.

[195] C.H. Chi, E. Durham, E.K. Neely, Pharmacodynamics of aqueous leuprolide acetate stimulation testing in girls: Correlation between clinical diagnosis and time of peak

luteinizing hormone level, Journal of Pediatrics 4 (2012) 757-759.

[196] R. Astaneh, M. Erfan, H. Moghimi, H. Mobedi, Changes in morphology of in situ forming PLGA implant prepared by different polymer molecular weight and its effect on release behavior, Journal of Pharmaceutical Sciences 1 (2009) 135-145.

[197] E. Ron, T. Turek, E. Mathiowitz, M. Chasin, M. Hageman, R. Langer, Controlled release of polypeptides from polyanhydrides, Proceedings of the National Academy of Science 9 (1993) 4176-4180.

[198] A.J. Domb, M. Maniar, Absorbable biopolymers derived from dimer fatty acids, Journal of Polymer Science Part A: Polymer Chemistry 5 (1993) 1275-1285.

[199] S. Dong, S. Wang, C. Zheng, W. Liang, Y. Huang, An in situ-forming, solid lipid/PLGA hybrid implant for long-acting antipsychotics, Soft Materials 7 (2011) 5873-5878.

[200] S. Herrmann, G. Winter, S. Mohl, F. Siepmann, J. Siepmann, Mechanisms controlling protein release from lipidic implants: Effects of PEG addition, Journal of Controlled Release 2 (2007) 161-168.

[201] S. Schulze, G. Winter, Lipid extrudates as novel sustained release systems for pharmaceutical proteins, Journal of Controlled Release 3 (2009) 177-185.

[202] C-L. Li, Y-J. Deng, Oil-based formulations for oral delivery of insulin, Journal of Pharmacy and Pharmacology 9 (2004) 1101-1107.

[203] X. Luan, R. Bodmeier, Modification of the tri-phasic drug release pattern of leuprolide acetate-loaded poly(lactide-co-glycolide) microparticles, European Journal of Pharmaceutics and Biopharmaceutics 2 (2006) 205-214.

[204] A. Calafi, N. Bormann, D. Scharnweber, B. Rentsch, B. Wildemann, A new concept for a drug releasing modular scaffold, Materials Letters 119 (2014) 119-122.

[205] M. Gallarate, L. Battaglia, E. Peira, M. Trotta, Peptide-loaded solid lipid nanoparticles prepared through coacervation technique, International Journal of Chemical Engineering 2011 (2011) 1-6.

[206] F. Ye, S.W. Larsen, A. Yaghmur, H. Jensen, C. Larsen, J. Østergaard, Real-time UV imaging of piroxicam diffusion and distribution from oil solutions into gels mimicking the subcutaneous matrix, European Journal of Pharmaceutical Sciences 1-2 (2012) 72-78.

[207] R.B. Schulz, W. Semmler, Fundamentals of optical imaging, Handbook of Experimental Pharmacology 185 (2008) 3-22.

[208] Thermofischer. Fluorescence SpectraViewer DiR. (2017). Available: https://www.thermofisher.com/de/de/home/life-science/cell-analysis/labelingchemistry/fluorescencespectraviewer.html?ICID=svtool&UID=12731lip

[209] R.W. Kalicharan, P. Schot, H. Vromans, Fundamental understanding of drug absorption from a parenteral oil depot, European Journal of Pharmaceutical Sciences

83 (2016) 19-27.

[210] K. Uekama, H. Arima, T. Irie, K. Matsubara, T. Kuriki. Sustained release of buserelin acetate, a luteinizing hormone-releasing hormone agonist, from an injectable oily preparation utilizing ethylated beta-cyclodextrin, Journal of Pharmacy and Pharmacology 12 (1989) 874-876.

[211] L. Kagan, Pharmacokinetic modeling of the subcutaneous absorption of therapeutic proteins, Drug Metabolism and Disposition 11 (2014) 1890-1905.

[212] R. Mathaes, A. Koulov, S. Joerg, H.C. Mahler, Subcutaneous injection volume of biopharmaceuticals pushing the boundaries, Journal of Pharmaceutical Sciences 8 (2016) 2255-2259.

[213] H.M. Kinnunen, V. Sharma, L.R. Contreras-Rojas, Y. Yu, C. Alleman, A. Sreedhara, S. Fischer, L. Khawli, S.T. Yohe, D. Bumbaca, T.W. Patapoff, A.L. Daugherty, R.J. Mrsny, A novel in vitro method to model the fate of subcutaneously administered biopharmaceuticals and associated formulation components, Journal of Controlled Release 214 (2015) 94-102.

[214] T. Heise, L. Nosek, S. Dellweg, E. Zijlstra, K.A. Praestmark, J. Kildegaard, G. Nielsen, T. Sparre, Impact of injection speed and volume on perceived pain during subcutaneous injections into the abdomen and thigh: A single-centre, randomized controlled trial, Diabetes, Obesity and Metabolism 10 (2014) 971-976.

[215] K.L. Stoner, H. Harder, L.J. Fallowfield, V.A. Jenkins, Intravenous versus subcutaneous drug administration. Which do patients prefer? A systematic review, Patient 2 (2015) 145-153.

[216] M.L. Slevin, E.M. Piall, A. Johnston, D.A. Levison, G.W. Aherne, S.B. Tree, T.A. Lister, The pharmacokinetics of subcutaneous bolus cytosine arabinoside in an arachis oil plus aluminium distearate suspension, Investigational New Drugs 3 (1984) 271-276.

[217] S. Ytzhak, J.P. Wuskell, L.M. Loew, B. Ehrenberg, Lipid composition affects the rate of photosensitized dissipation of cross-membrane diffusion potential on liposomes, The Journal of Physical Chemistry B 31 (2010) 10097-10104.

[218] P. Chytil, S. Hoffmann, L. Schindler, L. Kostka, K. Ulbrich, H. Caysa, T. Müller, K. Mäder, T. Etrych, Dual fluorescent HPMA copolymers for passive tumor targeting with pH-sensitive drug release II: Impact of release rate on biodistribution, Journal of Controlled Release 2 (2013) 504-512.

[219] G. Zhou, A. Liedmann, C. Chatterjee, T. Groth, In vitro study of the host responses to model biomaterials via a fibroblast/macrophage co-culture system, Biomaterials Science 1 (2016) 141-152.

[220] C. Hernandez, N. Gawlik, M. Goss, H. Zhou, S. Jeganathan, D. Gilbert, A.A. Exner, Macroporous acrylamide phantoms improve prediction of in vivo performance of in situ forming implants, Journal of Controlled Release 243 (2016) 225-231.

[221] K. Hayashi, F. Okamoto, S. Hoshi, T. Katashima, D.C. Zujur, X. Li, M. Shibayama,

E.P. Gilbert, U-il Chung, S. Ohba, T. Oshika, T. Sakai, Fast-forming hydrogel with ultralow polymeric content as an artificial vitreous body, Nature Biomedical Engineering 1 (2017) 1-7.

[222] Z. Wu, I.G. Tucker, M. Razzak, L. Yang, K. Mcsporran, N.J. Medlicott, Absorption and tissue tolerance of ricobendazole in the presence of hydroxypropyl-beta-cyclodextrin following subcutaneous injection in sheep, International Journal of Pharmaceutics 1-2 (2010) 96-102.

[223] M. Titford, The long history of hematoxylin, Biotechnic and Histochemistry 2 (2005) 73-78.

[224] E. Algin-Yapar, N. Ari, T. Baykara, Evaluation of in vitro and in vivo performance of granisetron in situ forming implants: Effect of sterilization, storage condition and degradation, Tropical Journal of Pharmaceutical Research 3 (2014) 319-325.

[225] W.F. Richter, S.G. Bhansali, M.E. Morris, Mechanistic determinants of biotherapeutics absorption following sc administration, American Association of Pharmaceutical Scientists 3 (2012) 559-570.

[226] J.M. Anderson, M.S. Shive, Biodegradation and biocompatibility of PLA and PLGA microspheres, Advanced Drug Delivery Reviews 28 (1997) 5-24.

[227] B. Vaisman, M. Motiei, A. Nyska, A.J. Domb, Biocompatibility and safety evaluation of a ricinoleic acid-based poly(ester-anhydride) copolymer after implantation in rats, Journal of Biomedical Materials Research Part A 2 (2010) 419-431.

[228] J. Skrobot, L. Zair, M. Ostrowski, El.M. Fray, New injectable elastomeric biomaterials for hernia repair and their biocompatibility, Biomaterials 75 (2016) 182-192.

[229] J.N. Korley, S. Yazdi, K. Mchugh, J. Kirk, J. Anderson, One-step synthesis, biodegradation and biocompatibility of polyesters based on the metabolic synthon, dihydroxyacetone, Biomaterials 98 (2016) 45-51.

[230] G. Helenius, H. Bäckdahl, A. Bodin, U. Nannmark, P. Gatenholm, B. Risberg, In vivo biocompatibility of bacterial cellulose, Journal of Biomedical Materials Research - Part A 2 (2006) 431-438.

[231] M. Licciardi, G. Amato, A. Cappelli, M. Paolino, G. Giuliani, B. Belmonte, C. Guarnotta, G. Pitarresi, G. Giammona, Evaluation of thermoresponsive properties and biocompatibility of polybenzofulvene aggregates for leuprolide delivery, International Journal of Pharmaceutics 1-2 (2012) 279-286.

7 Appendix
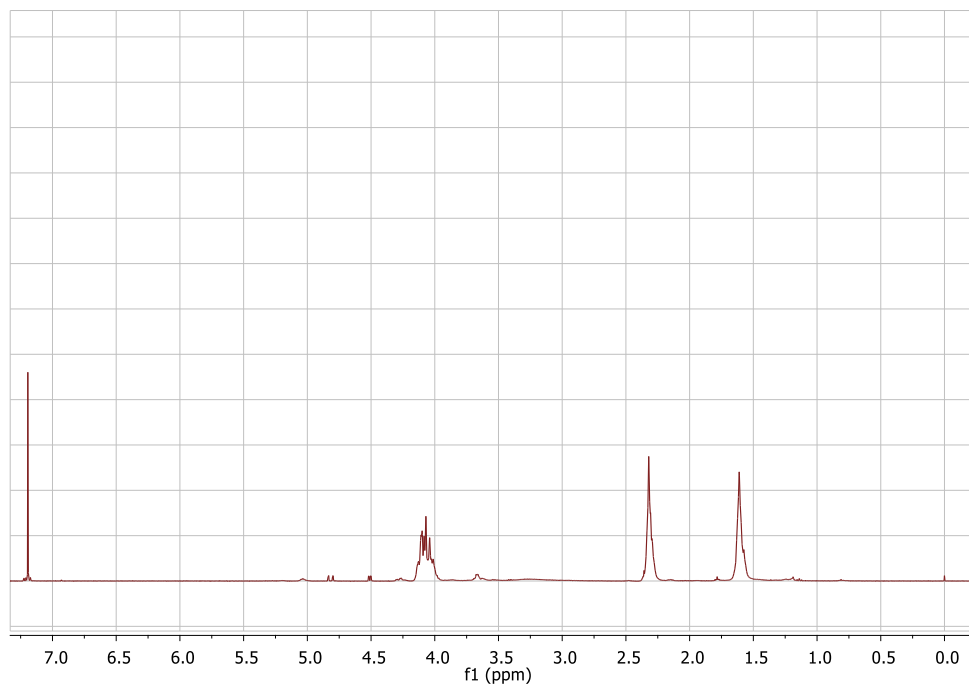
^{1}H NMR of PGA at 27 °C in CDCl$_3$.
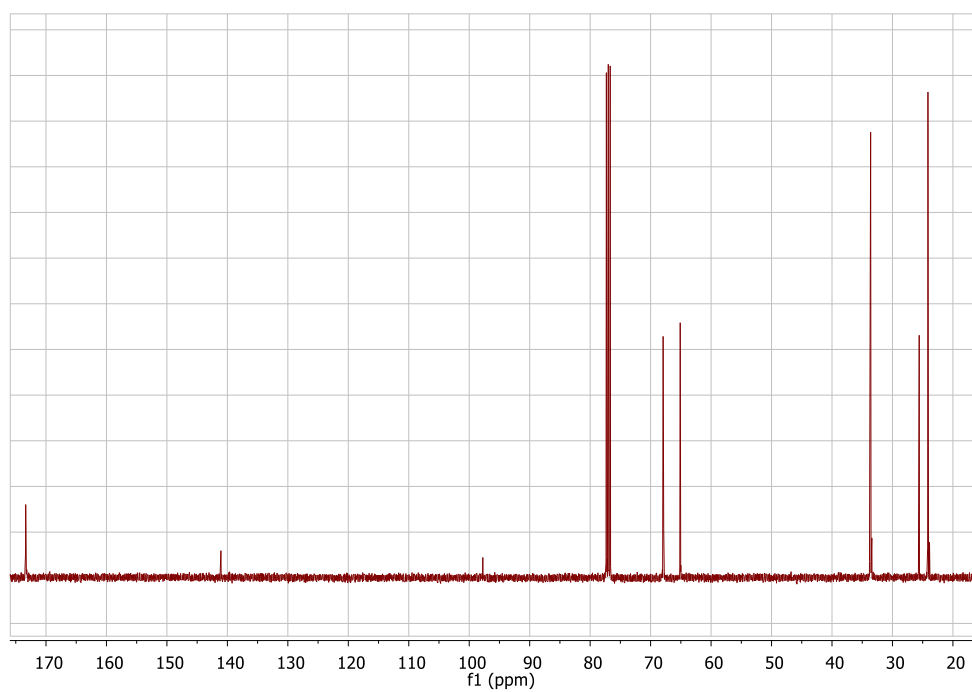
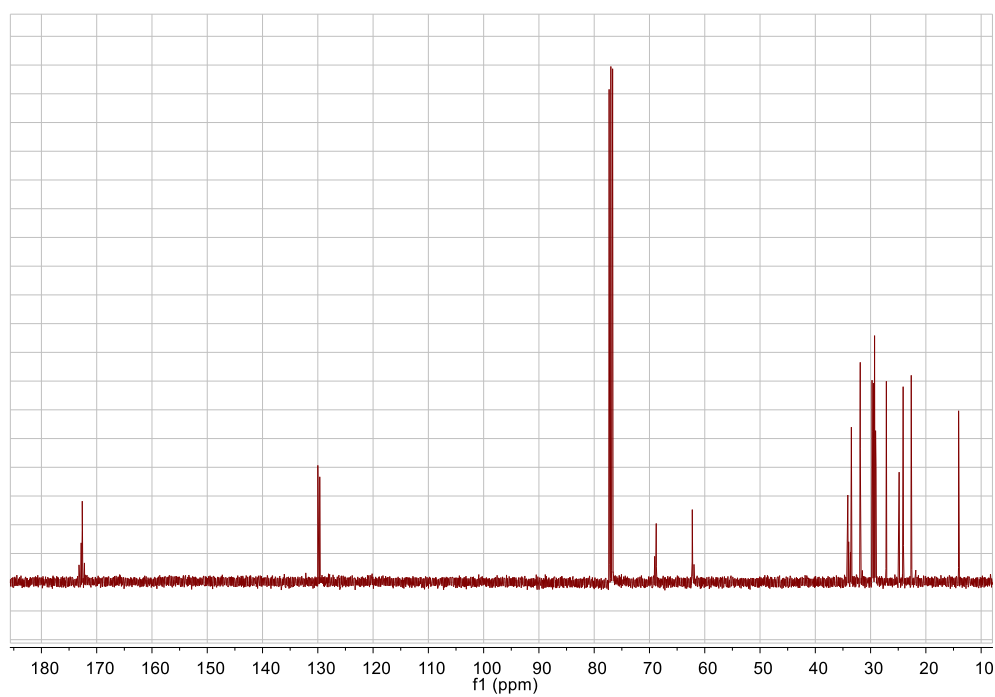^{13}C NMR of PGA at 27 °C in CDCl$_3$.
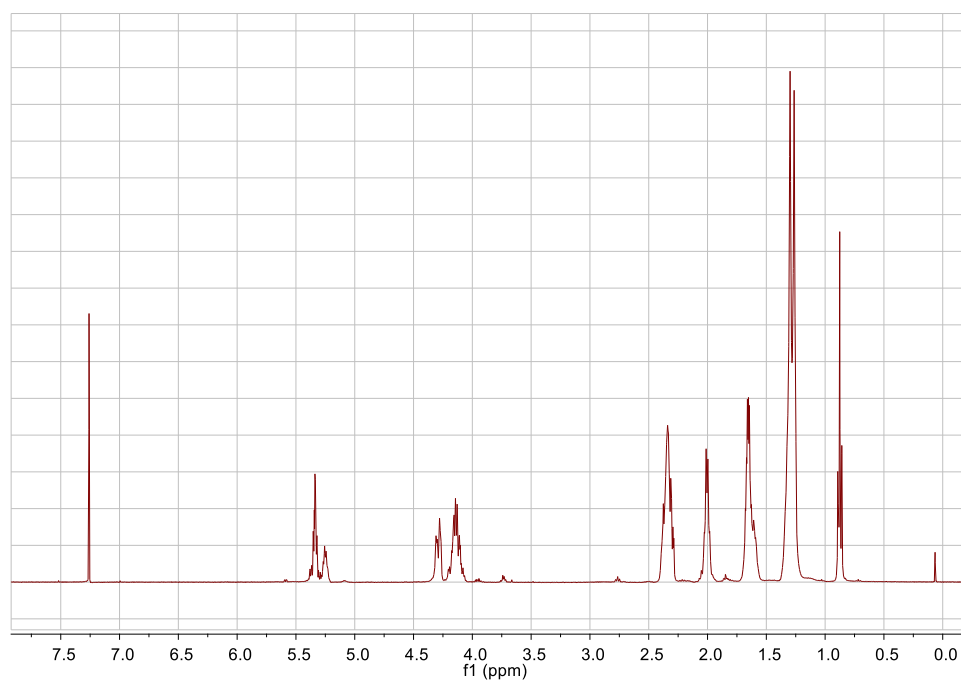
^{1}H NMR of PGA-*g*-O75 at 27 °C in CDCl$_3$.
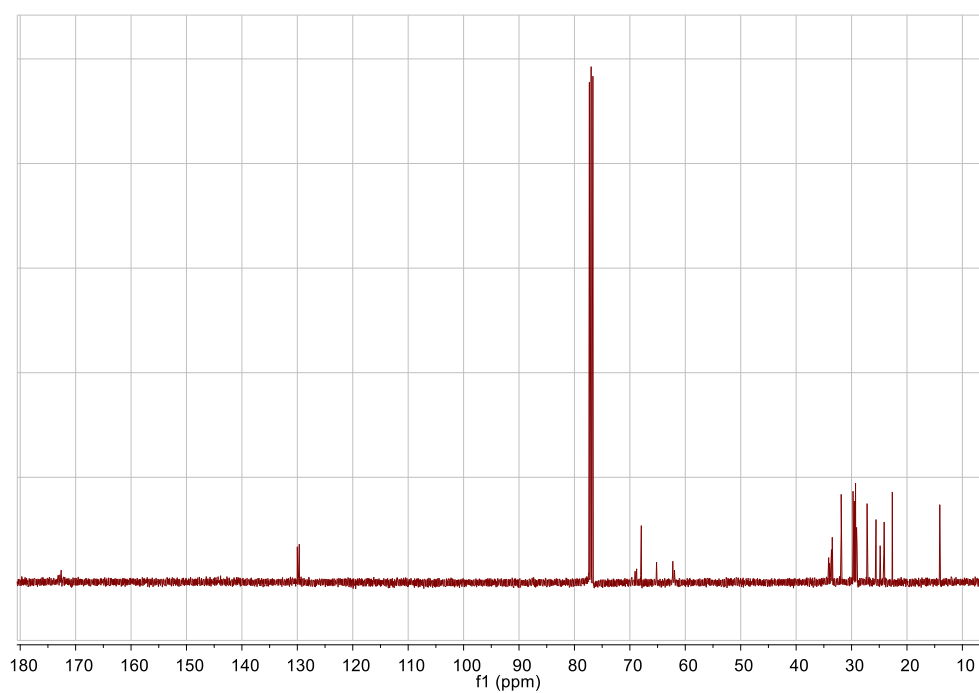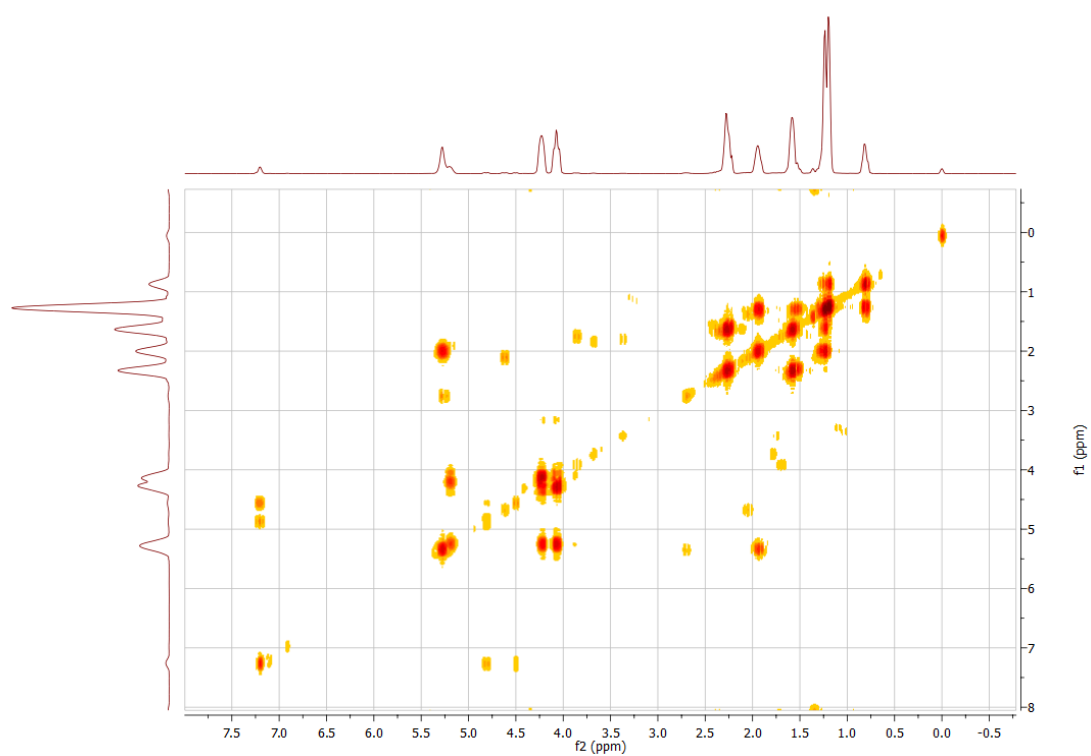

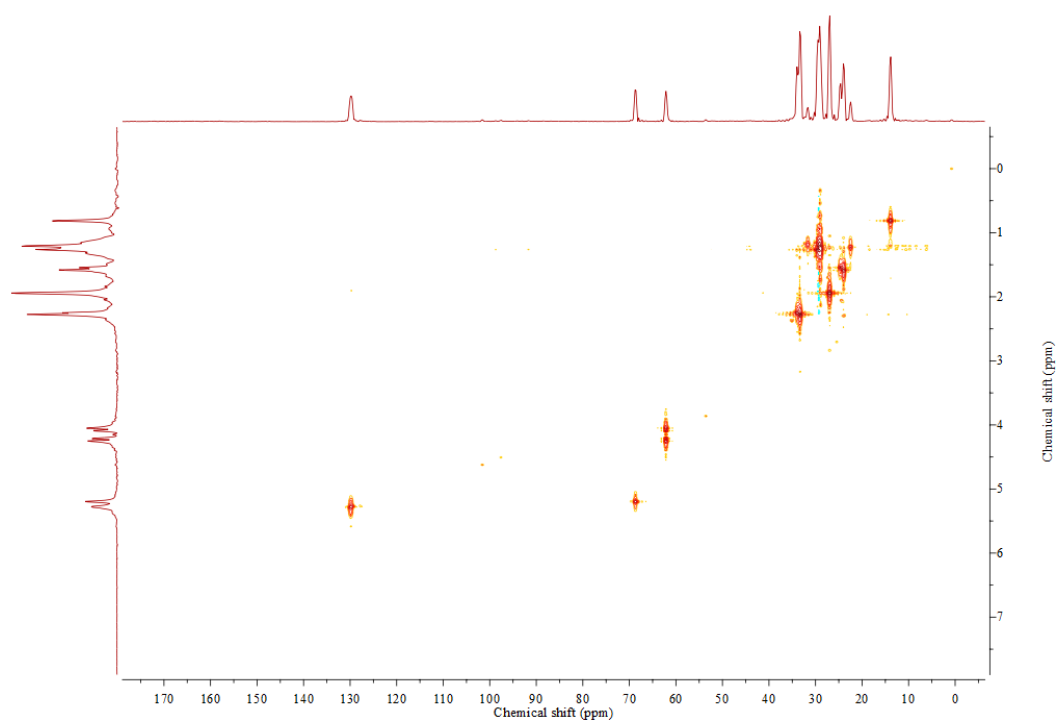^{13}C NMR PGA-*g*-O75 at 27 °C in CDCl$_3$.
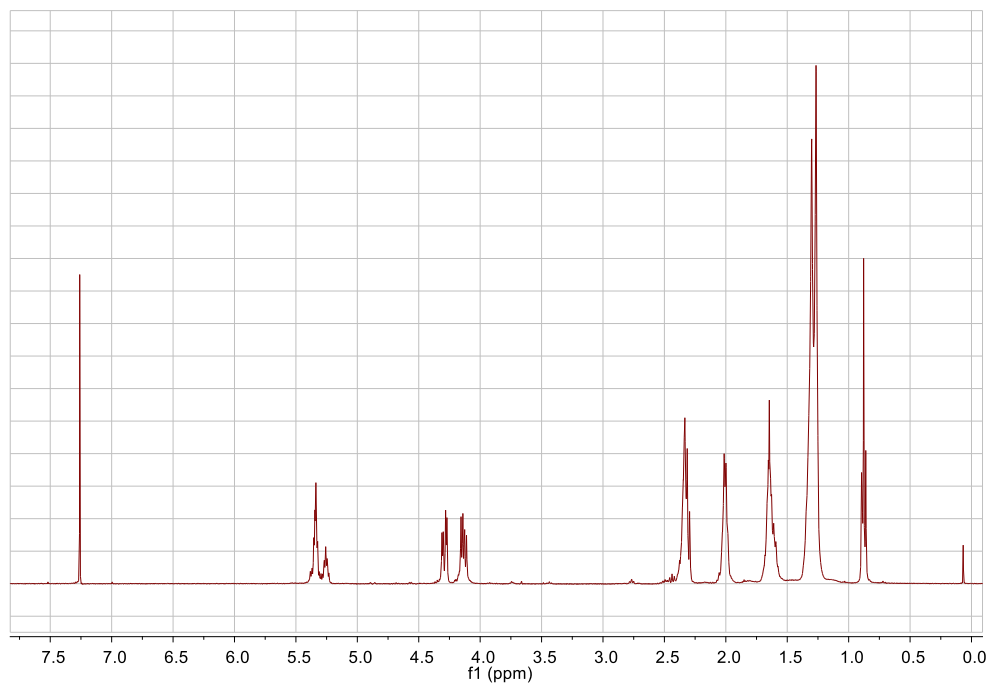
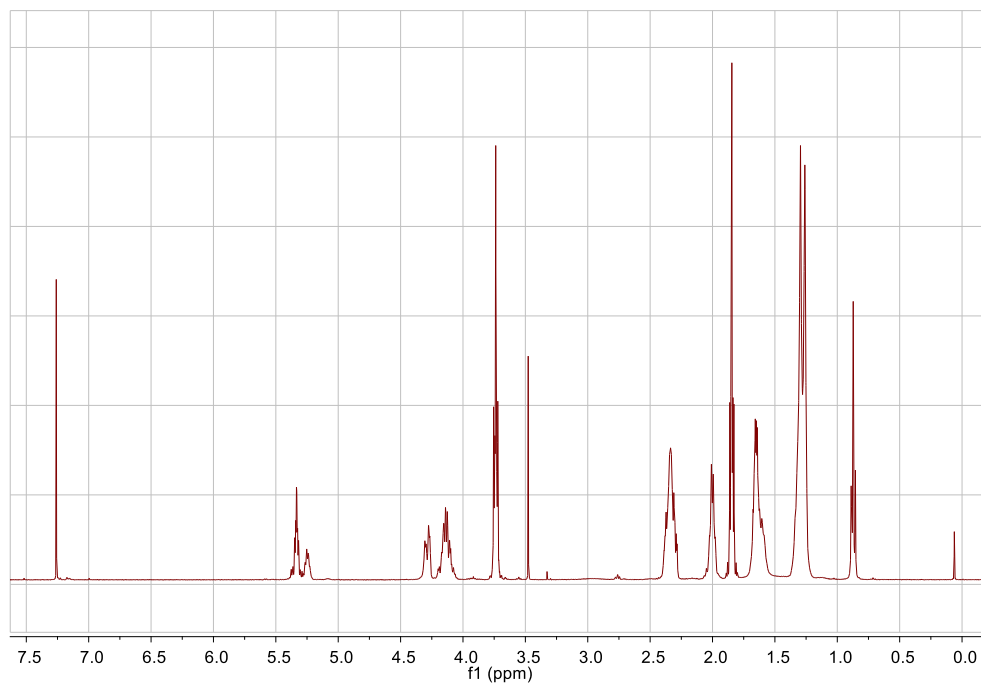^{1}H NMR of PGA-*g*-O100 at 27 °C in CDCl$_3$.

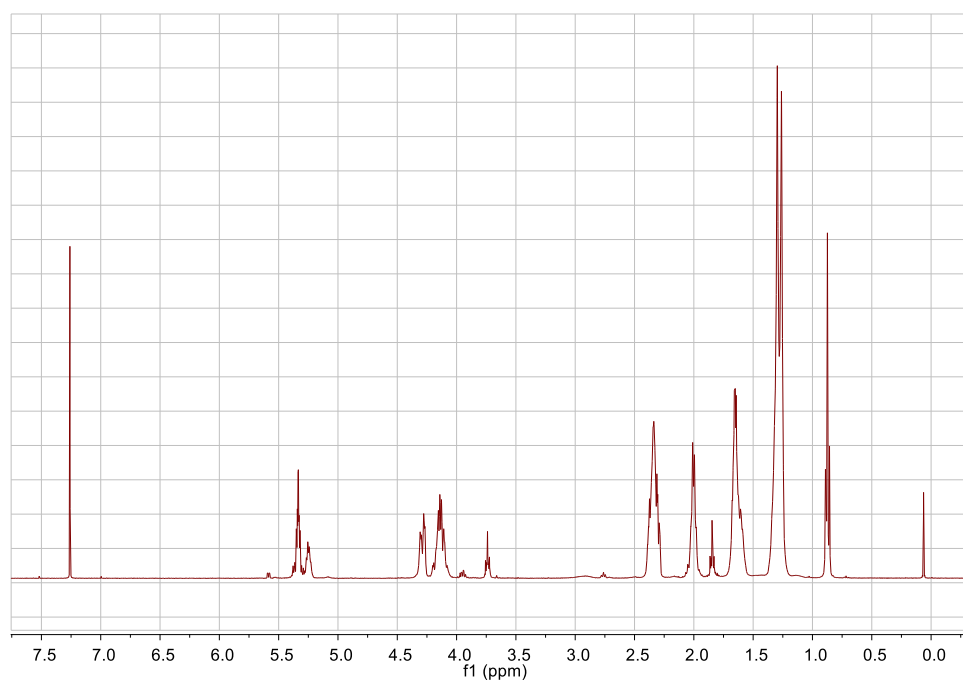^{13}C NMR PGA-*g*-O100 at 27 °C in CDCl$_3$.
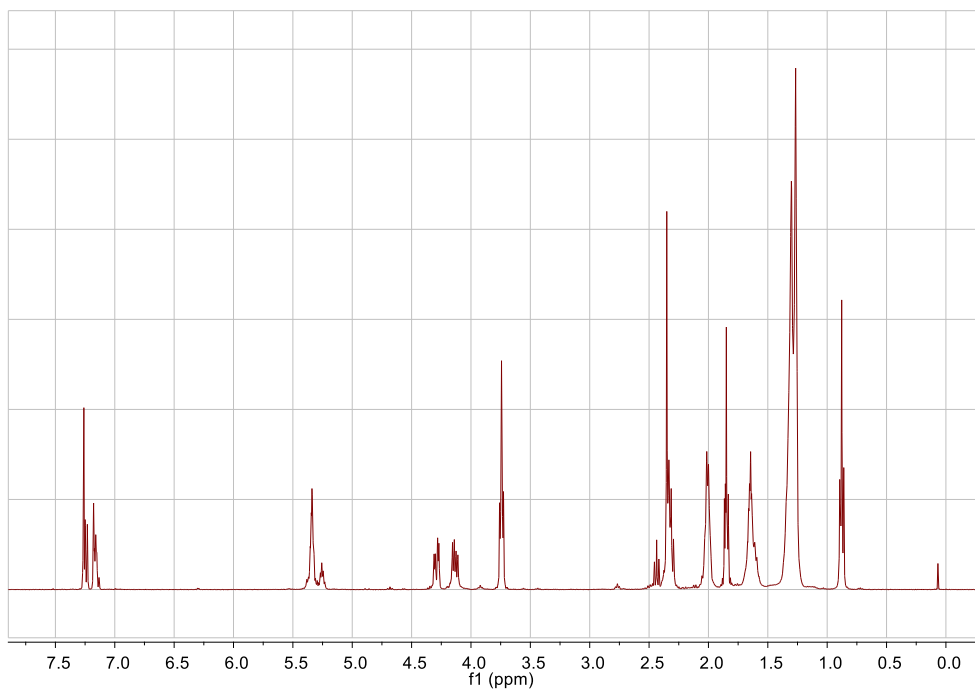
2D ^{1}H NMR PGA-*g*-O100 at 27 °C in CDCl$_3$.
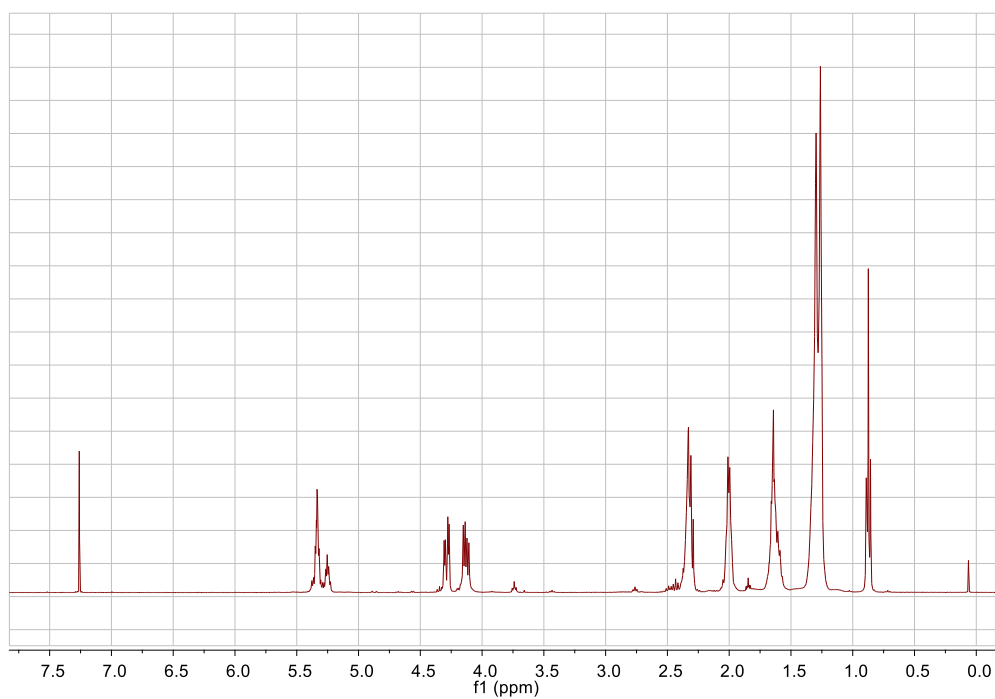

2D ^{13}C-^{1}H NMR PGA-*g*-O100 at 27 °C in CDCl$_3$.

^{1}H NMR PGA-*g*-O75 at 27 °C before irradiation in CDCl$_3$.

^{1}H NMR PGA-*g*-O75 at 27 °C after irradiation in CDCl$_3$.

^{1}H NMR PGA-*g*-O100 at 27 °C before irradiation in CDCl$_3$.

^{1}H NMR PGA-*g*-O100 at 27 °C before irradiation in CDCl$_3$.

Acknowledgments

I thank Professor Dr. Karsten Mäder immensely for offering me the chance to work in this exciting and interesting project, for his valuable guidance throughout the path I have gone, for giving me room to put my ideas into the work and for driving me into more assertive directions, with advice and criticisms. I also thank him for the opportunity of being in his research group, from which I have learned a lot, and allowing me to take up tasks in the whole spectrum of the activities in the University. I finally thank him for supporting me in a constructive way when it was necessary. It was very valuable for my life.

I thank Professor Dr. Jörg Kressler for co-supervising me constructively, for allowing me to learn the steps I needed in Chemistry from his group. For being open and supportive towards the work, and for providing necessary means I needed to conduct my research.

I thank all the group technicians as well, without whom our work would be quite harder, if even possible. In this case, I would like to name Mrs. Claudia Bertram, Dr. Hendrik Metz, Ms. Ute Mentzel, Ms. Kerstin Schwarz, Ms. Manuela Woigk and Mrs. Diana Rarisch. You all were always kind and very supportive. You are very good professionals and people.

I am delighted to dedicate heartful thanks to Dr. Stefan Hoffmann, who was a postdoc in our group and always helped me from the very start, including accompanying me in many official meetings, going out of his way to make my life here easier. For all discussions we had and very genuine conversations. I will never forget it.

I thank Dr. Henrike Lucas and Dr. Thomas Müller for their readiness and supportive work, especially regarding the experiments with animals.

I thank Muhammad H. Bilal for his good and valuable help with the chemical synthesis and important discussions during the preparation of this thesis.

I thank my working group (the current and all members with whom I had contact), for their suggestions, talks, trips, support, and so much more. Nice time with you.

I thank Tom Wersig for his help with the animal experiments.

I thank Professor Dr. Bernhard Hiebl and Mrs. Undine for conducting the *in vitro* tests of toxicity, his positive approach towards the work, and his friendly words.

List of Publications

Conference contributions

Rodrigues, A. G., Bilal, M. H., Weiss, V. M., Naulou, T., Metz, H., Kressler J. and Mäder, K. Solvent-free direct injectable biodegradable polymers for parenteral drug delivery. Annual Meeting Controlled Release Society, Edinburgh, 2015.

K. Mäder, J. Kutza, M. Windorf, V. Weiss, **A. Rodrigues**, T. Naolou, M.H. Bilal, J. Kreßler: Direct injectable Lipid and Polymer based Carriers for Controlled Release Applications. 5th Halle Conference on Recombinant Proteins, February 19-20, 2015, Halle/Saale, Germany (Poster).

Curriculum Vitae

Alexandre Gomes Rodrigues

Born in 12.11.1983 in Ribeirão Pires, São Paulo, Brazil

Work Experience

02/2014-11/2016   Research and Teaching Assistant at the Institute of Pharmacy,

Martin-Luther-University Halle-Wittenberg, Halle, Germany

02/2011-/02/2014 Research Assistant at Biochem and Biophys Lab, Butantã Instit, SP, Brazil

03/2010-01/2011   Research Assistant at Lab of Physico-Chemical QC at USP, Brazil

08/2009-10/2009   Internship, Gran Pharma Aline Ltda, Pharmacy, São Paulo, Brazil

11/2008-07/2009   Internship, Pharmacology Department, Funcional Card, São Paulo, Brazil

02/2008-07/2008   Research Assistant at Pharma. Tech. Lab, São Paulo University, Brazil

09/2007-11/2007   Internship, Cosmetics Develop. Lab, Gerbrás Quím. Farma., São Paulo, Brazil

Education

02/2014-01/2018 Doctorate at Martin Luther University, Halle-Wittenberg, Germany

02/2011-02/2014 Master of Science at São Paulo University, São Paulo, Brazil.

02/2007-12/2010 Bachelor in Pharmacy at Paulista University, São Paulo, Brazil

02/2005-06/2006 Technical Chemistry at Colégio Barão de Mauá, São Paulo, Brazil

02/2003-12/2003 Technical Industrial Mechanics (unfinished) at ETEC, São Paulo, Brazil

02/1999-12/2002 High School in São Paulo, Brazil

Prizes

2016   German Academic Exchange Service (DAAD). Highly Engaged PhD Student.

2016   International Office, Martin Luther University. Teaching Assistantship (TA).

2014   Brazilian research funding organization (CAPES). PhD Scholarship.

2011   Brazilian research funding organization (CAPES). M. Sc. Scholarship.

2008   Best poster presentation. São Paulo University.

Declaration under Oath

I hereby declare that the thesis I am submitting is entirely my own original work except than otherwise indicated. The results of this work were obtained under the guidance of Prof. rer. nat. habil. Karsten Mäder.

Furthermore, I have not received external help, and I have marked the contributions from cooperation partners. The texts and references used herein are appropriately cited and recognized. I respect the principles of good scientific practice of the German Research Foundation (DFG) and have not faked any data.

I have not pursued any doctoral studies previously and have not submitted this work to any other Faculty.

_____

Halle (Saale), 15.05.2018   Alexandre Gomes Rodrigues

.